

# Topics in MHD Turbulence

Thesis by  
Yoram Lithwick

In Partial Fulfillment of the Requirements  
for the Degree of  
Doctor of Philosophy

California Institute of Technology  
Pasadena, California

2002  
(Defended May 3, 2002)



## Acknowledgements

I thank my advisor, Peter Goldreich, for showing me how enjoyable physics can be. He is not only a great physicist, but a great advisor as well.

## Abstract

I consider two topics in MHD turbulence. First, I work out the theory of compressible MHD turbulence, including kinetic effects. I use this theory to understand features of interstellar scintillation that have hitherto been unexplained. Second, I work out the theory of imbalanced weak MHD turbulence.

# Contents

<b>Acknowledgements</b>	<b>iii</b>
<b>Abstract</b>	<b>iv</b>
<b>1 Compressible MHD Turbulence in Interstellar Plasmas</b>	<b>1</b>
1.1 Introduction . . . . .	2
1.1.1 Compressible MHD Turbulence for Explaining Scintillation . . . . .	2
1.1.2 Diffractive Interstellar Scintillation (DISS) . . . . .	3
1.1.3 Basic Theory of DISS and the Scattering Measure . . . . .	3
1.1.4 Examination of Assumptions . . . . .	5
1.1.5 Observational Overview . . . . .	6
1.1.6 Two Constraints on the Turbulence . . . . .	7
1.1.7 SM From Turbulence Behind Shocks . . . . .	10
1.2 Incompressible MHD Turbulence . . . . .	11
1.2.1 Alfvén Wave Spectrum . . . . .	12
1.2.2 Eddies . . . . .	13
1.2.3 Passive Scalar Spectrum . . . . .	15
1.2.4 Slow Wave Spectrum . . . . .	18
1.2.5 Numerical Simulations . . . . .	19
1.3 Compressible Turbulence: Overview . . . . .	20
1.4 The Outer Scale and the MHD Scale . . . . .	22
1.5 The Cooling Scale . . . . .	24
1.5.1 Density Fluctuations Below the Cooling Scale: $1 < \beta < L_{\text{out}}/c_s t_{\text{cool}}$ . . . . .	25
1.5.2 Density Fluctuations Below the Cooling Scale: $\beta > L_{\text{out}}/c_s t_{\text{cool}} > 1$ . . . . .	27
1.6 The Collisionless Scale of the Neutrals . . . . .	28
1.6.1 Frequency Change . . . . .	29
1.6.2 Effect of Neutrals on the Turbulent Cascade . . . . .	32
1.6.3 Neutral Hydrogen Atoms . . . . .	34
1.6.4 Neutral Helium Atoms . . . . .	34
1.6.5 If Neutrals Damp the Cascade . . . . .	35
1.7 The Collisionless Scale of the Ions . . . . .	36
1.7.1 The Electron Diffusion Scale . . . . .	37

1.7.2	The Electron-Proton Equilibration Scale . . . . .	38
1.7.3	The Proton Diffusion Scale: Death of the Slow Mode and Entropy Mode . . . . .	38
1.7.4	Density Spectrum Below the Proton Diffusion Scale . . . . .	40
1.8	The End: the Proton Gyroscale . . . . .	40
1.9	Summary . . . . .	40
1.10	Comparison with Higdon's Work . . . . .	41
1.11	Compressible Turbulence When $\beta < 1$ . . . . .	42
1.12	Future Work . . . . .	43
1.13	Appendix: Waves in Compressible MHD . . . . .	43
1.13.1	Alfvén Mode . . . . .	44
1.13.2	Slow Mode . . . . .	45
1.13.3	Entropy Mode . . . . .	45
	<b>Bibliography</b> . . . . .	<b>47</b>
<b>2</b>	<b>Imbalanced Weak MHD Turbulence</b> . . . . .	<b>49</b>
2.1	Introduction . . . . .	49
2.2	Basic Equations . . . . .	51
2.3	Weak Turbulence: Heuristic Discussion . . . . .	53
2.3.1	Scaling Relation . . . . .	53
2.3.2	Insufficiency of Scaling Arguments for the Imbalanced Cascade . . . . .	55
2.3.3	Dynamics at the Dissipation Scale: Pinned Spectra . . . . .	55
2.3.4	Two Peripheral Issues . . . . .	56
2.4	Steady State Energy Spectra . . . . .	58
2.4.1	Fixed Energy at the Outer Scale . . . . .	59
2.4.2	Fixed Flux . . . . .	59
2.5	Kinetic Equations in Weak Turbulence . . . . .	60
2.6	Numerical Simulations of Kinetic Equations . . . . .	62
2.6.1	Fixed Energy at the Outer Scale . . . . .	63
2.6.2	Fixed Flux . . . . .	65
2.6.3	Decaying Turbulence . . . . .	67
2.7	A Model of the Kinetic Equations: Coupled Diffusion Equations . . . . .	67
2.7.1	Derivation of Coupled Diffusion Equations . . . . .	69
2.7.2	Numerical Simulations of Coupled Diffusion Equations . . . . .	70
2.8	The Bottleneck Effect . . . . .	73
2.9	Discussion . . . . .	73
2.10	Appendix: Kinetic Equation in Weak Turbulence . . . . .	75

2.10.1 Preliminaries . . . . .	75
2.10.2 A Toy Problem: the Linear Random Oscillator . . . . .	76
2.10.3 Derivation of Kinetic Equation . . . . .	79
2.10.4 Steady State Fluxes . . . . .	81
<b>Bibliography</b>	<b>83</b>

## List of Figures

1.1	Wandering of Magnetic Fieldlines . . . . .	14
1.2	Three-Dimensional Spectrum . . . . .	16
2.1	Simulation of Kinetic Equations with Fixed Energies at the Outer Scale . . . . .	64
2.2	Simulation of Kinetic Equations with Fixed Fluxes . . . . .	66
2.3	Decaying Simulation of Kinetic Equations . . . . .	68
2.4	Simulation of Diffusion Equations with Fixed Energies at the Outer Scale . . . . .	71
2.5	Simulation of Diffusion Equations with Fixed Fluxes . . . . .	72
2.6	The Bottleneck Effect . . . . .	74

## List of Tables

1.1 Summary of Lengthscales . . . . .	22
---------------------------------------	----

# Chapter 1 Compressible MHD Turbulence in Interstellar Plasmas

Written with Peter Goldreich; published in the *Astrophysical Journal*, 562, 279 (2001).

(Introduction has been expanded for thesis.)

## ABSTRACT

Radio-wave scintillation observations reveal a nearly Kolmogorov spectrum of density fluctuations in the ionized interstellar medium. Although this density spectrum is suggestive of turbulence, no theory relevant to its interpretation exists. We calculate the density spectrum in turbulent magnetized plasmas by extending the theory of incompressible magnetohydrodynamic (MHD) turbulence given by Goldreich and Sridhar (1995) to include the effects of compressibility and particle transport. Our most important results are as follows. (1) Density fluctuations are due to the slow mode and the entropy mode. Both modes are passively mixed by the cascade of shear Alfvén waves. Since the shear Alfvén waves have a Kolmogorov spectrum, so do the density fluctuations. (2) Observed density fluctuation amplitudes constrain the nature of MHD turbulence in the interstellar medium. Slow mode density fluctuations are suppressed when the magnetic pressure is less than the gas pressure. Entropy mode density fluctuations are suppressed by cooling when the cascade timescale is longer than the cooling timescale. These constraints imply either that the magnetic and gas pressures are comparable, or that the outer scale of the turbulence is very small. (3) A high degree of ionization is required for the cascade to survive damping by neutrals and thereby to extend to small lengthscales. Regions that are insufficiently ionized produce density fluctuations only on lengthscales larger than the neutral damping scale. These regions may account for the excess of power that is found on large scales. (4) Provided that the thermal pressure exceeds the magnetic pressure, both the entropy mode and the slow mode are damped on lengthscales below that at which protons can diffuse across an eddy during the eddy's turnover time. Consequently, eddies whose extents *along the magnetic field* are smaller than the proton collisional mean free path do not contribute to the density spectrum. However, in MHD turbulence eddies are highly elongated along the magnetic field. From an observational perspective, the relevant lengthscale is that *transverse* to the magnetic field. Thus the cutoff lengthscale for density fluctuations is significantly smaller than the proton mean free path. (5) The Alfvén mode is critically damped at the transverse lengthscale of the proton gyroradius, and thus cascades to smaller lengthscales than either the slow mode or the entropy mode.

## 1.1 Introduction

### 1.1.1 Compressible MHD Turbulence for Explaining Scintillation

Diffractive scintillations of small angular-diameter radio sources indicate that the interstellar electron density spectrum on lengthscales  $10^8 - 10^{10}$  cm is nearly Kolmogorov; i.e., r.m.s. density fluctuations across a lengthscale  $\lambda$  are nearly proportional to  $\lambda^{1/3}$ .

Density fluctuations that obey the Kolmogorov scaling occur in homogeneous subsonic *hydrodynamic* turbulence. They are due to the entropy mode, a zero-frequency isobaric mode whose density fluctuations are offset by temperature fluctuations. Since subsonic turbulence is nearly incompressible, the velocity fluctuations follow Kolmogorov's scaling. To a good approximation, the entropy mode is passively mixed by the velocity field, so it also conforms to the Kolmogorov spectrum.<sup>1</sup> Density fluctuations in Earth's atmosphere, which cause stars to twinkle, obey the Kolmogorov scaling. They arise from the passive mixing of the entropy mode.

The electron density spectrum in the interstellar medium cannot be explained by hydrodynamic turbulence.<sup>2</sup> Because the medium is ionized, magnetic effects must be accounted for. This is evident since the lengthscales probed by diffractive scintillations are smaller than the collisional mean free paths of both electrons and protons. If the magnetic field were negligible, freely streaming plasma would wipe out density fluctuations at diffractive scales. In the presence of a magnetic field, electrons and protons are tied to fieldlines at the scale of their gyroradii. For typical interstellar field strengths, these gyroradii are smaller than the diffractive scales. A magnetic field thus impedes the plasma from streaming across fieldlines, and allows the turbulent cascade and the associated density fluctuations to reach very small scales across the fieldlines before dissipating. Therefore, a theory for compressible turbulence in magnetized plasmas is required to explain the observed density spectra. Our objective is to develop this theory.

Until now, the only description of density fluctuations in interstellar plasmas was by Higdon (1984, 1986). These papers, while prescient, preceded a theory for *incompressible* MHD turbulence, and therefore did not account for the full dynamics of the cascade. We compare Higdon's theory with ours in §1.10.

Before presenting our theory of compressible MHD turbulence, we give an overview of the observations.

---

<sup>1</sup>Density fluctuations due to the Reynolds stress scale as  $\lambda^{2/3}$ . In addition, the dissipation of turbulent kinetic energy yields entropy fluctuations. The ratio of the corresponding density fluctuations to the mean density is comparable to the square of the Mach number at the lengthscale of interest; hence these density fluctuations are also proportional to  $\lambda^{2/3}$ .

<sup>2</sup>Charge neutrality is maintained on diffractive scales, so electron density fluctuations include compensating fluctuations in the density of positive ions.

### 1.1.2 Diffractive Interstellar Scintillation (DISS)

Rickett (1977, 1990) and Armstrong, Rickett, and Spangler (1995) review the observations of diffractive interstellar scintillation (DISS) and their interpretation. They also discuss refractive scintillations and dispersion measure fluctuations. However, we focus primarily on diffractive measurements because they are much more sensitive.

Radio waves that propagate through ionized gas are affected by plasma dispersion: their phase speed depends on the density of free electrons. Since free electrons are distributed inhomogeneously in the interstellar medium, wavefronts in the ISM are distorted. One consequence is that point-like radio sources are observed to be scatter-broadened, i.e., their images have a finite angular extent,  $\theta_{\text{scatt}}$ . The scattering disks of a few dozen sources have been imaged—primarily extra-galactic radio sources, as well as a few Galactic sources such as the Galactic center and Galactic OH-IR stars. A much more common method for detecting scattering disks is through their effects on pulsars. The scattering disk of a pulsar is usually too small and too weak to be directly imaged. However, rays that travel through the center of the scattering disk arrive at Earth faster than those that travel through the edges. If the distance between the Earth and the region where scattering occurs is  $D$ , then the difference in travel time is  $\tau_{\text{scatt}} \simeq (D/c)(1 - \cos \theta_{\text{scatt}}) \simeq (D/c)(\theta_{\text{scatt}})^2/2$  (assuming that the distance from the scattering region to the pulsar is  $\gg D$ ). Therefore a pulse that is emitted for an infinitesimal time is observed at Earth to be broadened in time by  $\tau_{\text{scatt}}$ . Pulse broadening has been observed directly in many pulsars. There are also many pulsars whose pulse-broadenings, while not directly observable, can be inferred in frequency-space; i.e., because of pulse broadening, the observed pulsar signal is correlated with itself only over a narrow bandwidth,  $\Delta\nu_{\text{scatt}} \sim 1/\tau_{\text{scatt}}$ ; this is called the decorrelation bandwidth.

### 1.1.3 Basic Theory of DISS and the Scattering Measure

If a plane wave is incident on a localized region of scattering material, then fronts of constant phase are distorted. In this subsection, we calculate the typical angle by which phase fronts are bent. This angle is closely related to the observed angular size of a point-like radio source that is located at an infinite distance behind the scattering region. We will see that the angular size depends on a single combination of parameters within the scattering region: the scattering measure.

Because of plasma dispersion, a radio wave that travels through ionized plasma has phase speed  $c(1 - (\nu_p/\nu)^2)^{-1/2}$ , where  $c$  is the speed of light,  $\nu$  is the radio-wave frequency and  $\nu_p$  is the plasma frequency (e.g., Spitzer 1978). Neglecting factors of order unity throughout,  $(\nu_p/\nu)^2 \sim nr_e\tilde{\lambda}^2$ , where  $n$  is the electron number density,  $r_e$  is the classical electron radius, and  $\tilde{\lambda}$  is the radio-wavelength (we use a tilde to differentiate radio-wavelength from lengthscale, which we denote by  $\lambda$  in this thesis); for the observations of interest,  $nr_e\tilde{\lambda}^2 \ll 1$ . As a result, a wave that travels through a region of

plasma for a distance  $\lambda$ , has its phase increased by

$$\phi \sim n\lambda[r_e\tilde{\lambda}] \quad (1.1)$$

relative to the phase it would have had if it had travelled through vacuum.

Let us consider the scattering of a plane wave by fluctuations in the scattering region that have lengthscale  $\lambda$ .<sup>3</sup> We label the r.m.s. electron density fluctuation on this lengthscale  $n_\lambda$ . After a plane wave penetrates the scattering region a distance  $\lambda$  along the line of sight, it becomes distorted; the r.m.s. value of its phase is  $\sim n_\lambda\lambda[r_e\tilde{\lambda}]$ . As the plane wave penetrates further, the phase change along any line of sight due to plasma dispersion changes randomly every step of length  $\lambda$ , as in a random walk. The r.m.s. phase thus increases as the square root of the number of steps. If the scattering region has an extent  $L_{\text{turb}}$  along the line of sight (where  $L_{\text{turb}} \gg \lambda$ ), then the r.m.s phase of the wavefront after  $L_{\text{turb}}$  is

$$\phi_\lambda \sim n_\lambda\lambda(L_{\text{turb}}/\lambda)^{1/2}[r_e\tilde{\lambda}]. \quad (1.2)$$

Therefore a front of constant phase becomes corrugated; the r.m.s. bending angle is

$$\theta_\lambda \sim \tilde{\lambda}\phi_\lambda/\lambda. \quad (1.3)$$

As long as  $\phi_\lambda \gg 1$ ,  $\theta_\lambda$  is the angle by which rays are deflected.

Let us next consider the scattering when density fluctuations exist on a range of lengthscales. We assume a Kolmogorov density spectrum on lengthscales of interest,  $n_\lambda \propto \lambda^{1/3}$ . If we insert this  $n_\lambda$  into equation (1.2), we find  $\phi_\lambda \propto \lambda^{5/6}$ ; we then see from equation (1.3) that  $\theta_\lambda \propto \lambda^{-1/6}$ . Larger values of  $\theta_\lambda$  result from smaller lengthscales. The smallest relevant lengthscale is that at which  $\phi_\lambda \sim 1$ . It is called the diffractive lengthscale,  $\lambda_{\text{diff}}$ . On smaller scales,  $\phi_\lambda < 1$ , so two rays separated by  $\lambda < \lambda_{\text{diff}}$  at the scattering region can only partially interfere. As a result, the observed angular size of the scattering disk is  $\theta_{\lambda_{\text{diff}}}$ .

Before calculating  $\lambda_{\text{diff}}$  and  $\theta_{\lambda_{\text{diff}}}$ , it is convenient to introduce the scattering measure (SM),

$$\text{SM} \sim \frac{n_\lambda^2}{\lambda^{2/3}}L_{\text{turb}}, \quad (1.4)$$

which is independent of lengthscale. Equation (1.2) becomes

$$\phi_\lambda \sim \text{SM}^{1/2}\lambda^{5/6}[r_e\tilde{\lambda}]. \quad (1.5)$$

---

<sup>3</sup>We assume isotropy, so  $\lambda$  refers to lengthscales both transverse and parallel to the line of sight. Although MHD turbulence is anisotropic on small scales, the angle-averaged spectrum is nearly isotropic.

At the diffractive scale  $\phi_\lambda \sim 1$ , so

$$\lambda_{\text{diff}} \sim \text{SM}^{-3/5} [r_e \tilde{\lambda}]^{-6/5} . \quad (1.6)$$

Typically  $\lambda_{\text{diff}} \sim 10^8 - 10^{10}$  cm. Inserting  $\lambda_{\text{diff}}$  into equation (1.3), we have for the observed angular size of the scattering disk:

$$\theta_{\text{scatt}} \sim \theta_{\lambda_{\text{diff}}} \sim \tilde{\lambda} / \lambda_{\text{diff}} \sim \text{SM}^{3/5} \tilde{\lambda}^{11/5} r_e^{6/5} . \quad (1.7)$$

It is set by SM. Since  $\tau_{\text{scatt}} \sim 1/\Delta\nu_{\text{scatt}} \sim (D/c)(\theta_{\text{scatt}})^2$ , all DISS measurements are characterized by SM (in addition to  $D$  and the spectral slope).

### 1.1.4 Examination of Assumptions

One of our reasons for repeating the above well-known calculation of  $\theta_{\text{scatt}}$  is to clarify what assumptions have been made. We do that in this subsection.

First, we assumed that the amplitude of the Kolmogorov density spectrum,  $n_\lambda/\lambda^{1/3}$ , is constant along the line of sight. If it varies, then it is apparent from our derivation that SM should simply be defined as the integral of  $(n_\lambda)^2/\lambda^{2/3}$  along the line of sight (instead of eq. [1.4]); i.e., SM is an extensive quantity.

Second, we assumed that  $n_\lambda \propto \lambda^{1/3}$  in the vicinity of  $\lambda_{\text{diff}}$ . More generally, if  $n_\lambda \propto \lambda^a$  where  $a < 1/2$ , then instead of equation (1.7) we derive

$$\theta_{\text{scatt}} \sim [\text{SM}_a \tilde{\lambda}^{2a+3} r_e^2]^{1/(2a+1)} , \quad (1.8)$$

where  $\text{SM}_a$  is the generalized scattering measure,  $\text{SM}_a \sim (n_\lambda^2/\lambda^{2a})L_{\text{turb}}$ .<sup>4</sup> The exponent on  $\tilde{\lambda}$ , i.e.,  $(2a+3)/(2a+1)$ , is observable from the scalings of DISS measurements with radio-wavelength. While it is often observed to be near 11/5 (implying the Kolmogorov value  $a = 1/3$ ), there are a number of lines of sight where it differs substantially from this value.

Third, we assumed that the radio source is at infinity. To consider the more general case, we first define  $D_1$  as the Earth-to-scattering region distance and  $D_2$  as the scattering region-to-radio source distance. Then, as long as  $D_1 < D_2$ , the  $\theta_{\text{scatt}}$  given by equation (1.7) is approximately the angular size of the scattering spot (viewed from Earth). If the converse is true ( $D_1 > D_2$ ), then the  $\theta_{\text{scatt}}$  given by equation (1.7) corresponds to the angular spot size at the scattering screen as viewed from the source; from Earth, the observed spot size would be  $\theta_{\text{obs}} \sim (D_2/D_1)\theta_{\text{scatt}} < \theta_{\text{scatt}}$ . When

<sup>4</sup>Cordes et al. (1991) define their SM as follows. They assume that the density power spectrum is given by  $|n_k|^2 = C_n^2 k^{-\alpha}$ , where  $n_k$  is the Fourier transform of the density field  $n(x)$ . They then define SM as the integral of  $C_n^2$  along the line of sight. So their  $C_n^2$  is nearly equal to our  $n_\lambda^2/\lambda^{2a}$ , aside from an order unity multiplicative factor that can easily be calculated by performing the Fourier transform; their SM is nearly equal to our  $\text{SM}_a$ ; and  $\alpha = 2a + 3$ .

inferring SM from observations of angular broadening, one often assumes that  $D_1 < D_2$ , which allows the distance correction to be ignored. However, this could underestimate SM.

The corresponding problem exists also for measurements of either temporal broadening or decorrelation bandwidth, which form the bulk of DISS observations. For arbitrary  $D_1$  and  $D_2$ ,  $\tau_{\text{scatt}} \sim (\min\{D_1, D_2\}/c)(\theta_{\text{scatt}})^2$ , where  $\theta_{\text{scatt}}$  is given by equation (1.7), and similarly for  $\Delta\nu_{\text{scatt}}$  (i.e.,  $\Delta\nu_{\text{scatt}} \sim 1/\tau_{\text{scatt}}$ ). Typically, the Earth-to-pulsar distance is estimated from the observed dispersion measure together with a model of the electron density distribution within the Galaxy. The scattering region is assumed to lie halfway to the pulsar, so the inferred SM is typically an underestimate.

### 1.1.5 Observational Overview

Within a kiloparsec of the galactic plane, the contributions to  $C_n^2 \sim (n_\lambda)^2/\lambda^{2/3}$  appear to be of two kinds. There is a mean background with  $C_n^2 \sim 10^{-3.5}\text{m}^{-20/3}$ , together with localized regions, mostly close to the galactic plane, in which  $C_n^2$  is considerably larger (Cordes, Weisberg, and Boriakoff 1985). Along one line of sight through the HII region complex NGC 6334,  $\theta \sim 3''$  at radio-frequency  $\sim 1.5$  GHz, making this the strongest scattered source yet observed (Moran et al. 1990). Equation (1.7) implies that  $\text{SM} \sim 2 \times 10^3 \text{m}^{-20/3} \text{kpc}$ . The authors assume that the thickness of the scattering screen is  $\sim 1$  pc, which means that  $C_n^2 \sim 2 \times 10^6 \text{m}^{-20/3}$ . By contrast, in the local bubble of hot gas surrounding the sun,  $C_n^2 \lesssim 10^{-4.5} \text{m}^{-20/3}$  (Phillips and Clegg 1992).

The background value of  $C_n^2$  is contributed by the diffuse, ionized, interstellar medium (DIM). The DIM has mean (local) electron density  $n \sim 0.1 \text{cm}^{-3}$ , and temperature  $T \sim 10^4$  K. With a filling factor of about 0.2 in the galactic plane, which some evidence suggests approaches unity at  $|z| \gtrsim \text{kpc}$ , it probably accounts for most of the electron density deduced from pulsar dispersion measures (Reynolds 1991). The DIM appears to be ionized by O stars (Mathis 1986). This requires that about 0.14 of the ionizing photons from O stars manage to escape being absorbed by neutral gas near the galactic plane. A detailed model of the ionization structure produced by O stars within 2.5 kpc of the sun shows good agreement with observational determinations of both electron density and emission measure (Miller and Cox 1993).

A useful diagnostic of turbulence in the Galaxy is the relation of a pulsar's SM to its dispersion measure, DM. The dispersion measure is defined as the integral of  $n$  along the line of sight. It can be used as a surrogate for distance. Cordes et al. (1991) plot the SM's and DM's of over a hundred pulsars. They find that for nearby pulsars (with small DM), SM increases roughly linearly with DM. This is consistent with a constant level of  $C_n^2$ , contributed by the DIM. However,  $\text{SM} \propto \text{DM}^3$  when  $\text{DM} \gtrsim 100 \text{pc cm}^{-3}$ , i.e., for distances greater than a few kpc.

Scattering measures that increase faster than distance can arise if scattering occurs in localized structures, such as HII regions, supernova shocks, or stellar wind bubbles. To be specific, let us

consider HII regions. The denser an HII region, the more it contributes to SM. The integrated SM through the Galaxy will increase faster than distance if high-density HII regions are sufficiently rare. Quantitatively, we denote the number of HII regions per unit volume that have electron densities between  $n$  and  $n + dn$  by  $\mathcal{N}(n)dn$ . If the distance to the source of radio waves is  $D$ , then the ‘‘optical depth’’ for the line of sight to intersect HII regions with electron density between  $n$  and  $n + dn$  is  $(\mathcal{N}(n)dn) \cdot A(n) \cdot D$ , where  $A(n)$  is the cross-section of these HII regions. So the expected value of SM is

$$\langle \text{SM} \rangle \sim \int dn \mathcal{N}(n) \cdot A(n) \cdot D \cdot \text{SM}_{\text{reg}}(n) , \quad (1.9)$$

where  $\text{SM}_{\text{reg}}(n)$  is the SM through a single region with density  $n$ . To determine the limits of this integral, we assume that most of the contribution to  $\langle \text{SM} \rangle$  is from regions with large  $n$ , i.e., that  $n\mathcal{N} \cdot A \cdot \text{SM}_{\text{reg}}$  is an increasing function of  $n$  for the  $n$ 's of interest; otherwise, we would have  $\langle \text{SM} \rangle \propto D$ . For  $\langle \text{SM} \rangle$  not to diverge, the optical depth,  $n\mathcal{N} \cdot A \cdot D$ , must decrease with increasing  $n$ . The largest  $n$  which contributes to  $\langle \text{SM} \rangle$  is that at which the optical depth is unity. Therefore,

$$\langle \text{SM} \rangle \sim \text{SM}_{\text{reg}}(n_{\text{max}}) , \quad (1.10)$$

where  $n_{\text{max}}$  is given by

$$n_{\text{max}} \mathcal{N}(n_{\text{max}}) \cdot A(n_{\text{max}}) \cdot D \sim 1 . \quad (1.11)$$

Thus far we have kept our discussion sufficiently general that it can be applied to other objects, such as supernova shocks or extreme density fluctuations in a turbulent cascade (i.e., Lévy flights, see Boldyrev and Gwinn 2002);  $n$  could represent any property that varies from object to object, such as the age of supernova remnants. Let us now compute the distribution function of HII regions, assuming that HII regions are responsible for the scattering, and that  $\langle \text{SM} \rangle \propto D^3$ . We take the distribution function to be given by

$$n\mathcal{N} \propto n^b . \quad (1.12)$$

Our goal is to calculate  $b$ . The radius of an HII region (the Strömngren radius) is  $R_s \sim 70(\text{cm}^{-3}/n)^{2/3}$  pc (e.g., Spitzer 1978). Its cross-sectional area is  $A \sim R_s^2 \propto n^{-4/3}$ . If the outer scale of the turbulent density spectrum is  $\sim R_s$ , then  $\text{SM}_{\text{reg}} \sim n^2 R_s^{1/3} \propto n^{16/9}$  (eq. [1.4]). From equation (1.11), with  $n\mathcal{N}_{\text{reg}}$  given by equation (1.12),  $n_{\text{max}} \propto D^{3/(4-3b)}$ . Substituting this into equation (1.10), we have  $\langle \text{SM} \rangle \propto D^{16/(12-9b)}$ . For this to be proportional to  $D^3$ , we must have  $b = (4/3) - (16/27) \sim 0.74$ .

### 1.1.6 Two Constraints on the Turbulence

We consider two general constraints on the turbulence.

### Constraint From EM/SM

The first constraint comes from comparing observations of SM with observations of EM, the emission measure. This constraint has been considered by other authors, e.g., by Cordes et al. (1991). Assuming that the density spectrum is Kolmogorov in the vicinity of the diffraction scale and that the scattering material is homogeneous,  $SM \sim (n_\lambda^2/\lambda^{2/3})L_{\text{turb}}$ , where  $L_{\text{turb}}$  is the path-length through the turbulence along the line of sight (eq. 1.4). We define the dimensionless amplitude  $\epsilon$ ,

$$\epsilon \equiv \frac{n_\lambda/\lambda^{1/3}}{n/L_{\text{out}}^{1/3}}, \quad (1.13)$$

where  $n$  is the number density of ionized particles and  $L_{\text{out}}$  is the outer scale, i.e., the lengthscale at which the turbulence is stirred; it satisfies  $L_{\text{out}} < L_{\text{turb}}$ . If the Kolmogorov spectrum extends to  $L_{\text{out}}$ , then  $\epsilon = n_{L_{\text{out}}}/n$ . In terms of  $\epsilon$ , we have

$$SM \sim \frac{\epsilon^2 n^2 L_{\text{turb}}}{L_{\text{out}}^{2/3}}. \quad (1.14)$$

The emission measure is defined as the integral of  $n^2$  along the line of sight. It has been measured along many lines of sight, e.g., from free-free emission or from  $\text{H}\alpha$ . The turbulent gas contributes  $n^2 L_{\text{turb}}$  to EM. If a fraction  $f < 1$  of the ionized gas along the line of sight contributes to SM, then

$$EM \sim \frac{n^2 L_{\text{turb}}}{f}. \quad (1.15)$$

We divide equation (1.15) by (1.14), which yields an expression for the outer scale:

$$L_{\text{out}} \sim \epsilon^3 f^{3/2} \left( \frac{EM}{SM} \right)^{3/2} = \epsilon^3 f^{3/2} L_{EM/SM}, \quad (1.16)$$

where we define  $L_{EM/SM} \equiv (EM/SM)^{3/2}$ . Since  $f < 1$  and, typically,  $\epsilon < 1$ , the outer scale is smaller than  $L_{EM/SM}$ . Lines of sight with large SM tend to have surprisingly small EM;  $L_{EM/SM}$  is often much smaller than a parsec. It is a challenge to find a site in the ISM that gives such small outer scales.

One of the main goals of the body of this chapter is to calculate  $\epsilon$  in a compressible MHD cascade. We summarize our result as follows (neglecting neutral damping and assuming that the proton damping scale is smaller than the diffraction scale):

$$\epsilon = \max \left\{ \mathcal{M}^{5/2} \left( \frac{c_s t_{\text{cool}}}{L_{\text{out}}} \right)^{1/2}, \frac{1}{\beta^{1/2}} \right\}, \quad (1.17)$$

where  $\mathcal{M}$  is the Mach number of the turbulence,  $t_{\text{cool}}$  is the cooling time, and  $\beta$  is the ratio of thermal to magnetic pressure. In deriving this result, we assume that  $\mathcal{M} c_s t_{\text{cool}} < L_{\text{out}}$ ,  $\mathcal{M} < 1$ , and

$\beta > 1$ , so  $\epsilon < 1$ . If the magnetic field is amplified by the turbulence, the smallest  $\beta$  achievable is  $\beta_{\min} \sim \mathcal{M}^{-2}$ .

### Constraint From Energetics

The second constraint on  $L_{\text{out}}$  is based on energetics. In all of the sources that we shall consider, we expect that the kinetic energy that is required to stir the turbulence is less than the thermal energy that is radiated away by the gas. If this were not true, then the turbulence would heat the gas faster than it could cool. Furthermore, most astrophysical sources are inefficient in converting their energy output into kinetic energy—most of the energy is radiated away. To be quantitative, kinetic energy must be put into the turbulence at the rate  $\dot{E}_{\text{kin}} \sim (m_p v_\lambda^2 / t_\lambda)(n L_{\text{turb}} A)$ , where  $m_p$  is the proton mass,  $v_\lambda$  is the velocity of the gas on lengthscale  $\lambda$ ,  $t_\lambda$  is the cascade time on this scale, and  $A$  is the area occupied by the turbulence transverse to the line of sight. In both hydro and strong MHD turbulence,  $t_\lambda \sim \lambda / v_\lambda$ . Since the energy cascade rate must be independent of lengthscale in steady state, this cascade time implies that  $v_\lambda \propto \lambda^{1/3}$ . We denote the Mach number of the turbulence as follows

$$\mathcal{M} \equiv \frac{v_\lambda / \lambda^{1/3}}{c_s / L_{\text{out}}^{1/3}}, \quad (1.18)$$

where  $c_s$  is the sound speed. In terms of  $\mathcal{M}$ , we have

$$\dot{E}_{\text{kin}} \sim \mathcal{M}^3 \frac{nm_p c_s^3}{L_{\text{out}}} L_{\text{turb}} A. \quad (1.19)$$

We wish to compare this with  $\dot{E}_{\text{cool}}$ , the rate at which energy is radiated away by the ionized gas along the line of sight (both turbulent and quiescent gas):

$$\dot{E}_{\text{cool}} \sim \frac{1}{f} \frac{nm_p c_s^2}{t_{\text{cool}}} L_{\text{turb}} A, \quad (1.20)$$

where  $t_{\text{cool}}$  is the cooling time. So  $\dot{E}_{\text{kin}} / \dot{E}_{\text{cool}} \sim \mathcal{M}^3 f (c_s t_{\text{cool}} / L_{\text{out}})$ , and our requirement that  $\dot{E}_{\text{kin}} < \dot{E}_{\text{cool}}$  can be rewritten as follows:

$$L_{\text{out}} > \mathcal{M}^3 f c_s t_{\text{cool}}. \quad (1.21)$$

Interstellar gas in photoionization equilibrium typically has a temperature of  $\sim 10^4 \text{K}$  and  $c_s t_{\text{cool}} \sim 0.2(\text{cm}^{-3}/n) \text{ pc}$ . This  $c_s t_{\text{cool}}$  probably characterizes much of the interstellar gas that is responsible for DISS. If the turbulence is trans-sonic ( $\mathcal{M} \sim 1$ ) and  $f \sim 1$ , then  $L_{\text{out}}$  should be larger than  $c_s t_{\text{cool}}$ .

## Combining the Two Constraints

Inequality (1.21) can be combined with our other constraint (eq. [1.16]). For given EM/SM,  $t_{\text{cool}}$ ,  $\mathcal{M}$ , and  $\epsilon$ , this leads to a lower limit on  $f$  and hence a lower limit on  $L_{\text{out}}$ ; e.g., if  $\epsilon \sim 1/\sqrt{\beta} < 1$  and  $\mathcal{M} \sim 1$ ,

$$L_{\text{out}} > \beta^3 \frac{(c_s t_{\text{cool}})^3}{(L_{\text{EM/SM}})^2}. \quad (1.22)$$

Alternatively, we can address the following question: given EM, what is the largest possible SM? From equations (1.14) and (1.15),  $\text{SM} \sim \epsilon^2 f \text{EM}/L_{\text{out}}^{2/3}$ . So we should maximize  $\epsilon$  and  $f$  (i.e.,  $\epsilon \sim 1$  and  $f \sim 1$ ) and minimize  $L_{\text{out}}$ . The smallest  $L_{\text{out}}$  that can be achieved without overheating the medium is given by equation (1.21); so the maximum SM is

$$\text{SM}_{\text{max}} \sim \frac{1}{\mathcal{M}^2} \frac{\text{EM}}{(c_s t_{\text{cool}})^{2/3}}. \quad (1.23)$$

For sufficiently small  $\mathcal{M}$ ,  $\text{SM}_{\text{max}}$  can be made as large as desired. However, we shall see that many astrophysical sites are expected to have  $\mathcal{M} \sim 1$ .

### 1.1.7 SM From Turbulence Behind Shocks

Radio waves that pass through a shock front in the ISM are scattered both by the density discontinuity across the shock and by density fluctuations in the turbulence behind the shock. In this subsection, we show that scattering in the turbulence always dominates.

Let us consider the scattering across a single adiabatic shock, where the density jump across the shock is  $\sim n$ , with  $n$  the post-shock density. We assume that the post-shock gas is fully ionized. To calculate the amount of scattering, we first calculate the difference between the accumulated phases along two lines of sight separated by  $\lambda$  (see §1.1.3). Associated with turbulence behind the shock, from equation (1.2),

$$\phi_{\lambda}^{\text{turb}} \sim n_{\lambda} \lambda (L_{\text{out}}/\lambda)^{1/2} [r_e \tilde{\lambda}] \sim n \lambda^{5/6} L_{\text{out}}^{1/6} [r_e \tilde{\lambda}], \quad (1.24)$$

where we have assumed that the extent of the turbulence is comparable to the outer scale ( $L_{\text{turb}} \sim L_{\text{out}}$ ) and that  $n_{\lambda} \sim n(\lambda/L_{\text{out}})^{1/3}$ . Associated with the discontinuity across the front,

$$\phi_{\lambda}^{\text{disc}} \sim n \lambda [r_e \tilde{\lambda}], \quad (1.25)$$

since the column densities along the two lines of sight differ by  $\sim n \lambda$ . Therefore

$$\phi_{\lambda}^{\text{disc}} \sim \left( \frac{\lambda}{L_{\text{out}}} \right)^{1/6} \phi_{\lambda}^{\text{turb}}, \quad (1.26)$$

and as long as  $L_{\text{out}}$  is larger than the diffractive scale,  $\phi_{\lambda}^{\text{disc}}$  is negligible. We expect  $L_{\text{out}} \gg \lambda_{\text{diff}} \sim$

$10^8 - 10^{10}$  cm, so the signature of the shock front is always smothered by the turbulence behind it.

If we erroneously neglect the turbulence, we find from using equation (1.25) that  $\theta_{\text{scatt}} \propto \tilde{\lambda}^2$ , which is consistent with observations along certain lines of sight. (Recall that the Kolmogorov result is  $\theta_{\text{scatt}} \propto \tilde{\lambda}^{11/5}$ , eq. [1.7].) Therefore it has been frequently claimed in the literature that the  $\tilde{\lambda}^2$  scaling can be explained by shocks (e.g., Lambert and Rickett 2000). However, shocks give  $\tilde{\lambda}^{11/5}$  because of the turbulence behind them. A more plausible explanation for the  $\tilde{\lambda}^2$  scaling is a turbulent cascade with an inner scale that is larger than the diffractive scale (e.g., if the cascade is cut off at a relatively large scale by damping caused by neutral atoms, see §1.6.5).

## 1.2 Incompressible MHD Turbulence

Our compressible theory extends the theory of incompressible MHD turbulence given by Goldreich and Sridhar (1995) by including a slightly compressible slow mode and a passive entropy mode. We also consider kinetic effects: on sufficiently short lengthscales, the mean free paths of the particles are significant, and the equations of compressible MHD must be modified. This is especially important for damping. Before considering compressible turbulence, we discuss incompressible MHD turbulence, focusing on issues that are important for the compressible case.

Goldreich and Sridhar (1995, 1997) propose a picture of the dynamics of incompressible strong MHD turbulence and describe the power spectra of Alfvén waves, slow waves, and passive scalars. We extend their picture to cover additional features such as the parallel cascades of both slow waves and passive scalars. Unless explicitly stated otherwise, throughout this chapter “parallel” and “transverse” refer to the orientation relative to the local mean magnetic field, which is the magnetic field averaged over the scale of interest. Our discussion of incompressible MHD turbulence, while somewhat lengthy, is important for understanding the extension to compressible turbulence that follows.

Consider a uniform unperturbed plasma with an embedded magnetic field. Turbulence is excited at the MHD outer scale,  $L_{\text{MHD}}$ , by random and statistically isotropic forcing, with r.m.s. velocity fluctuations and r.m.s. magnetic field fluctuations (in velocity units) which are comparable to the Alfvén speed,  $v_A$ .<sup>5</sup>

As the turbulence cascades from the MHD outer scale to smaller scales, power concentrates in modes with increasingly transverse wave vectors. The inertial range velocity spectrum applies to lengthscales below  $L_{\text{MHD}}$  but above the dissipation scale. It is anisotropic and is characterized by

$$v_{\lambda_{\perp}} = v_A \left( \frac{\lambda_{\perp}}{L_{\text{MHD}}} \right)^{1/3}, \quad (1.27)$$

---

<sup>5</sup>The forcing fluctuations may also be less  $v_A$ , in which case  $L_{\text{MHD}}$  would be defined as the lengthscale at which the fluctuations extrapolate to  $v_A$ .

$$\Lambda_{\parallel} = \lambda_{\perp}^{2/3} L_{\text{MHD}}^{1/3}; \quad (1.28)$$

the inertial range magnetic field spectrum is identical. Here  $\lambda_{\perp}$  is the lengthscale transverse to the local mean magnetic field,  $v_{\lambda_{\perp}}$  is the r.m.s. velocity fluctuation across  $\lambda_{\perp}$ , and  $\Lambda_{\parallel}$  is the lengthscale parallel to the local mean magnetic field across which the velocity fluctuation is  $v_{\lambda_{\perp}}$ . We interpret  $\Lambda_{\parallel}$  as the elongation along the magnetic field of an eddy which has a size  $\lambda_{\perp}$  transverse to the magnetic field; it is not an independent variable, but is a function of  $\lambda_{\perp}$ . Deep within the inertial range, where  $\lambda_{\perp} \ll L_{\text{MHD}}$ , eddies are highly elongated along the magnetic field:  $\Lambda_{\parallel} \gg \lambda_{\perp}$ . In the following subsections, we explain the physics underlying the spectrum, and consider some of the implications.

### 1.2.1 Alfvén Wave Spectrum

Arbitrary disturbances can be decomposed into Alfvén waves and slow waves. The Appendix summarizes the properties of these waves in the more general case of compressible MHD. In incompressible MHD, Alfvén waves and slow waves are usually referred to as shear-Alfvén waves and pseudo-Alfvén waves, but the former designation is more convenient for making the connection with compressible MHD.

Our understanding of the MHD turbulence is based on two facts: (i) MHD wave-packets propagate at the Alfvén speed either parallel or antiparallel to the local mean magnetic field; and (ii) nonlinear interactions are restricted to collisions between oppositely directed wave-packets. These facts imply that in encounters between oppositely directed wave-packets, each wave-packet is distorted as it follows field lines perturbed by its collision partner. A wave-packet cascades when the fieldlines that it is propagating along have spread by a distance comparable to its transverse size.

Alfvén waves have quasi two-dimensional velocity and magnetic field fluctuations which are confined to planes perpendicular to the local mean magnetic field. As their more complete name shear-Alfvén implies, they dominate the shear of the mapping of planes transverse to the local mean magnetic field produced by field line wander. Thus, Alfvén waves control the dynamics of MHD cascades; slow waves may be ignored when considering the dynamics of Alfvén waves.

In strong MHD turbulence the cascade time of an Alfvén wave-packet is comparable to its travel time across the parallel length of a single oppositely directed Alfvén wave-packet of similar size. Goldreich and Sridhar (1995) refer to this balance of timescales as critical balance. It relates the parallel size of a wave-packet,  $\Lambda_{\parallel}$ , to its transverse size,  $\lambda_{\perp}$ . Wave-packets of transverse size  $\lambda_{\perp}$  cascade when the fieldlines they follow wander relative to each other by a transverse distance  $\lambda_{\perp}$ . Critical balance implies that this occurs over a parallel distance  $\Lambda_{\parallel}$ .

The Alfvén wave spectrum is given by equations (1.27) and (1.28), with  $v_{\lambda_{\perp}}$  referring to the velocity fluctuations of the Alfvén waves. It is deduced from two scaling arguments: (i) Kolmogorov's

argument that the cascade time  $t_{\lambda_{\perp}} \simeq \lambda_{\perp}/v_{\lambda_{\perp}}$  leads to an energy cascade rate,  $v_{\lambda_{\perp}}^2/t_{\lambda_{\perp}} \simeq v_{\lambda_{\perp}}^3/\lambda_{\perp}$ , which is independent of lengthscale; and (ii) the critical balance assertion that the linear wave period which characterizes the Alfvén waves in a wave-packet is comparable to the nonlinear cascade time of that wave-packet, i.e.,  $v_A/\Lambda_{\parallel} \simeq 1/t_{\lambda_{\perp}}$ .

Before considering slow waves in MHD turbulence, we discuss two topics that are governed by the dynamics of Alfvén waves only: eddies and passive scalars.

### 1.2.2 Eddies

Because of their transverse polarization, Alfvén waves are responsible for the wandering of magnetic fieldlines. A snapshot of wandering fieldlines is shown in Figure 1.1. Each of these fieldlines passes through a localized region of size  $\lambda_{\perp}$  in one plane transverse to the mean magnetic field. Away from this plane the bundle of fieldlines diverges due to the differential wandering of the individual lines. At a second plane, the bundle’s cross sectional area has approximately doubled. Critical balance implies that the distance to this second plane is comparable to the parallel wavelength which characterizes the bundle,  $\Lambda_{\parallel}$ . As the bundle spreads, other fieldlines, not depicted, enter from its sides. In general, the neighboring fieldlines of any individual field line within a region of transverse size  $\lambda_{\perp}$  change substantially over a parallel distance of order  $\Lambda_{\parallel}$ . It is natural to think of  $\Lambda_{\parallel}$  as the parallel size of an eddy that has transverse size  $\lambda_{\perp}$ . Two eddies with the same transverse lengthscale that are separated by a parallel distance greater than their  $\Lambda_{\parallel}$  incorporate different fieldlines, and hence are statistically independent. Eddies are distinct from wave-packets. The former are rooted in the fluid whereas the latter propagate up and down magnetic fieldlines at the Alfvén speed.

Aside from their anisotropy, eddies in MHD turbulence are similar to those in hydrodynamic turbulence. They are spatially localized structures with characteristic velocity fluctuations and lifetimes. The r.m.s. velocity difference between two points is determined by the smallest eddy that contains both. Different eddies of a given size are statistically independent. The three-dimensional spectrum for r.m.s. velocity fluctuations across transverse lengthscales  $\lambda_{\perp}$  and parallel lengthscales  $\lambda_{\parallel}$  is

$$v_{\lambda_{\perp},\lambda_{\parallel}} = v_A \times \begin{cases} (\lambda_{\perp}/L_{\text{MHD}})^{1/3}, & \text{for } \lambda_{\parallel} \ll \Lambda_{\parallel} \\ (\lambda_{\parallel}/L_{\text{MHD}})^{1/2} = (\lambda_{\perp}/L_{\text{MHD}})^{1/3}(\lambda_{\parallel}/\Lambda_{\parallel})^{1/2}, & \text{for } \lambda_{\parallel} \gg \Lambda_{\parallel} \end{cases} . \quad (1.29)$$

There is negligible additional power within an eddy on parallel lengthscales smaller than  $\Lambda_{\parallel}$ , so for  $\lambda_{\parallel} \ll \Lambda_{\parallel}(\lambda_{\perp})$ ,  $v_{\lambda_{\perp},\lambda_{\parallel}} = v_{\lambda_{\perp}}$ . For  $\lambda_{\parallel} \gg \Lambda_{\parallel}(\lambda_{\perp})$ , the smallest eddy that contains both  $\lambda_{\perp}$  and  $\lambda_{\parallel}$  has a transverse lengthscale  $\lambda'_{\perp}$  which satisfies  $\Lambda_{\parallel}(\lambda'_{\perp}) = \lambda_{\parallel}$ . The velocity fluctuation of this eddy is obtained by solving this equation for  $\lambda'_{\perp}$  (eq. [1.28]), and inserting this  $\lambda'_{\perp}$  in equation (1.27). Contours of the three-dimensional spectrum are plotted in Figure 1.2. Each contour represents

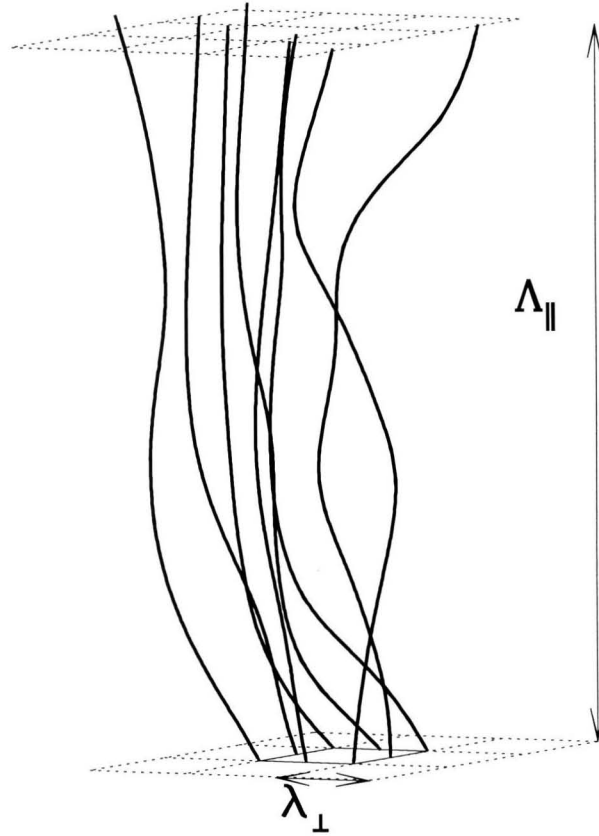


Figure 1.1: Wandering of Magnetic Fieldlines

A fieldline bundle of transverse size  $\lambda_{\perp}$  diverges after a parallel distance  $\Lambda_{\parallel}$ , where  $\Lambda_{\parallel}$  is the parallel size of an eddy (eq. [1.28]) as determined by critical balance.

eddies of a characteristic size.

Maron and Goldreich (2001) give the three-dimensional spectrum in Fourier-space. Since eddies that are separated by more than  $\Lambda_{\parallel}$  are statistically independent, the power spectrum at a fixed transverse wavenumber  $k_{\perp}$  is independent of the parallel wavenumber  $k_{\parallel}$  in the corresponding region of Fourier-space, i.e., where  $k_{\parallel}^{-1} \gtrsim \Lambda_{\parallel}(k_{\perp}^{-1})$ .

The turbulent cascade is generally viewed as proceeding from larger eddies to smaller eddies as this is the direction of energy transfer. However, smaller eddies cascade many times in the time that a large eddy cascades. This is particularly important in turbulent mixing. Consider the evolution of two fluid elements whose initial separation is larger than the dissipation scale. On cascade timescale  $t_{\lambda_{\perp}}$ , their transverse separation will random walk a distance  $\lambda_{\perp}$  as the result of the cascade of smaller eddies. Therefore, on a timescale comparable to an eddy's cascade time, the transverse locations of its component fluid elements—whose sizes may be considered to be comparable to the dissipation scale—are completely randomized. Moreover, since mixing at the dissipation scale causes neighbouring fluid elements to be rapidly homogenized, transverse smoothing of the eddy occurs on the timescale that it cascades. Rapid transverse mixing in MHD turbulence is similar to the more familiar isotropic mixing in hydrodynamic turbulence.

### 1.2.3 Passive Scalar Spectrum

A passive scalar,  $\sigma$ , satisfies the continuity equation,  $(\partial/\partial t + \mathbf{v} \cdot \nabla)\sigma = 0$ , and does not affect the fluid's evolution. It could represent, for example, the concentration of a contaminant. We consider the spectrum of a passive scalar mixed by the Alfvén wave cascade. These considerations are important for our subsequent investigation of compressible turbulence. They are also helpful for understanding the slow wave spectrum. We discuss the passive scalar spectrum both in the inertial range and also below the scale at which the Alfvén wave spectrum is cut off.

#### Passive Scalar Spectrum in the Inertial Range

As we show in this subsection, the transverse spectrum of the passive scalar in the inertial range is

$$\sigma_{\lambda_{\perp}} \propto \lambda_{\perp}^{1/3}, \quad (1.30)$$

where  $\lambda_{\perp}$  is the lengthscale transverse to the local mean magnetic field and  $\sigma_{\lambda_{\perp}}$  is the r.m.s. fluctuation in the passive scalar across  $\lambda_{\perp}$ . The passive scalar parallel spectrum is the same as the Alfvén wave parallel spectrum given in equation (1.28), where  $\Lambda_{\parallel}$  is now to be interpreted as the lengthscale parallel to the local mean magnetic field across which the passive scalar fluctuation is  $\sigma_{\lambda_{\perp}}$ .

Mixing of the passive scalar is due to Alfvén waves. Slow wave mixing is negligible. This is because transverse velocity gradients are much larger than parallel ones in MHD turbulence. Thus

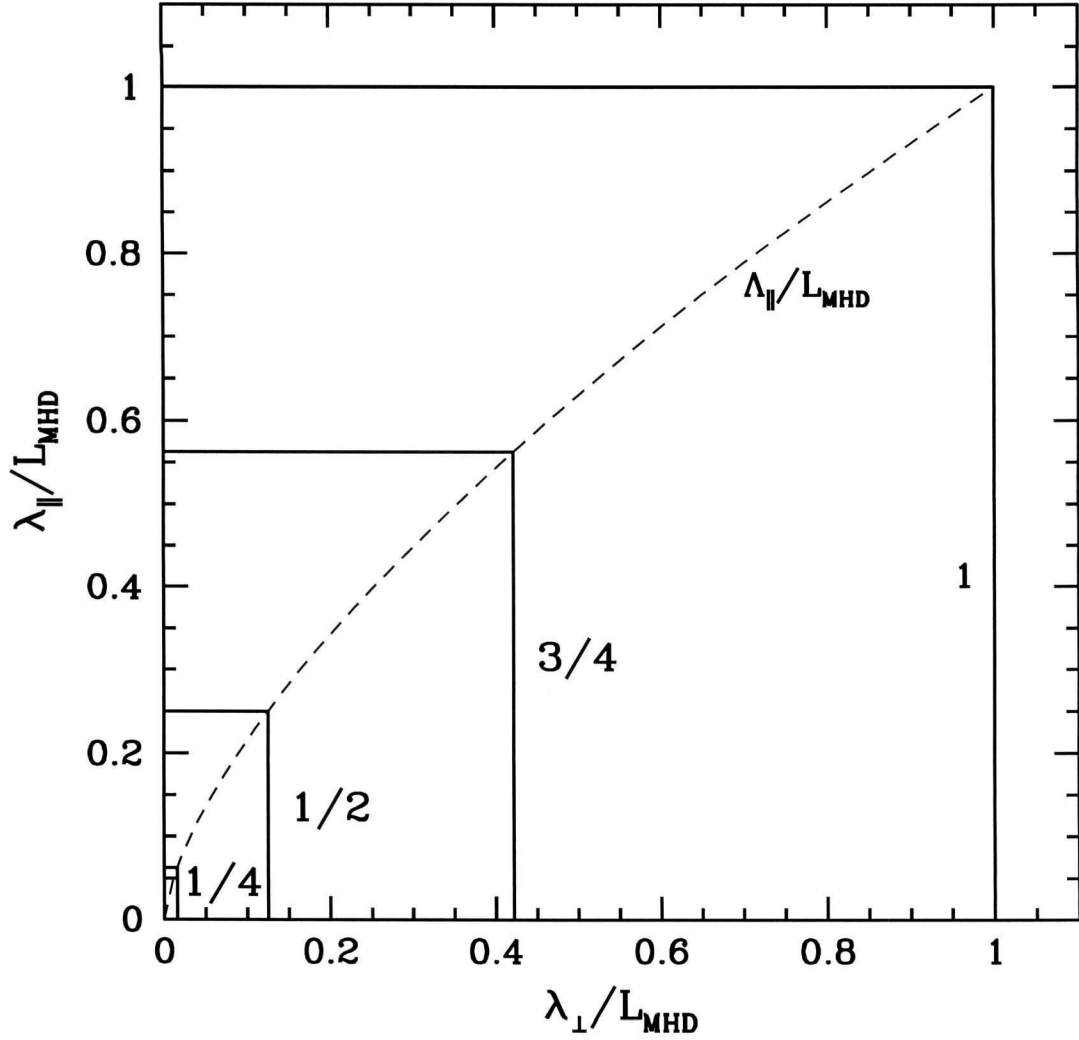


Figure 1.2: Three-Dimensional Spectrum

Contours of constant  $v_{\lambda_{\perp}, \lambda_{\parallel}}$  (eq. [1.29]), labelled by the value of  $v_{\lambda_{\perp}, \lambda_{\parallel}}/v_A$ . Along the  $\lambda_{\perp}$ -axis,  $v_{\lambda_{\perp}, 0}/v_A = (\lambda_{\perp}/L_{\text{MHD}})^{1/3}$ ; along the  $\lambda_{\parallel}$ -axis,  $v_{0, \lambda_{\parallel}}/v_A = (\lambda_{\parallel}/L_{\text{MHD}})^{1/2}$ .

Alfvén waves, whose velocity fluctuations are perpendicular to the magnetic field, are much more effective at mixing than slow waves, whose velocity fluctuations are nearly parallel to the magnetic field. The transverse cascade arises from the shuffling of fieldlines as Alfvén waves propagate through the fluid.

The transverse spectrum (eq. [1.30]) follows from the Kolmogorov-like hypothesis that the cascade rate of the “energy” in the scalar field is independent of lengthscale; i.e.,  $\sigma_{\lambda_{\perp}}^2/t_{\lambda_{\perp}}$  is constant, where  $t_{\lambda_{\perp}}$  is the passive scalar cascade time, which is assumed to be proportional to the cascade time of Alfvén waves. Comparing this with the constancy of the kinetic energy cascade rate,  $v_{\lambda_{\perp}}^2/t_{\lambda_{\perp}}$ , we conclude that  $\sigma_{\lambda_{\perp}} \propto v_{\lambda_{\perp}}$ , which implies equation (1.30). A similar argument holds for the cascade of a passive scalar in hydrodynamic turbulence (e.g., Tennekes and Lumley 1972).

The parallel cascade of a passive scalar is more subtle. It might appear that a passive scalar cannot cascade along fieldlines since, neglecting dissipation, both the scalar and the magnetic field are frozen to the fluid, and thus the scalar must be frozen to fieldlines. In that case there certainly could not be a parallel cascade. If the scalar were injected on large scales, then fluctuations with smaller wavelengths along the magnetic field would not be generated. However, dissipation cannot be neglected. It is an essential part of MHD turbulence, as it is of hydrodynamic turbulence. For example, the description of turbulent mixing in §1.2.2 depends crucially upon small scale dissipation.

Perhaps the best way to understand the parallel cascade is to consider mixing on the transverse lengthscale  $\lambda_{\perp}$  within two planes which are perpendicular to the local mean magnetic field, and which are separated by a parallel distance larger than  $\Lambda_{\parallel}$ . Velocity fluctuations within the two planes are statistically independent. This is evident because a bundle of fieldlines cannot be localized within a transverse distance  $\lambda_{\perp}$  over a parallel separation greater than  $\Lambda_{\parallel}$ . Even a pair of fluid elements, one in each plane, that are initially on the same fieldline are mixed into two regions with different values of passive scalar concentration. It follows that the parallel cascade of the passive scalar also obeys equation (1.28).

### Passive Scalar Spectrum Below Alfvén Wave Cutoff

A passive scalar cascade may extend below the transverse scale at which the MHD cascade is cut off. Mixing on these scales is driven by fluid motions at  $\lambda_{\text{cutoff}}$  which results in a scale-independent mixing time equal to the cascade time at  $\lambda_{\text{cutoff}}$ . This yields

$$\sigma_{\lambda_{\perp}} = \text{constant} , \quad \lambda_{\perp} < \lambda_{\text{cutoff}} . \quad (1.31)$$

A similar argument applies in hydrodynamic turbulence. Tennekes and Lumley (1972) call this regime in hydrodynamic turbulence the viscous-convective subrange.

### 1.2.4 Slow Wave Spectrum

The slow wave spectrum is the same as that of the Alfvén waves. It is given by equations (1.27) and (1.28), with  $v_{\lambda_{\perp}}$  referring to the velocity fluctuations of the slow waves. This is a consequence of the similar kinematics of slow waves and shear Alfvén waves and the fact that both are cascaded by shear Alfvén waves.

Slow waves obey the same linear wave equation as Alfvén waves, and to lowest nonlinear order they travel up and down the local mean magnetic field lines at the Alfvén speed just as Alfvén waves do. However, the dynamics of the MHD cascade is controlled by the Alfvén waves (Goldreich and Sridhar 1997, Maron and Goldreich 2001) because their velocity and magnetic field fluctuations are perpendicular to the local mean magnetic field, whereas those of the slow waves are nearly parallel to it. Since perpendicular gradients are much larger than parallel ones in the MHD cascade, Alfvén waves are much more effective at mixing than are slow waves. Hence, Alfvén waves cascade both themselves and slow waves, whereas slow waves cascade neither.<sup>6</sup>

The transverse mixing of the slow waves by Alfvén waves is analogous to the mixing of a passive scalar. As discussed in §1.2.3, a passive scalar assumes the same inertial range spectrum as that of the velocity field which is responsible for its mixing. Thus, equation (1.27) is also applicable to the velocity fluctuations of the slow waves.

Similarly, the parallel cascade of slow waves is analogous to the parallel cascade of a passive scalar. Since Alfvén waves cascade in the time they move a distance  $\Lambda_{\parallel}$ , slow waves separated by this distance are independently mixed. Thus, equation (1.28) also applies to slow waves. There is, however, a conceptual difference between the parallel cascades of the passive scalar and of the slow mode. In the absence of dissipation a passive scalar is frozen to fieldlines, whereas slow mode wave-packets travel along them at the Alfvén speed. A passive scalar has a parallel cascade because Alfvénic fluctuations are statistically independent within two transverse planes frozen in the fluid and separated by  $\Lambda_{\parallel}$ . The parallel cascade of slow waves occurs because two transverse planes separated by  $\Lambda_{\parallel}$  and travelling at the Alfvén speed in the same direction experience uncorrelated sequences of distortions suffered as a result of interactions with oppositely directed Alfvén waves. Nevertheless, these two requirements are both satisfied in the MHD cascade when the transverse planes are separated by a distance greater than  $\Lambda_{\parallel}$ , and so the passive scalar and the slow mode have the same parallel spectrum. Whereas passive scalar mixing is due to eddies, slow wave mixing may be thought of as due to travelling eddies, i.e., eddies which travel up and down the magnetic field at the Alfvén speed.

---

<sup>6</sup>We are assuming that Alfvén and slow waves have comparable strengths at a given lengthscale.

### 1.2.5 Numerical Simulations

Numerical simulations offer some support for the above description of incompressible MHD turbulence. Those by Cho and Vishniac (2000b) support both equations (1.27) and (1.28), and those by Müller and Biskamp (2000) support equation (1.27). However, although the simulations of Maron and Goldreich (2001) support equation (1.28), they yield  $v_{\lambda_{\perp}} \propto \lambda_{\perp}^{1/4}$  instead of equation (1.27). Because the simulations of Maron and Goldreich (2001) are stirred highly anisotropically, whereas those of Cho and Vishniac (2000b) and Müller and Biskamp (2000) are stirred isotropically, it is not clear whether these disparate results conflict. Maron and Goldreich (2001) speculate that the discrepancy between their spectrum and the scaling prediction of Goldreich and Sridhar (1995) results from intermittency. In any case, we expect that the physical picture of a critically balanced cascade, which underlies Goldreich and Sridhar’s description of MHD turbulence, remains valid. Even if the spectrum is proportional to  $\lambda_{\perp}^{1/4}$ , we expect that the results of this investigation—which assumes a spectrum proportional to  $\lambda_{\perp}^{1/3}$ —would not be significantly altered.

The simulations of Maron and Goldreich (2001) confirm that a passive scalar has the same transverse spectrum as that of Alfvén waves, although both are proportional to  $\lambda_{\perp}^{1/4}$ . They also indicate that the parallel cascade of a passive scalar conforms to equation (1.28).

Maron and Goldreich (2001) present results from simulations of the interaction between oppositely directed slow and Alfvén waves; the slow waves cascade whereas the Alfvén waves do not. They also compute the spectrum of slow waves in a simulation of MHD turbulence and find that both its transverse and longitudinal behavior matches that of the Alfvén wave spectrum.

### Kolmogorov Constants

Scaling arguments do not yield values for the Kolmogorov constants, the order-unity multiplicative constants of the spectrum. However, they can be obtained from simulations. We define them such that equation (1.27) remains valid; i.e., we take  $L_{\text{MHD}}$  to be the separation at which the r.m.s. velocity difference is equal to, or extrapolates to,  $v_A$ . Two Kolmogorov constants,  $M_{\parallel}$  and  $M_t$ , are needed in this chapter:

$$M_{\parallel} \equiv \frac{v_A}{v_{\lambda_{\perp}}} \frac{\lambda_{\perp}}{\Lambda_{\parallel}} \Rightarrow \Lambda_{\parallel} = M_{\parallel}^{-1} \lambda_{\perp}^{2/3} L_{\text{MHD}}^{1/3} \quad (1.32)$$

$$M_t \equiv \frac{v_A t_{\lambda_{\perp}}}{\Lambda_{\parallel}}. \quad (1.33)$$

In these definitions,  $\lambda_{\perp}$  and  $\Lambda_{\parallel}$  are the inverses of the wavenumbers transverse and parallel to the local mean magnetic field, and  $t_{\lambda_{\perp}}$  is the cascade time of waves with transverse wavenumber  $\lambda_{\perp}^{-1}$ .

From the numerical simulations of Maron and Goldreich (2001),

$$M_{\parallel} \simeq 3.4 \quad \text{and} \quad M_t \simeq 1.4. \quad (1.34)$$

Because these simulations yield a transverse spectrum which is proportional to  $\lambda_{\perp}^{1/4}$  instead of  $\lambda_{\perp}^{1/3}$ , the resulting Kolmogorov constants are not truly constant.

### 1.3 Compressible Turbulence: Overview

Our primary concern is interstellar scintillation, which is affected by electron density fluctuations on very small scales, typically  $10^8 - 10^{10}$  cm for diffractive scintillation. In the remainder of this chapter, we calculate the spectrum of density fluctuations which results from compressible turbulence in magnetized plasmas with parameters appropriate to the interstellar medium. Throughout, we consider plasmas that have more ions than neutrals, and that have  $1 \lesssim \beta < \infty$ , where  $\beta$  is the ratio of the thermal pressure to the mean magnetic pressure:  $\beta \equiv 8\pi p/B^2 = 2c_T^2/v_A^2$ . Here,  $c_T \equiv (p/\rho)^{1/2}$  is the isothermal sound speed,  $v_A$  is the Alfvén speed,  $p$  is the thermal pressure,  $B$  is the magnetic field strength, and  $\rho$  is the mass density.<sup>7</sup> The incompressible limit corresponds to  $\beta = \infty$ .

On the lengthscales that we consider, compressible MHD is a good approximation for the dynamics of the ionized interstellar medium. Kinetic effects, where important, may be accounted for by simple modifications to the MHD equations. Therefore, we turn our attention to turbulence in compressible MHD.

The turbulent velocity spectrum in compressible MHD is approximately the same as the turbulent velocity spectrum in incompressible MHD, because the Alfvén mode remains incompressible in a compressible medium, and the slow mode is only slightly compressible. Thus, the velocity spectrum for both of these modes is given by equations (1.27) and (1.28). The Appendix summarizes the properties of the relevant modes in compressible MHD.

There are two additional modes in compressible MHD which are not present in incompressible MHD. One of these is the fast mode. However, as long as  $\beta \gtrsim$  a few, the fast mode is essentially a sound wave. Its phase speed is larger than the phase speed of either the Alfvén mode or the slow mode, and so the fast mode does not couple to them. Thus, we ignore the fast mode. An analogous approximation is often made in subsonic hydrodynamic turbulence, where sound waves have little influence on the turbulent cascade. Some support for our neglect of the fast mode is provided by numerical simulations. Balsara and Pouquet (1999) show that in simulations of turbulence with Mach number of order unity, the compressible component of the velocity is significantly smaller than the solenoidal component; they argue that this is because shocks dissipate much of the irrotational

<sup>7</sup>We briefly discuss plasmas with  $\beta < 1$  in §1.11.

component of the velocity.

The second mode that is present only in compressible MHD is the entropy mode. When turbulent motions are adiabatic, the entropy mode is a zero-frequency mode with unperturbed pressure, and with density perturbation offset by temperature perturbation (see Appendix). In hydrodynamics, simple scaling arguments show that the entropy mode does not affect the dynamics of the fluid—i.e., the fluid obeys the incompressible equations of motion—provided that fluid motions are subsonic and that density fluctuations are smaller than the mean density; these arguments carry over directly to MHD (e.g., Higdon 1986, and references therein). Furthermore, since the entropy of any fluid element is conserved in the inertial range of adiabatic turbulence, the mixing of the entropy mode is identical to the mixing of a passive scalar (see eq. [1.30]), yielding the transverse spectrum

$$s_{\lambda_{\perp}} \propto \lambda_{\perp}^{1/3}, \quad (1.35)$$

where  $s_{\lambda_{\perp}}$  is the r.m.s. entropy fluctuation across  $\lambda_{\perp}$ . The parallel spectrum is given by equation (1.28). Analogously, in hydrodynamic turbulence the effect of the entropy mode on turbulent motions can often be neglected, and the entropy mode is mixed as a passive scalar (Monin and Yaglom 1971).

Based on the above discussion, there are two sources of density fluctuations on small scales: the slow mode and the entropy mode. Since the slow mode density perturbation is proportional to its velocity perturbation, and since the entropy mode density perturbation is proportional to its entropy perturbation, both yield a Kolmogorov spectrum of density perturbations:

$$n_{\lambda_{\perp}} \propto \lambda_{\perp}^{1/3}. \quad (1.36)$$

In the remainder of this chapter, we investigate the density spectrum in more detail. We calculate the density spectrum on diffractive lengthscales for given values of the number density,  $n$ , and outer scale,  $L_{\text{out}}$ . Typically, in regions of the interstellar medium which are relevant for scintillation,  $1 \text{ cm}^{-3} < n < 100 \text{ cm}^{-3}$ . Values of  $L_{\text{out}}$  are more uncertain, though it is likely that  $L_{\text{out}}$  is typically within a few orders of magnitude of 1 pc. It is also plausible that the value of  $L_{\text{out}}$  is related to that of  $n$ . In a future paper, we discuss in much more detail the values of these parameters in turbulent regions of the ionized interstellar medium, e.g., in supernova shocks, HII regions, and stellar winds.

A naive guess for the resulting density fluctuation at the lengthscale  $\lambda_{\perp}$  is  $n_{\lambda_{\perp}} = n(\lambda_{\perp}/L_{\text{out}})^{1/3}$ , which we refer to as the fiducial spectrum. However, there are a number of physical effects which suppress the small-scale density spectrum in the interstellar medium relative to the fiducial spectrum.

When considering scintillation observations, it is the transverse—not parallel—lengthscale which is relevant. Each line of sight crosses regions with different orientations of the local mean magnetic field. The observational effects of the parallel lengthscale are washed out if the orientation varies by an angle greater than a tiny ratio:  $\lambda_{\perp}/\Lambda_{\parallel}$  at the diffractive scale. Since the variation in angle due

Table 1.1: Summary of Lengthscales

Symbol	Description
$\lambda_{\perp}$	lengthscale transverse to the mean magnetic field; it is comparable to the observed lengthscale.
$\lambda_{\parallel}$	lengthscale parallel to the mean magnetic field
$\Lambda_{\parallel}$	parallel size of an eddy; it is a function of $\lambda_{\perp}$ (eq. [1.28]).
$L_{\text{out}}$	$\lambda_{\perp} = L_{\text{out}}$ at the outer scale
$L_{\text{MHD}}$	$\lambda_{\perp} = L_{\text{MHD}}$ at the MHD scale
$L_{\text{cool}}$	$\lambda_{\perp} = L_{\text{cool}}$ at the cooling scale
$L_{\text{H}}$	$\lambda_{\perp} = L_{\text{H}}$ at the collisionless scale of hydrogen atoms
$L_{\text{He}}$	$\lambda_{\perp} = L_{\text{He}}$ at the collisionless scale of helium atoms
$L_{\text{mfp}}$	mean free path of protons and of electrons
$L_{\text{ed}}$	$\Lambda_{\parallel} = L_{\text{ed}}$ at the electron diffusion scale
$L_{\text{eq}}$	$\Lambda_{\parallel} = L_{\text{eq}}$ at the electron-proton equilibration scale
$L_{\text{pd}}$	$\Lambda_{\parallel} = L_{\text{pd}}$ at the proton diffusion scale
$L_{\text{pd}}^{(\perp)}$	$\lambda_{\perp} = L_{\text{pd}}^{(\perp)}$ at the proton diffusion scale
$L_{\text{p,gyr}}$	$\lambda_{\perp} = L_{\text{p,gyr}}$ at the proton gyro scale

to eddies on scales larger than the diffractive scale is  $\lambda_{\perp}/\Lambda_{\parallel} \propto \lambda_{\perp}^{1/3}$ , it increases with scale, so these eddies render the parallel lengthscale unobservable. As a result, we frequently refer to the transverse lengthscale as, simply, the lengthscale.

Because of the multitude of special lengthscales involved, we organize the discussion by decreasing lengthscale. We begin at the outer scale, and proceed down to the smallest scales relevant to interstellar scintillation, while considering the effects of the Alfvén mode, the slow mode, and the entropy mode simultaneously. Since most of the relevant lengthscales in the interstellar medium have a similar dependence on the background density—they decrease with increasing density—the ordering of lengthscales is fairly universal. The lengthscales which we consider are the outer scale, the MHD scale, the cooling scale, the collisionless scale of the neutrals, the collisionless scale of the ions, and the proton gyro scale. We conclude with a summary of the most important effects. Table 1.3 lists the lengthscales that are used in this chapter.

## 1.4 The Outer Scale and the MHD Scale

As a model for the excitation of the turbulence, we consider plasma which is stirred on an outer scale  $L_{\text{out}}$  with velocity fluctuations that are of order the sound speed:  $v_{L_{\text{out}}} \sim c_s$ . The generalization from this case of Mach 1 turbulence to subsonic turbulence with arbitrary Mach number  $\mathcal{M} < 1$  is trivial:  $L_{\text{out}}$  would be interpreted as an effective outer scale at which velocity fluctuations extrapolate to  $c_s$ . However, we focus on the Mach 1 case because it is probably the most relevant for interstellar scintillation.

If, initially, the strength of the magnetic field is negligible, then random fieldline stretching amplifies the mean field (Cho and Vishniac 2000a). It is uncertain both how quickly the magnetic field is amplified, and whether its energy density is amplified until it approaches equipartition with the turbulent kinetic energy density. If it does reach equipartition within a few outer-scale crossing times, then  $\beta \sim 1$  would be appropriate for Mach 1 turbulence. Recall that  $\beta$  is the ratio of thermal pressure to magnetic pressure, or equivalently,  $\beta = 2c_T^2/v_A^2$ . We generally assume that the mean magnetic field can approach equipartition with the gas pressure, so we think of  $\beta$  as close to but a little larger than unity, although we leave its exact value unspecified.

Provided  $\beta$  is larger than unity and  $\mathcal{M} \sim 1$  on scale  $L_{\text{out}}$ , the turbulent kinetic energy dominates the mean magnetic energy on scales just below  $L_{\text{out}}$ . Thus the cascade is hydrodynamic on these lengthscales, and the velocity fluctuations are given by Kolmogorov's isotropic scaling:  $v_{\lambda_{\perp}} \sim c_s(\lambda_{\perp}/L_{\text{out}})^{1/3}$ .

The kinetic energy density decreases towards smaller scales. At a critical scale, which we denote  $L_{\text{MHD}}$ , the kinetic energy density is sufficiently small that it is comparable to the mean magnetic energy density:  $v_{L_{\text{MHD}}}^2 \sim v_A^2$ , which implies that

$$L_{\text{MHD}} \sim L_{\text{out}}\beta^{-3/2} . \quad (1.37)$$

Below this scale, the turbulent kinetic energy density is smaller than the magnetic energy density, and the theory of compressible MHD turbulence is applicable. Note that the effects of large-scale velocity fields can be neglected when considering fluctuations on smaller scales, because a large-scale velocity field can be eliminated by a Galilean transformation. However, since large-scale magnetic fields cannot be transformed away, they affect the dynamics of small-scale eddies.

Hydrodynamic turbulent motions on scales slightly larger than  $L_{\text{MHD}}$  have speeds  $\sim v_A$ . Thus they couple to, and efficiently excite, Alfvén waves and slow waves whose phase velocities  $\omega/k \approx v_A(k_z/k)$  are of comparable magnitude. Provided  $\beta > 1$  and  $\mathcal{M} \leq 1$ , fast waves, which have  $\omega/k \sim c_s > v_A$ , are weakly excited at  $L_{\text{MHD}}$ . In what follows, we neglect fast waves.

Alfvén waves excited at  $L_{\text{MHD}}$  cascade to smaller scales, and these cascading Alfvén waves in turn cascade slow waves. The spectra of both of these cascades are given by equations (1.27) and (1.28), so that

$$v_{\lambda_{\perp}} \sim c_s \left( \frac{\lambda_{\perp}}{L_{\text{out}}} \right)^{1/3} \quad (1.38)$$

for both modes, even on scales smaller than  $L_{\text{MHD}}$ .

We have not yet discussed density fluctuations on the scales which have been considered in this section. It is more convenient to do so in the following section.

## 1.5 The Cooling Scale

On the lengthscales in the interstellar medium that we have considered thus far, the radiative cooling time is shorter than the eddy turnover time.<sup>8</sup> Consequently, in photoionized regions, turbulence on these lengthscales is expected to be isothermal (Sridhar 1998; Goldreich 1998; Higdon and Conley 1998). This has only a marginal effect on the turbulent dynamics described in the previous section, because isothermal Alfvén waves are identical to adiabatic Alfvén waves, and isothermal slow waves are only slightly different from adiabatic slow waves. However, the entropy mode is rapidly damped in isothermal turbulence. As a consequence, small-scale density fluctuations may be significantly suppressed. There are two possible solutions to this “cooling catastrophe”: either (i) the outer scale is extremely small, small enough that the turbulence at the outer scale is nearly adiabatic; or (ii) there are significant density fluctuations associated with the slow mode. However, in the latter case, the mean magnetic field must be amplified almost to equipartition with the gas pressure, so that  $\beta \sim 1$ . Either of these two solutions would place stringent constraints on the nature of the turbulence which is responsible for observed density fluctuations. In the following, we consider the cooling scale in more detail.

There is a critical scale for the turbulence, which we call the cooling scale,  $L_{\text{cool}}$ . Above this scale the turbulence is isothermal, and below it the turbulence is adiabatic. We assume that  $L_{\text{cool}} < L_{\text{MHD}}$  throughout this chapter, except in §1.5.2 where we consider the case in which this inequality is reversed. The cooling scale is where the eddy turnover time,  $\lambda_{\perp}/v_{\lambda_{\perp}}$ , is equal to the cooling time,  $t_{\text{cool}}$ ; i.e., with  $v_{\lambda_{\perp}} \sim c_s(\lambda_{\perp}/L_{\text{out}})^{1/3}$ ,

$$\frac{L_{\text{cool}}}{L_{\text{out}}} \sim \left( \frac{c_s t_{\text{cool}}}{L_{\text{out}}} \right)^{3/2}. \quad (1.39)$$

As we will discuss in detail in a future paper, most plausible astrophysical sources of interstellar scintillation have  $c_s t_{\text{cool}} \lesssim L_{\text{out}}$ , and thus  $L_{\text{cool}} \lesssim L_{\text{out}}$ . In general, the kinetic power per unit mass that is dissipated in Mach 1 turbulence is  $\sim c_s^2/t_{L_{\text{out}}} \sim c_s^3/L_{\text{out}}$ , where  $t_{L_{\text{out}}}$  is the eddy turnover time at the outer scale. The thermal power per unit mass required to keep the gas hot is  $\sim c_s^2/t_{\text{cool}}$ . Hence, only if the energy that goes into turbulent motions is as large as the total energy that goes into heating can the outer scale be as small as the cooling scale. Nonetheless, in plasmas that are thermally unstable, and in isothermal shocks (assuming that the outer scale is comparable to the scale across which the density doubles), the two powers are comparable, and the cooling scale is comparable to the outer scale.

As an example, we consider an HII region. Photoionized plasma is thermally stable. Heating is primarily due to photoionizing photons, and cooling is primarily due to electron impact excitation

---

<sup>8</sup>For definiteness, we consider plasma that is thermally stable; deviations of the temperature from its equilibrium value decay in a cooling time,  $t_{\text{cool}}$ .

of metal line transitions (e.g., Spitzer 1978).<sup>9</sup> A characteristic temperature for plasma photoionized by hot stars is  $T \sim 8,000\text{K}$ , which implies that the speed of sound is  $c_s \sim 10 \text{ km/sec}$ . The cooling time is  $t_{\text{cool}} \sim 20,000(\text{cm}^{-3}/n)$  years, where  $n$  is the number density of electrons. Therefore,

$$c_s t_{\text{cool}} \sim 0.2 \left( \frac{\text{cm}^{-3}}{n} \right) \text{ pc} . \quad (1.40)$$

A plausible value for  $L_{\text{out}}$  might be the radius an HII region (the Strömngren radius), which is  $\sim 70(\text{cm}^{-3}/n)^{2/3} \text{ pc}$  (Spitzer 1978). Therefore, with typical values of  $n$  in HII regions ( $1 \text{ cm}^{-3} < n < 100 \text{ cm}^{-3}$ ),  $L_{\text{out}}$  is significantly larger than  $c_s t_{\text{cool}}$ , and so the cooling scale is significantly smaller than the outer scale.

The fact that the turbulence is isothermal on large scales has important implications. Had cooling been ignored, i.e., had it been implicitly assumed that the cooling time is infinite, then one would have calculated the density spectrum as follows: there should be density fluctuations of order unity on the outer scale, implying excitation of entropy modes on the outer scale which are passively mixed by the Alfvénic turbulence to small scales. This would yield the fiducial density spectrum,  $n_{\lambda_{\perp}} \simeq n(\lambda_{\perp}/L_{\text{out}})^{1/3}$ .

However, since the turbulence is isothermal on large scales, the above calculation is incorrect. The entropy mode is not passively mixed on these scales, since it is damped by cooling before it can be mixed. In the following, we consider separately two cases: first, the low- $\beta$  case ( $\beta < L_{\text{out}}/c_s t_{\text{cool}}$ ), and then the high- $\beta$  case ( $\beta > L_{\text{out}}/c_s t_{\text{cool}}$ ). In each case, we show that the small-scale density fluctuations are substantially smaller than those predicted by the fiducial spectrum unless a relatively stringent condition holds: either  $\beta \sim 1$  or  $L_{\text{out}} \sim c_s t_{\text{cool}}$ .

### 1.5.1 Density Fluctuations Below the Cooling Scale: $1 < \beta < L_{\text{out}}/c_s t_{\text{cool}}$

With regards to interstellar scintillation, the crucial difference between high- $\beta$  and low- $\beta$  turbulence lies in the compressibility of the slow mode. Since the sum of thermal pressure and magnetic pressure vanishes for the slow mode, the mode's density perturbation satisfies  $n_{\lambda_{\perp}}/n \sim p_{\lambda_{\perp}}/p \sim \beta^{-1} B_{\lambda_{\perp}}/B \sim \beta^{-1} v_{\lambda_{\perp}}/v_A \sim \beta^{-1/2} v_{\lambda_{\perp}}/c_s$  (see Appendix). So, assuming that the energy in slow waves is comparable to that in Alfvén waves,

$$\frac{n_{\lambda_{\perp}}}{n} \sim \frac{1}{\sqrt{\beta}} \left( \frac{\lambda_{\perp}}{L_{\text{out}}} \right)^{1/3} \quad \lambda_{\perp} < L_{\text{MHD}} , \quad (1.41)$$

<sup>9</sup>In this case, there is another lengthscale, the photoionization scale, which we do not consider because its effects are unimportant for scintillations. This is the scale at which the eddy turnover time is comparable to the recombination time. It is slightly larger than the cooling scale because the recombination time is approximately five times larger than the cooling time (Spitzer 1978). On scales larger than the photoionization scale, the turbulence is in photoionization equilibrium, whereas on scales smaller than this, the ionization fraction of a fluid element is conserved. Nonetheless, the temperature of the gas is only weakly dependent on ionization fraction: metal-line cooling by free electrons is exponentially dependent on temperature, and thus acts as a thermostat which is only slightly affected by the ion or neutral density. Thus, the photoionization lengthscale does not play an important role in the density spectrum.

from the slow mode, both above and below the cooling scale. Thus, slow waves can produce density fluctuations which are not much smaller than the fiducial spectrum if  $\beta$  is not much larger than unity. Comparing with equation (1.47) below, the contribution of the slow mode to the density fluctuations at  $L_{\text{cool}}$  exceeds the contribution from Reynolds stresses provided  $\beta < L_{\text{out}}/c_s t_{\text{cool}}$ .

The compressibility of the slow mode also yields density fluctuations associated with the entropy mode. The reason is as follows. Entropy fluctuations are associated with isothermal compressible waves. Those due to isothermal slow modes are passively mixed by Alfvén waves. Mixing due to Alfvén waves with wavelengths smaller than the cooling scale takes place in less than the cooling time. It produces a spectrum of entropy modes for  $\lambda_{\perp} < L_{\text{cool}}$  that gives rise to a density spectrum similar to the one given in equation (1.41). Nonetheless, there is some damping of entropy fluctuations when they are mixed from scales larger than the cooling scale to scales smaller than the cooling scale. We expect that the damping is of order unity. Since, as we show in the following section, the damping of the slow mode is not very large, we expect that the amplitudes of the slow and entropy modes below the cooling scale are roughly comparable. In this chapter, however, we do not quantify the amount of damping of the entropy mode more precisely, because it is a difficult calculation. We have attempted to quantify this damping by performing numerical simulations. However, the limited dynamical range made the interpretation of the results difficult. Nevertheless, the relative amplitude of slow and entropy waves on small scales does not appear to be observationally important; as we show in §1.7.3 below, both slow and entropy waves damp at the same scale.

### Slow Mode Damping at the Cooling Scale

Although there is negligible damping of the slow mode on lengthscales that are either much larger or much smaller than the cooling scale, there is some damping on lengthscales that are comparable to the cooling scale. As we show in this section, the damping of the slow wave cascade is small, because the slow mode is not very compressible. In the limit that  $\beta \rightarrow \infty$ , the slow mode is incompressible, and the damping disappears. In the following, we calculate the damping to first order in  $1/\beta$ .

First, we calculate the damping rate of a slow wave of a fixed wavenumber. The damping rate is obtained by substituting  $\bar{c}$  (given in the Appendix, eq. [1.95]) into the slow mode dispersion relation (eq. [1.99]); noting that  $c_T^2 \equiv p/\rho = \beta v_A^2/2$ , this gives, to lowest order in  $1/\beta$ ,

$$\frac{\omega_i}{v_A k_{\parallel}} = \frac{-v_A k_{\parallel} t_{\text{cool}}}{\beta[1 + (5v_A k_{\parallel} t_{\text{cool}}/2)^2]}, \quad (1.42)$$

where  $\omega_i$  is the imaginary part of  $\omega$ , and  $k_z$  from the Appendix is here relabelled  $k_{\parallel}$ . Only on lengthscales where  $v_A k_{\parallel} t_{\text{cool}} \sim 1$  is this ratio non-negligible.

To obtain the total decrement in the amplitude of the slow mode through the cooling scale, we solve a kinetic equation obtained by balancing the slow mode  $k$ -space energy flux with the loss-rate

of slow mode  $k$ -space energy density due to damping; i.e.,

$$\frac{d}{dk} \frac{v_{\lambda_{\perp}}^2}{t_{\lambda_{\perp}}} = 2\omega_i \frac{v_{\lambda_{\perp}}^2}{k}, \quad (1.43)$$

where  $\lambda_{\perp}^{-1} \equiv k_{\perp}$  is the transverse wavenumber,  $t_{\lambda_{\perp}}$  is the cascade time of a slow wave with this wavenumber, and  $v_{\lambda_{\perp}}$  is the velocity perturbation of the slow mode; since  $k_{\perp} \simeq k$ , we drop the  $\perp$  subscript on  $k$ . We rewrite the kinetic equation as follows:

$$\frac{d}{d \ln k} \ln \frac{v_{\lambda_{\perp}}^2}{t_{\lambda_{\perp}}} = 2\omega_i t_{\lambda_{\perp}} = 2M_t \frac{\omega_i}{v_A k_{\parallel}}, \quad (1.44)$$

where  $M_t \equiv v_A k_{\parallel} t_{\lambda_{\perp}} \simeq 1.4$  is a Kolmogorov constant (see §1.2.5). Substituting equation (1.42) into equation (1.44) and integrating, using  $k_{\parallel} \propto k^{2/3}$  (eq. [1.28]) and  $t_{\lambda_{\perp}} \propto k^{-2/3}$ , yields the net damping through the cooling scale:

$$\begin{aligned} \frac{[v_{\lambda_{\perp}}/\lambda_{\perp}^{1/3}]|_{\lambda_{\perp} \ll L_{\text{cool}}}}{[v_{\lambda_{\perp}}/\lambda_{\perp}^{1/3}]|_{\lambda_{\perp} \gg L_{\text{cool}}}} &= \exp\left(-\frac{M_t}{\beta} \int_0^{\infty} \frac{v_A k_{\parallel} t_{\text{cool}}}{1 + (5v_A k_{\parallel} t_{\text{cool}}/2)^2} \frac{dk}{k}\right) \\ &= \exp\left(-\frac{3\pi M_t}{10\beta}\right) \\ &\simeq 1 - 1.3/\beta, \end{aligned} \quad (1.45)$$

to lowest order in  $1/\beta$ . Thus for  $\beta$  slightly larger than unity, slow mode damping can be ignored.

### 1.5.2 Density Fluctuations Below the Cooling Scale: $\beta > L_{\text{out}}/c_s t_{\text{cool}} > 1$

In this subsection only, we assume that  $\beta > L_{\text{out}}/c_s t_{\text{cool}}$ , which implies  $L_{\text{MHD}} < L_{\text{cool}}$ . In this case, the isothermal hydrodynamic turbulent cascade extends from the outer scale down to the cooling scale. Because the entropy mode is rapidly damped under isothermal conditions and hydrodynamic turbulence is incompressible to order  $v_{\lambda_{\perp}}/c_s$ , to this order there are no density fluctuations on lengthscales larger than  $L_{\text{cool}}$ . However, pressure fluctuations due to Reynolds stresses,  $p_{\lambda_{\perp}} \sim \rho v_{\lambda_{\perp}}^2$ , create second order density and entropy fluctuations,

$$\frac{n_{\lambda_{\perp}}}{n} = \frac{p_{\lambda_{\perp}}}{p} = s_{\lambda_{\perp}} \sim \left(\frac{v_{\lambda_{\perp}}}{c_s}\right)^2, \quad L_{\text{cool}} < \lambda_{\perp} < L_{\text{out}}. \quad (1.46)$$

These entropy fluctuations couple to the entropy mode at the cooling scale. On scales below the cooling scale, the entropy mode is mixed as a passive scalar yielding

$$\frac{n_{\lambda_{\perp}}}{n} \sim \frac{v_{L_{\text{cool}}}^2}{c_s^2} \left(\frac{\lambda_{\perp}}{L_{\text{cool}}}\right)^{1/3} \sim \left(\frac{L_{\text{cool}}}{L_{\text{out}}}\right)^{2/3} \left(\frac{\lambda_{\perp}}{L_{\text{cool}}}\right)^{1/3} \sim \left(\frac{c_s t_{\text{cool}}}{L_{\text{out}}}\right)^{1/2} \left(\frac{\lambda_{\perp}}{L_{\text{out}}}\right)^{1/3}, \quad \lambda_{\perp} < L_{\text{cool}}. \quad (1.47)$$

Hydrodynamic turbulence mixes the entropy mode down to  $L_{\text{MHD}}$ . At this scale, the hydrodynamic motions turn into Alfvén and slow waves, so the entropy mode continues to be mixed below  $L_{\text{MHD}}$ , and equation (1.47) remains valid. Comparing with equation (1.41), the density fluctuations associated with the entropy mode exceed those associated with the slow mode when  $\beta > L_{\text{out}}/c_s t_{\text{cool}}$ .

The entropy mode’s density spectrum (eq. [1.47]) is smaller than the fiducial spectrum by the small factor  $(c_s t_{\text{cool}}/L_{\text{out}})^{1/2}$ . As will be seen in a future paper, it yields density fluctuations that are too small to explain much of the observed interstellar scintillation for most plausible values of  $L_{\text{out}}$ , such as those given by Strömgren radii of HII regions. There are two alternatives; either  $L_{\text{out}}$  is not much larger than  $c_s t_{\text{cool}}$ , or  $\beta < L_{\text{out}}/c_s t_{\text{cool}}$ .

## 1.6 The Collisionless Scale of the Neutrals

In the remainder of this chapter, we consider lengthscales which are comparable to, or smaller than, the mean free paths of the various particles; thus, kinetic effects must be considered.

In this section, we calculate the damping of the turbulence by neutrals. We assume that the neutral density is smaller than the electron density, i.e.,  $n_N \lesssim n$ , and that most of the ions are protons. The neutral particles which we consider are hydrogen atoms and helium atoms. The relevant lengthscales are the hydrogen and helium mean free paths for collisions with protons:  $L_{\text{H}} = 5 \times 10^{13} (\text{cm}^{-3}/n)$  cm and  $L_{\text{He}} = 1.5 \times 10^{15} (\text{cm}^{-3}/n)$  cm (Banks 1966). The hydrogen mean free path is significantly smaller than the helium mean free path because its collisions with protons are due to resonant charge exchange.

There are two main results for this section.

- (i) Only if the neutral fraction is sufficiently small (eq. [1.75], below) can the cascade survive on lengthscales smaller than  $L_{\text{H}}$ . If the neutral fraction does not satisfy this condition, then all three modes—Alfvén, slow, and entropy—are damped at the same lengthscale.
- (ii) Regions where the cascade does not survive contribute to an excess of density fluctuations on large scales. This might explain observations which detect an excess of power in large-scale density fluctuations.

The organization of the calculation is as follows: first, the change in wave frequency due to neutrals is calculated. Second, we consider the effect of the frequency change on the cascade. Third, we consider the cases in which the neutrals are hydrogen atoms and in which they are helium atoms. Although helium atoms have a larger mean free path, we consider them after neutral hydrogen atoms because they are of lesser importance. Finally, we consider regions where neutral damping terminates the cascade.

A similar, though less detailed calculation is performed by Goldreich and Sridhar (1995) for the case in which the neutrals are hydrogen atoms.

### 1.6.1 Frequency Change

Consider an incompressible wave, either an Alfvén wave or a slow wave in the incompressible limit. Although the slow wave is, in fact, slightly compressible, this does not have a large effect on the final result. We calculate the frequency change of an incompressible wave with fixed  $\mathbf{k}$ :  $k_{\parallel}$  along the mean magnetic field and  $k_{\perp}$  transverse to the mean magnetic field, where  $k_{\parallel} \ll k_{\perp} \simeq k$ .

We define  $\mathbf{v}$  to be the mean velocity of the protons averaged over the proton distribution function. Thus  $\mathbf{v}$  satisfies the equation of motion for the Alfvén wave or for the slow wave derived in the Appendix. We then calculate the force that these protons exert on the neutrals. Since this force is the same as the force of the neutrals on the protons, inserting it into the equation of motion for the protons yields the change in frequency.

We denote the perturbed distribution function for the neutrals, i.e., perturbed to first-order in  $\mathbf{v}_N$ , after being Fourier-transformed in space and time, by  $\delta f_N(\mathbf{k}, \omega, \mathbf{v}_N)$ , where  $\mathbf{v}_N$  is the velocity of the neutrals. The evolution of the neutrals is determined by the Boltzmann equation:

$$-i\omega \delta f_N + i(\mathbf{k} \cdot \mathbf{v}_N) \delta f_N = \mathcal{C} , \quad (1.48)$$

where  $\mathcal{C}$  is the Fourier-transformed, perturbed, collision integral of the neutrals with the protons. Neutral-neutral collisions are negligible relative to neutral-proton collisions. The collision integral is simplified by making the approximation that, on the timescale that a neutral collides with protons,  $\delta f_N$  is driven towards a Maxwellian with mean velocity  $\mathbf{v}$ :

$$\mathcal{C} = \nu_{N,p} \left[ \frac{(\mathbf{v} \cdot \mathbf{v}_N)}{T/m_N} \frac{n_N \exp(-m_N v_N^2/2T)}{(2\pi T/m_N)^{3/2}} - \delta f_N \right] , \quad (1.49)$$

where the first term in the square brackets is generated by expanding a Maxwellian distribution function with mean velocity  $\mathbf{v}$  to linear order in  $\mathbf{v}$  and retaining only the perturbation, and  $\nu_{N,p}$  is the frequency with which a given neutral atom collides with protons. With the above approximation to the collision integral, the solution to the Boltzmann equation reads

$$\delta f_N = \frac{(\mathbf{v} \cdot \mathbf{v}_N)}{T/m_N} \frac{n_N \exp(-m_N v_N^2/2T)}{(2\pi T/m_N)^{3/2}} \frac{\nu_{N,p}}{\nu_{N,p} - i\omega + i\mathbf{k} \cdot \mathbf{v}_N} . \quad (1.50)$$

Next we verify that the perturbed neutral number density vanishes,

$$\int \delta f_N d^3 \mathbf{v}_N = \frac{n_N v \nu_{N,p}}{(2\pi)^{3/2} (T/m_N)^{5/2}}$$

$$\begin{aligned} & \times \left[ \int dv_{N\parallel} v_{N\parallel} \exp(-m_N v_{N\parallel}^2 / 2T) \right] \\ & \times \left[ \int d^2 \mathbf{v}_{N\perp} \frac{\exp(-m_N v_{N\perp}^2 / 2T)}{\nu_{N,p} - i\omega + i\mathbf{k} \cdot \mathbf{v}_{N\perp}} \right] \end{aligned} \quad (1.51)$$

$$= 0, \quad (1.52)$$

since the first square-bracketed integral vanishes by antisymmetry. For the purpose of evaluating the above integrals, we use  $\perp$  and  $\parallel$  for the perpendicular and parallel projections of  $\mathbf{v}_N$  relative to  $\mathbf{v}$ , and not relative to the magnetic field as in the rest of this chapter; i.e.,  $\mathbf{v}_{N\parallel} \equiv (\mathbf{v} \cdot \mathbf{v}_N) \mathbf{v} / v^2$  and  $\mathbf{v}_{N\perp} \equiv \mathbf{v}_N - \mathbf{v}_{N\parallel}$ . We also use the incompressibility relation  $\mathbf{k} \cdot \mathbf{v} = 0$ , which implies that  $\mathbf{k} \cdot \mathbf{v}_{N\parallel} = 0$ .

With the neutral distribution function given by equation (1.50), the force per unit volume of the protons on the neutrals may be calculated as

$$\mathbf{F} = m_N \int \mathbf{v}_N (-i\omega \delta f_N + i(\mathbf{k} \cdot \mathbf{v}_N) \delta f_N) d^3 \mathbf{v}_N \quad (1.53)$$

$$\begin{aligned} &= \frac{m_N n_N \mathbf{v} \nu_{N,p}}{(2\pi)^{3/2} (T/m_N)^{5/2}} \\ & \times \left[ \int dv_{N\parallel} v_{N\parallel}^2 \exp(-m_N v_{N\parallel}^2 / 2T) \right] \\ & \times \left[ \int d^2 \mathbf{v}_{N\perp} \frac{(-i\omega + i\mathbf{k} \cdot \mathbf{v}_{N\perp}) \exp(-m_N v_{N\perp}^2 / 2T)}{\nu_{N,p} - i\omega + i\mathbf{k} \cdot \mathbf{v}_{N\perp}} \right] \end{aligned} \quad (1.54)$$

$$\begin{aligned} &= \frac{m_N n_N \mathbf{v} \nu_{N,p}}{(2\pi T/m_N)^{1/2}} \\ & \times \int_{-\infty}^{\infty} ds \frac{(-i\omega + iks) \exp(-m_N s^2 / 2T)}{\nu_{N,p} - i\omega + iks} \end{aligned} \quad (1.55)$$

$$= \frac{m_N n_N \mathbf{v} \nu_{N,p}}{\pi^{1/2} \Pi_1} \int_{-\infty}^{\infty} \frac{it}{1 + it} \exp[-(t/\Pi_1 + \Pi_2/\Pi_1)^2] dt. \quad (1.56)$$

The second equality follows after replacing the overall multiplicative  $\mathbf{v}_N (= \mathbf{v}_{N\parallel} + \mathbf{v}_{N\perp})$  by  $\mathbf{v}_{N\parallel}$ , because the  $\mathbf{v}_{N\perp}$  term vanishes by antisymmetry of the integral over  $v_{N\parallel}$ . In the second equality, the first bracketed integral is equal to  $(2\pi)^{1/2} (T/m_N)^{3/2}$ . The second bracketed integral is a double integral; the integral over the component of  $\mathbf{v}_{N\perp}$  which is perpendicular to  $\mathbf{k}$  is equal to  $(2\pi T/m_N)^{1/2}$ . The remaining integral is over the component of  $\mathbf{v}_{N\perp}$  which is parallel to  $\mathbf{k}$ ; we label this component  $s$  in the third equality. Finally, the fourth equality follows from the change of variables  $t \equiv (ks - \omega) / \nu_{N,p}$ , and from the following definitions

$$\Pi_1 \equiv \frac{k}{\nu_{N,p}} \left( \frac{2T}{m_N} \right)^{1/2} = \frac{v_A k}{\nu_{N,p}} \beta^{1/2} \left( \frac{m_p}{m_N} \right)^{1/2} \quad (1.57)$$

$$\Pi_2 \equiv \frac{\omega}{\nu_{N,p}} = \frac{v_A k_{\parallel}}{\nu_{N,p}}, \quad (1.58)$$

where  $m_p$  is the proton mass. The dimensionless parameter  $\Pi_1$  is the number of wavelengths a

neutral crosses before colliding, and the dimensionless parameter  $\Pi_2$  is the number of waveperiods a neutral travels before colliding. Since  $k \gg k_{\parallel}$  and  $\beta \gtrsim 1$ ,  $\Pi_1 \gg \Pi_2$  in the inertial range of the MHD cascade.

Performing the integral for the real and imaginary parts of  $\mathbf{F}$  to lowest order in  $\Pi_2/\Pi_1$  yields

$$\mathbf{F} = m_N n_N \mathbf{v} \nu_{N,p} \left(1 - 2i \frac{\Pi_2}{\Pi_1^2}\right) g(\Pi_1), \quad (1.59)$$

where

$$g(\Pi_1) \equiv 1 - \sqrt{\pi} \exp(\Pi_1^{-2}) \operatorname{erfc}(\Pi_1^{-1}) / \Pi_1 \quad (1.60)$$

$$= \begin{cases} \frac{1}{2} \Pi_1^2, & \text{for } \Pi_1 \ll 1 \\ 1, & \text{for } \Pi_1 \gg 1 \end{cases}. \quad (1.61)$$

Since  $-\mathbf{F}$  is equal to the force of the neutrals on the protons, we insert  $-\mathbf{F}$  into the equation of momentum conservation for the protons. More precisely, we add  $-i\mathbf{F}/(m_p n)$  to the right-hand side of equation (1.90) in the Appendix. We label the resulting change of frequency caused by the presence of neutrals as  $\Delta\omega$ . Assuming that  $\Delta\omega \ll v_A k_{\parallel}$ , it follows that

$$\frac{\Delta\omega}{v_A k_{\parallel}} = -\frac{m_N n_N}{m_p n} \left( \frac{1}{\Pi_1^2} + \frac{i}{2\Pi_2} \right) g(\Pi_1). \quad (1.62)$$

### Discussion of the Frequency Change

The physical interpretation of this frequency change is straightforward. Recall that  $k \gg k_{\parallel}$ , so that the wavelength,  $2\pi/k$ , is nearly identical to the wavelength transverse to the magnetic field,  $2\pi/k_{\perp}$ . It is convenient to define the neutral mean free path,  $L_N$ , as follows:

$$L_N \equiv \frac{\Pi_1}{k} = \frac{c_T}{\nu_{N,p}} \left( \frac{2m_p}{m_N} \right)^{1/2}, \quad (1.63)$$

where  $c_T = (p/\rho)^{1/2}$  is the isothermal sound speed.

The imaginary part of  $\Delta\omega$  is the negative of the damping rate, and is given by

$$\omega_i = -\frac{1}{2} \frac{m_N n_N}{m_p n} \nu_{N,p} g(kL_N) \quad (1.64)$$

$$= -\frac{1}{2} \frac{m_N n_N}{m_p n} \nu_{N,p} \times \begin{cases} \frac{1}{2} (kL_N)^2, & \text{for } kL_N \ll 1 \\ 1, & \text{for } kL_N \gg 1 \end{cases}. \quad (1.65)$$

The above expression may be explained as follows (Goldreich and Sridhar 1995). The neutrals are nearly locked to the protons only if both  $\Pi_1 < 1$  and  $\Pi_2 < 1$ . These conditions hold for wavelengths larger than the neutral mean free path ( $kL_N < 1$ ). So on these scales damping is due to the viscosity

of the neutrals. For wavelengths smaller than the neutral mean free path, the neutral atoms are decoupled from the ions, and hence are effectively at rest. The damping rate is thus the ion-neutral collision frequency.

The real part of the frequency change,  $\Delta\omega_r$ , is

$$\frac{\Delta\omega_r}{v_A k_{\parallel}} = -\frac{m_N n_N}{m_p n} \times \begin{cases} \frac{1}{2}, & \text{for } kL_N \ll 1 \\ (kL_N)^{-2}, & \text{for } kL_N \gg 1 \end{cases}. \quad (1.66)$$

Its physical significance is apparent. For small wavelengths the neutral atoms are effectively freely streaming, the motion of the protons nearly decouples from the motion of the neutrals, and there is negligible real frequency change associated with the presence of the neutrals. For large wavelengths the neutrals are locked to the protons, so the mass density of the fluid which participates in the waves is larger than that of the protons. Since the Alfvén speed, and hence the wave frequency, is inversely proportional to the square root of the mass density, i.e.,  $\omega \propto v_A \propto \rho^{-1/2}$ , this results in a decrease of the frequency by a fractional amount which is equal to one-half of the mass ratio of neutrals to protons.

## 1.6.2 Effect of Neutrals on the Turbulent Cascade

### Effect of $\omega_i$ on the Cascade

The turbulent cascade is quenched if the damping rate exceeds the eddy cascade rate or, equivalently, if  $|\omega_i|/v_A k_{\parallel} > 1$ . From equation (1.65) and  $k_{\parallel} \propto k^{2/3}$ , it is seen that for small wavenumbers  $|\omega_i|/v_A k_{\parallel} \propto k^{4/3}$ , and for large wavenumbers  $|\omega_i|/v_A k_{\parallel} \propto k^{-2/3}$ . Therefore  $|\omega_i|/v_A k_{\parallel}$  is a maximum for transverse wavelengths,  $k^{-1}$ , comparable to the neutral mean free path, and decreases for both larger and smaller wavelengths. The requirement that the cascade survive damping by neutrals is then that  $|\omega_i|/v_A k_{\parallel} < 1$  for  $k^{-1}$  comparable to the neutral mean free path, or equivalently,  $n_N \nu_{N,p}/n \lesssim v_A k_{\parallel}$  at this scale (eq. [1.65]). Since  $n_N \nu_{N,p}/n$  is the rate at which a given proton collides with neutrals, the cascade survives to small scales if the wave frequency, and hence the cascade rate, at the scale of the neutral mean free path is faster than the rate at which a proton collides with neutrals.

To obtain the total decrement in the amplitude of both the Alfvén mode and the slow mode through the damping scale, we solve the kinetic equation for the cascade.<sup>10</sup> As in §1.5.1, the kinetic equation is obtained by balancing the  $k$ -space energy flux with the loss-rate of  $k$ -space energy density

<sup>10</sup>The calculation of the amplitude decrement in this section is similar to that given in §1.5.1 for slow mode damping at the cooling scale. The principal difference, aside from the fact that the imaginary part of the frequency is different, is that here we must account for the decrease in the cascade rate,  $t_{\lambda_{\perp}}$ , caused by damping. This is not necessary when treating slow mode damping at the cooling scale because there the Alfvén modes which control the cascade rate are undamped.

due to damping:

$$\frac{d}{dk} \frac{v_{\lambda_{\perp}}^2}{t_{\lambda_{\perp}}} = 2\omega_i \frac{v_{\lambda_{\perp}}^2}{k}, \quad (1.67)$$

where  $\lambda_{\perp}^{-1} \equiv k_{\perp} \simeq k$  is the transverse wavenumber, and  $t_{\lambda_{\perp}}$  is the cascade time. The kinetic equation can be rewritten as follows:

$$\frac{d}{d \ln k} \ln \frac{v_{\lambda_{\perp}}^2}{t_{\lambda_{\perp}}} = 2M_t \frac{\omega_i}{v_A k_{\parallel}}, \quad (1.68)$$

where  $M_t$  is a Kolmogorov constant (see §1.2.5). Before integrating this equation, we re-express the damping frequency in terms of the relevant lengthscales,  $L_{\text{out}}$  and  $L_N$ :

$$\frac{\omega_i}{v_A k_{\parallel}} = -\frac{1}{2} \frac{m_N n_N}{m_p n} \nu_{N,p} \frac{g(kL_N)}{v_A k_{\parallel}} \quad (1.69)$$

$$= -\frac{1}{2M_{\parallel}} \frac{m_N n_N}{m_p n} \nu_{N,p} \frac{g(kL_N)}{v_{\lambda_{\perp}} k} \quad (1.70)$$

$$= -\frac{1}{\sqrt{2}M_{\parallel}} \left(\frac{m_N}{m_p}\right)^{1/2} \frac{n_N}{n} \left(\frac{L_{\text{out}}}{L_N}\right)^{1/3} \frac{g(kL_N)}{(kL_N)^{2/3}}. \quad (1.71)$$

The first equality above follows from equation (1.64). The second equality follows from the Kolmogorov constant  $M_{\parallel} = v_A k_{\parallel} / v_{\lambda_{\perp}} k$  (see §1.2.5). The third equality follows from the velocity spectrum,  $v_{\lambda_{\perp}} = c_T (kL_{\text{out}})^{-1/3}$  (eq. [1.38]), and from the definition of the neutral mean free path (eq. [1.63]). For convenience, we define  $L_{\text{out}}$  in this section such that  $v_{\lambda_{\perp}} = c_T$  when  $k^{-1} = L_{\text{out}}$ .

Integrating the kinetic equation (eq. [1.68]), and using  $t_{\lambda_{\perp}} \sim \lambda_{\perp} / v_{\lambda_{\perp}}$ , yields the net decrement due to damping by collisions with neutrals:

$$\begin{aligned} \frac{[v_{\lambda_{\perp}} / \lambda_{\perp}^{1/3}]|_{\lambda_{\perp} \ll L_N}}{[v_{\lambda_{\perp}} / \lambda_{\perp}^{1/3}]|_{\lambda_{\perp} \gg L_N}} &= \exp \left[ \frac{2M_t}{3} \int_0^{\infty} \frac{\omega_i}{v_A k_{\parallel}} \frac{dk}{k} \right] \\ &= \exp \left[ -0.2 \left(\frac{m_N}{m_p}\right)^{1/2} \frac{n_N}{n} \left(\frac{L_{\text{out}}}{L_N}\right)^{1/3} \right], \end{aligned} \quad (1.72)$$

after substituting from equation (1.71). The numerical prefactor in the second equality, 0.2, follows after inserting the values of the Kolmogorov constants (eq. [1.34]) and the value of the integral

$$\int_0^{\infty} g(x) x^{-5/3} dx \simeq 1.1, \quad (1.73)$$

which was integrated numerically; see equation (1.60) for the definition of  $g(x)$ .

For the cascade to continue to small scales, the right-hand side of equation (1.72) cannot be very small. This can be viewed as an upper limit on the neutral fraction:  $n_N/n \lesssim (L_N/L_{\text{out}})^{1/3}$ . Recall that the condition for the cascade to reach small scales is that the cascade rate at  $L_N$  be faster than the rate at which a proton collides with neutrals. If the neutral fraction is too large, then so is the proton collision rate, and the cascade is quenched. Moreover, for a fixed  $L_N$ , a large value for

$L_{out}$  implies that the cascade time at  $L_N$  is large, and hence that the cascade is more susceptible to damping by neutrals.

We postpone consideration of the damping due to hydrogen and helium atoms until after we evaluate the effect of  $\Delta\omega_r$  on the cascade.

### Effect of $\Delta\omega_r$ on the Cascade

We can picture the cascade as proceeding from large scales to small scales. As it crosses the scale of the neutral mean free path (eq. [1.66]), the effective Alfvén speed, and hence the real part of wave frequency, increases by the fraction  $m_N n_N / 2m_p n$ . Consequently, the cascade time decreases by the same amount. To the extent that the flux of energy in Alfvén waves from large scales to small scales is constant in the turbulent cascade,  $v_{\lambda_\perp}^2 / t_{\lambda_\perp} = \text{constant}$ , where  $t_{\lambda_\perp}$  is the cascade time. Therefore, a fractional decrease of  $m_N n_N / 2m_p n$  in the cascade time causes a decrement in the small-scale Alfvénic velocity perturbation by the fractional amount  $m_N n_N / 4m_p n$ . This decrement is in addition to that due to damping. Moreover, it applies to the slow mode and the entropy mode as well as to the Alfvén mode. Because  $n_N/n$  must be small for the cascade to pass through the scale of neutral damping, this decrement is also small, and we ignore it from here on.

### 1.6.3 Neutral Hydrogen Atoms

When the neutrals are hydrogen atoms we set  $n_N = n_H$ ,  $\nu_{N,p} = \nu_{H,p}$ ,  $L_N = L_H$ , and  $m_N = m_p$ . Collisions between hydrogen atoms and protons are due to resonant charge exchange. From equation (1.63), with the value of  $\nu_{H,p}$  taken from Banks (1966),

$$L_H = 5 \times 10^{13} \left( \frac{\text{cm}^{-3}}{n} \right) \text{ cm} \quad (1.74)$$

at  $8 \times 10^3$  K; the temperature dependence of  $L_H$  is very weak.

For the cascade to survive damping by neutral hydrogen atoms, the right-hand side of equation (1.72) cannot be very small. This sets an upper limit on the neutral fraction of

$$\frac{n_H}{n} \lesssim 5 \left( \frac{L_H}{L_{out}} \right)^{1/3} \sim \left( \frac{6 \times 10^{15} \text{ cm}}{(n/\text{cm}^{-3}) L_{out}} \right)^{1/3}. \quad (1.75)$$

The real part of  $\omega/v_A k_{\parallel}$  is larger on scales below  $L_H$  than it is on scales above  $L_H$  by the fractional value  $n_H/2n$ .

### 1.6.4 Neutral Helium Atoms

Although helium has a lower abundance than hydrogen, it has a higher ionization potential. Therefore, in some regions helium might comprise the majority of neutrals. When the neutrals are helium

atoms we set  $n_N = n_{\text{He}}$ ,  $\nu_{N,p} = \nu_{\text{He},p}$ ,  $L_N = L_{\text{He}}$ , and  $m_N = 4m_p$ . From equation (1.63), with the value of  $\nu_{\text{He},p}$  taken from Banks (1966),

$$L_{\text{He}} = 1.5 \times 10^{15} \left( \frac{\text{cm}^{-3}}{n} \right) \text{ cm} \quad (1.76)$$

at  $8 \times 10^3 \text{ K}$ , and  $L_{\text{He}} \propto T^{1/2}$ .

To place an upper bound on damping by helium atoms, we assume that most of the helium is neutral, i.e.,  $n_{\text{He}} \approx 0.1n$ . Then the decrement is given by the right-hand side of equation (1.72):

$$\frac{[v_{\lambda_{\perp}}/\lambda_{\perp}^{1/3}]|_{\lambda_{\perp} \ll L_{\text{He}}}}{[v_{\lambda_{\perp}}/\lambda_{\perp}^{1/3}]|_{\lambda_{\perp} \gg L_{\text{He}}}} = \exp \left[ - \left( \frac{(n/\text{cm}^{-3})L_{\text{out}}}{2 \times 10^{19} \text{ cm}} \right)^{1/3} \right]. \quad (1.77)$$

Only if  $L_{\text{out}} \gtrsim 2 \times 10^{19} (\text{cm}^{-3}/n) \text{ cm}$  could the cascade be terminated at the scale of the helium mean free path. If there are not many neutral helium atoms, or if the outer scale is not sufficiently large, then damping at  $L_{\text{He}}$  may be neglected, and the cascade extends at least to the scale of the hydrogen mean free path.

Collisions of neutral helium atoms with singly ionized helium ions might also be significant. Although there are fewer helium atoms than protons,  $\text{He}^0\text{-He}^+$  collisions have a larger cross-section than  $\text{He}^0\text{-proton}$  collisions because they are due to resonant charge exchange. Nonetheless, given the cosmic abundance of helium, the mean free path of neutral helium due to  $\text{He}^0\text{-He}^+$  collisions cannot be significantly smaller than that due to  $\text{He}^0\text{-proton}$  collisions regardless of the ionization fraction of helium.

The real part of  $\omega/v_A k_{\parallel}$  increases by  $2n_{\text{He}}/n$  below the scale  $L_{\text{He}}$ , or 0.2 if most of the helium is neutral.

### 1.6.5 If Neutrals Damp the Cascade

In subsequent sections, we consider regions in the interstellar medium where there are too few neutrals to damp the cascade. However, there are almost certainly many regions where the neutrals do damp the cascade. We discuss these regions here.

Suppose both Alfvén waves and slow waves are damped by neutrals. What happens to the entropy waves? If undamped, they would be mixed down to smaller scales by Alfvén waves at the neutral damping scale. The resulting density spectrum would be  $n_{\lambda_{\perp}} = \text{constant}$  (see eq. [1.31]). Because it is flatter than  $n_{\lambda_{\perp}} \propto \lambda_{\perp}^{1/3}$ , regions in which damping by neutrals truncated the Alfvén cascade might be important contributors to small scale density fluctuations. However, the fact that they would contribute a density spectrum different from that which is observed suggests that the entropy wave cascade is not more resistant than the Alfvén wave cascade to damping by neutrals. Indeed that is the case. Recall that the condition for the truncation of Alfvén and slow wave cascades

is that each proton collide with at least one neutral atom during one wave period at the neutral damping scale. Under this condition, the neutrals would damp the entropy waves by conducting heat across them.

Although regions in which the cascade is damped by neutrals do not contribute small scale density fluctuations, they may still be significant. Observational evidence indicates that there is more power in density fluctuations on large scales,  $10^{13} - 10^{14}$  cm, than would be predicted by extrapolating from small scales,  $10^8 - 10^{10}$  cm, with the Kolmogorov scaling. See, for example, Lambert and Rickett (2000) for a review of the observations. Perhaps this excess arises in regions where the cascade is damped by neutrals.

We complete this section by briefly considering and then rejecting the possibility that a turbulent cascade truncated at the neutral damping scale might be regenerated on a much smaller scale due to stirring by eddies at the damping scale. Although the ratio of the damping rate to the wave frequency decreases below the scale of the neutral mean free path, the absolute damping rate approaches a constant value. Provided the cascade is truncated by neutral damping, this rate is larger than the stirring rate and the cascade cannot be regenerated.

## 1.7 The Collisionless Scale of the Ions

If the cascade survives the neutral collisionless scales, then, proceeding to smaller scales, the next scale of importance is the ion collisionless scale. This scale is set by the mean free path of protons to collide with other protons:

$$L_{\text{mfp}} = 6 \times 10^{11} \left( \frac{\text{cm}^{-3}}{n} \right) \text{ cm} \quad (1.78)$$

at a temperature of 8,000K (Braginskii 1965). Since the electron and proton gyroradii (see eq. [1.88] for protons) are very small compared to the proton mean free path, the electrons and protons are tied to magnetic fieldlines. Therefore, when considering the collisionless effects of electrons and protons, the relevant lengthscales are those parallel to the magnetic field. Since turbulent eddies are highly elongated along the magnetic field, their transverse lengthscales are much smaller than their parallel ones (eq. [1.28]). It is the transverse lengthscale which is relevant when considering observations of the density spectrum, because each line of sight averages over regions with different magnetic field orientations. In this section, we show that both the slow mode and the entropy mode are cut off at the lengthscale where the parallel eddy size is comparable to the proton mean free path. The lengthscale where the density spectrum is observed to cut off, i.e., the transverse lengthscale, is therefore significantly smaller than the mean free path.

Before discussing the damping of the slow mode and the entropy mode, we consider two larger lengthscales, which are set by the effects of the electrons. Although the behaviour of the cascade at these lengthscales is interesting, it is shown to be unimportant for our purposes.

Throughout this section, we neglect numerical factors of order unity, such as the factors which are associated with kinetic corrections to the fluid equations (given in Braginskii 1965) and the Kolmogorov constants. However, we retain the dependences on  $\beta$ , which is assumed to satisfy  $\beta > 1$ , and on the ratio of the proton mass to the electron mass:  $m_p/m_e = 1840$ .

### 1.7.1 The Electron Diffusion Scale

The electrons have the same mean free path as the protons, but they are faster than the protons by the square root of the mass ratio:

$$c_{s,e} \approx \left(\frac{m_p}{m_e}\right)^{1/2} c_s, \quad (1.79)$$

where  $c_{s,e}$  is the electron thermal speed and  $c_s$  is the sound speed, which is comparable to the proton thermal speed. Because of charge neutrality, the electrons have the same density, both perturbed and unperturbed, as the protons. Viscous damping caused by the electrons may be neglected: since the dynamic viscosity of the electrons is smaller than that of the protons by the square root of their mass ratio, electron viscous damping is always subdominant.

As we now show, electrons are important for conducting heat on parallel lengthscales slightly larger than the proton mean free path. Electrons diffuse parallel to the magnetic field across a distance  $\Lambda_{\parallel}$  in the time  $(L_{\text{mfp}}/c_{s,e})(\Lambda_{\parallel}/L_{\text{mfp}})^2$ . This is equal to the cascade time of an eddy with parallel lengthscales  $\Lambda_{\parallel}$ , i.e., it is equal to  $\Lambda_{\parallel}/v_A$ , at the electron diffusion scale, given by  $\Lambda_{\parallel} \sim L_{\text{ed}}$ , where

$$L_{\text{ed}} \approx \frac{c_{s,e}}{v_A} L_{\text{mfp}} \approx \beta^{1/2} \left(\frac{m_p}{m_e}\right)^{1/2} L_{\text{mfp}}. \quad (1.80)$$

In eddies with parallel lengths smaller than this, the electrons diffuse across the parallel lengths of the eddies, thereby conducting heat, and the electrons are isothermal; in eddies with parallel lengths larger than this, conduction is unimportant.

We must also consider the effect of electron conduction on the protons. Electrons and proton temperatures approach a common value on the timescale that there are  $m_p/m_e$  collisions per particle. Since electrons are faster, the collision time is set by the electron speed, and the time for electron and proton temperatures to equilibrate is

$$\tau_{\text{eq}} \approx \frac{m_p}{m_e} \frac{L_{\text{mfp}}}{c_{s,e}} \approx \frac{1}{v_A} \frac{1}{\beta^{1/2}} \left(\frac{m_p}{m_e}\right)^{1/2} L_{\text{mfp}}. \quad (1.81)$$

This time is smaller, by a factor  $\beta$ , than the cascade time of eddies with parallel size  $L_{\text{ed}}$ . Thus in eddies of this parallel size, and in those which are slightly smaller, protons are at the same temperature as the electrons. And, since the electrons are isothermal, so are the protons.

As a result of the above considerations, when the parallel cascade crosses the electron diffusion scale, the cascade becomes isothermal. This is similar to the crossing of the cooling scale, discussed

in §1.5.1, though backwards, and similar considerations apply. In particular, the Alfvén mode is incompressible, and hence unaffected. The slow mode is nearly incompressible, and is only slightly affected: it suffers some damping to first order in  $1/\beta$ . The entropy mode, however, is rapidly damped under isothermal conditions; as the electron diffusion scale is crossed, entropy waves are converted into slow waves, and the density fluctuations which had been associated with entropy waves now become associated with slow waves.

### 1.7.2 The Electron-Proton Equilibration Scale

Continuing to slightly smaller scales, the isothermal cascade reaches the equilibration scale, where the cascade time,  $\Lambda_{\parallel}/v_A$ , is comparable to the electron-proton equilibration time (eq. [1.81]). At this scale,  $\Lambda_{\parallel} \sim L_{\text{eq}}$ , where

$$L_{\text{eq}} \approx \frac{1}{\beta^{1/2}} \left( \frac{m_p}{m_e} \right)^{1/2} L_{\text{mfp}} . \quad (1.82)$$

On larger scales, the protons are thermally coupled to the electrons, and hence they are isothermal on slightly larger scales; on smaller scales, the protons are thermally independent of the electrons, and hence adiabatic. The transition through the equilibration scale is nearly identical to the transition through the cooling scale (§1.5.1): the Alfvén waves are unaffected, and they mix larger-scale isothermal slow waves into smaller-scale adiabatic slow waves and into smaller-scale entropy waves, although with some damping. Therefore, below the equilibration scale, the entropy mode reappears.

The result of the calculations in both this subsection and the previous subsection is that, in crossing the electron diffusion scale and the equilibration scale, density fluctuations which were associated with the entropy mode on large scales are transferred from the entropy mode to the slow mode and then back to the entropy mode. Density fluctuations which were associated with the slow mode on large scales are unaffected.<sup>11</sup> Therefore, for our purposes, these two lengthscales have little net effect on the density spectrum. Although there is some damping, the amount of damping is comparable to the amount at the cooling scale, and hence is not very significant.

### 1.7.3 The Proton Diffusion Scale: Death of the Slow Mode and Entropy Mode

Entropy waves and slow waves with parallel wavelengths smaller than the proton mean free path both damp on the timescale that protons stream across their parallel wavelengths (Barnes 1966). However, because we consider  $\beta > 1$ , there is a scale slightly larger than the proton mean free path

---

<sup>11</sup>However, if the density fluctuations in the large-scale slow mode were less than the density fluctuations in the large-scale entropy mode, then, on small scales, the slow mode would be boosted so that its density fluctuations would be comparable to those of the entropy mode: the slow mode can steal approximately half of the entropy mode. Note that, since the behaviour of the cascade at the electron-proton equilibration scale is nearly identical to the the behaviour at the cooling scale, similar uncertainties apply; see discussion in §1.5.1. In particular, we are unable to quantify the damping of the entropy fluctuations, although we expect that this damping is not so large as to render the entropy mode negligible relative to the slow mode on small scales.

at which these waves damp in the turbulent cascade. This is the proton diffusion scale, which is the scale at which protons can diffuse across an eddy within a cascade time. Below the proton diffusion scale, proton viscosity kills the slow waves and proton heat conduction kills the entropy waves. Alfvén waves are unaffected by either of these effects. The density spectrum therefore cuts off below the proton diffusion scale.

To evaluate the proton diffusion scale, we equate the time for protons to diffuse across an eddy of parallel lengthscale  $\Lambda_{\parallel}$ , i.e.,  $(L_{\text{mfp}}/c_s)(\Lambda_{\parallel}/L_{\text{mfp}})^2$ , with the cascade time,  $\Lambda_{\parallel}/v_A$ . This gives  $\Lambda_{\parallel} \sim L_{\text{pd}}$ , where

$$L_{\text{pd}} \approx \frac{c_s}{v_A} L_{\text{mfp}} \approx \beta^{1/2} L_{\text{mfp}} . \quad (1.83)$$

However, from an observational point of view, it is the transverse size of a damped eddy,  $\lambda_{\perp}$ , which would be observed. This is related to the parallel size through equation (1.28). Alternatively, we use the Kolmogorov constant  $M_{\parallel} \equiv v_A \lambda_{\perp} / v_{\lambda_{\perp}} \Lambda_{\parallel}$  (see §1.2.5).<sup>12</sup> Then, the transverse scale of a damped eddy, i.e., an eddy with parallel size  $\Lambda_{\parallel} \sim L_{\text{pd}}$ , is

$$\begin{aligned} \lambda_{\perp} &\approx M_{\parallel} \frac{v_{\lambda_{\perp}}}{v_A} L_{\text{pd}} \\ &\approx M_{\parallel} \beta L_{\text{mfp}} \left( \frac{\lambda_{\perp}}{L_{\text{out}}} \right)^{1/3} , \end{aligned} \quad (1.84)$$

which we solve for the cutoff lengthscale:  $\lambda_{\perp} \sim L_{\text{pd}}^{(\perp)}$ , where

$$L_{\text{pd}}^{(\perp)} \approx M_{\parallel}^{3/2} \beta^{3/2} L_{\text{mfp}} \left( \frac{L_{\text{mfp}}}{L_{\text{out}}} \right)^{1/2} \quad (1.85)$$

$$\approx 2 \times 10^9 \left( \frac{\text{pc}}{L_{\text{out}}} \right)^{1/2} \left( \frac{\beta}{n/\text{cm}^{-3}} \right)^{3/2} \text{ cm} . \quad (1.86)$$

Below this scale, the density spectrum is cut off. For plausible values of  $\beta$ ,  $L_{\text{out}}$ , and  $n$ , this lengthscale is significantly smaller than  $L_{\text{mfp}}$ . It is also larger than the proton gyroradius (eq. [1.88], below).

Armstrong, Rickett, and Spangler (1995) summarize the observations of the density spectrum cutoff. There is considerable evidence that the cutoff scale is smaller than about  $10^{10}$  cm along many directions. There is weaker evidence, from refractive scintillation, that along some lines of sight the cutoff scale is larger than around  $10^9$  cm. Our theory might have implications for these observations.

We conclude this section with two remarks. First, we re-emphasize the importance of the fact that the cascade is anisotropic. It is this fact which allows the density spectrum to reach lengthscales which are significantly smaller than the proton mean free path. Second, we note an important

<sup>12</sup>Although we drop other factors of order unity, we keep the dependence on this one because of the importance of the proton diffusion scale.

consequence of the parallel cascades of the slow mode and of the passive scalar; these parallel cascades were explained in great detail when considering incompressible MHD turbulence (§1.2). Had there been no parallel cascade, then neither the slow mode nor the entropy mode would damp at the proton diffusion scale. The wavelength along the magnetic field would be effectively infinite, and so the ions could not diffuse across wavelengths. Rather, the slow mode and the entropy mode would be mixed down to the proton gyro scale, where the Alfvénic cascade is cut off.

#### 1.7.4 Density Spectrum Below the Proton Diffusion Scale

On scales smaller than  $L_{\text{pd}}^{(\perp)}$ , density fluctuations are wiped out. Since on these scales protons diffuse across the lengths of many eddies before the eddies cascade, the density within neighbouring eddies is homogenized. Homogenization occurs not only in the direction parallel to the local mean magnetic field—as might have been expected since protons are tied to fieldlines—but also in the transverse direction. This is because eddies that are adjacent in the parallel direction incorporate substantially different fieldlines, so proton diffusion also wipes out density differences amongst eddies with transverse separations. The result is that the density spectrum on scales smaller than  $L_{\text{pd}}^{(\perp)}$  is determined by density fluctuations at  $L_{\text{pd}}^{(\perp)}$ ; equivalently,

$$n_{\lambda_{\perp}} \propto \lambda_{\perp}^{-3}, \quad \text{for } \lambda_{\perp} < L_{\text{pd}}^{(\perp)}. \quad (1.87)$$

### 1.8 The End: the Proton Gyroscale

The Alfvén mode is undamped in a collisionless medium (Barnes 1966). Thus, the Alfvén wave cascade survives below the proton diffusion scale, without the accompaniment of the slow waves and entropy waves. The Alfvénic cascade is damped at the scale of the proton gyroradius:

$$L_{\text{p,gyr}} = \sqrt{2} c_T \frac{m_p c}{e B} = 2.5 \times 10^7 \left( \frac{\beta}{n/\text{cm}^{-3}} \right)^{1/2} \text{ cm}. \quad (1.88)$$

At this scale, Alfvén waves are converted into whistlers. The whistlers cascade to smaller scales, where they are damped by the collisionless effects of the electrons (Quataert 1998, viz. the curve in his Fig. 1b that corresponds to equal electron and proton temperatures).

### 1.9 Summary

The primary goal of this chapter has been to calculate the small-scale density spectrum in turbulent interstellar plasmas. Our theory of compressible MHD turbulence is based upon the incompressible theory of Goldreich and Sridhar (1995), for which there is growing support from numerical simula-

tions. We hypothesize that the compressible theory is similar to the incompressible theory of MHD turbulence, but with two main modifications: a compressible slow mode and an entropy mode which is passively advected. While we believe that this hypothesis is plausible, it can, and should, be tested with numerical simulations of compressible MHD.

Because of the multitude of special lengthscales encountered when discussing the turbulent cascade in the interstellar medium, a recapitulation might be useful. In the following, we list the most important lengthscales and summarize their significance to the turbulent cascade.

*The Outer Scale* ( $L_{\text{out}}$ ): This is the lengthscale at which the turbulent motions are stirred. On slightly smaller scales, there is isothermal hydrodynamic turbulence for most plausible astrophysical sources.

*The MHD Scale* ( $L_{\text{MHD}}$ ): At this lengthscale there is a transition from hydrodynamic to MHD turbulence. Larger-scale hydrodynamic motions couple to smaller-scale Alfvén waves and slow waves.

*The Cooling Scale* ( $L_{\text{cool}}$ ): At this lengthscale there is a transition from isothermal to adiabatic turbulence. In high- $\beta$  turbulence, where small scale density fluctuations are due to the entropy mode, entropy—and hence density—fluctuations are suppressed by cooling. In low- $\beta$  turbulence, i.e.,  $1 \lesssim \beta < L_{\text{out}}/c_s t_{\text{cool}}$ , density fluctuations due to the slow mode are important, and cooling has a negligible effect on the small-scale density spectrum.

*The Collisionless Scale of the Neutrals* ( $L_{\text{H}}$ ;  $L_{\text{He}}$ ): Neutrals decouple from ions across these scales. If the neutral fraction is not sufficiently small, then all three modes—Alfvén, slow, and entropy—are damped.

*The Collisionless Scale of the Ions* ( $\Lambda_{\parallel} = L_{\text{ed}}$ ;  $\Lambda_{\parallel} = L_{\text{eq}}$ ;  $\Lambda_{\parallel} = L_{\text{pd}} \Leftrightarrow \lambda_{\perp} = L_{\text{pd}}^{(\perp)}$ ): Across these lengthscales there is a gradual transition from fluid behaviour to collisionless plasma behaviour. The first two of these lengthscales, the electron diffusion scale and the equilibration scale, are set by the electrons. These lengthscales have only a small net effect on the cascade. The proton diffusion scale, however, is critically important for density fluctuations: both the slow mode and the entropy mode are cut off at this scale, and hence there are no density fluctuations below  $L_{\text{pd}}^{(\perp)}$ .

*The Proton Gyro Scale* ( $L_{\text{p,gyr}}$ ): Alfvén waves are cut off at this scale. However, this scale has little importance for the density spectrum, because there are no density fluctuations below the proton diffusion scale.

## 1.10 Comparison with Higdon’s Work

In his 1984 paper, Higdon attributes small-scale density fluctuations to the passive mixing of the entropy mode. In his 1986 paper, Higdon notes that if the entropy mode varies along the magnetic field, it is damped in a collisionless medium. He then attributes small-scale density fluctuations to the passive mixing of tangential pressure balances. Tangential pressure balances are structures

which are parallel to the mean magnetic field. They are composed of both entropy waves and slow waves that have purely transverse wave vectors.

Considering that Higdon's papers preceded even a theory of incompressible MHD turbulence, they are a remarkable accomplishment. However, Higdon does not account for the parallel cascade. Entropy and slow waves with purely transverse wave vectors contain negligible power. They are cascaded along the magnetic field by Alfvén waves. Consequently, they are damped when protons can diffuse across eddies in a cascade time, i.e., below the proton diffusion scale.

## 1.11 Compressible Turbulence When $\beta < 1$

In this section only, we consider compressible turbulence in plasmas that have  $\beta < 1$ , e.g., in strong oblique isothermal shocks and in the solar wind.

Since Alfvén waves are unaffected by the value of  $\beta$ , and since nearly transverse slow waves are only slightly affected (see Appendix), the dynamics of the cascade is nearly independent of  $\beta$ . While the dispersion relation of the slow mode is changed from  $\omega = v_A k_z$  to  $\omega = c_s k_z$ , the slow waves are still passively mixed by the Alfvén waves. Therefore, the Alfvén, slow, and entropy spectra in  $\beta < 1$  MHD turbulence are the same as when  $\beta > 1$ .

However, the damping of the slow and entropy waves is significantly changed. When  $\beta > 1$ , the proton thermal speed is faster than the Alfvén speed. Therefore protons can stream across small eddies before they cascade. Conversely, when  $\beta < 1$ , the time for protons to cross an eddy is always shorter than the cascade time. Therefore slow and entropy waves cannot be damped by protons which cross eddies, and the density spectrum extends to smaller scales.

We have ignored the effects of the electrons. However, in the following we show that the electrons' behaviour may be ignored for our purposes. Our discussion closely parallels that when  $\beta > 1$  in §1.7, and uses similar notation. When  $\beta < 1$ , the equilibration scale (eq. [1.82]) is larger than the electron diffusion scale (eq. [1.80]). Thus the largest scale at which kinetic effects are significant is the scale at which the cascade time is comparable to the time for electrons and protons to equilibrate their temperatures. Below this scale, electrons and protons are thermally decoupled. Nonetheless, this thermal decoupling has no effect on the Alfvén, slow, or entropy waves on scales larger than the electron diffusion scale. At the electron diffusion scale, the cascade time is comparable to the electron diffusion time. Below this scale, the electrons are isothermal. However, since the protons are thermally decoupled from the electrons, the slow waves and entropy waves are cascaded to smaller scales.<sup>13</sup>

Continuing to smaller scales, the next scale of importance is that at which the parallel size of an eddy is comparable to the proton mean free path. Below this scale, the cascade is collisionless. The

---

<sup>13</sup>There is a change in the density spectrum at this scale which is of order unity; it is due to the change in the electrons' equation of state.

Alfvén waves are undamped by collisionless effects. The entropy waves are undamped since protons cannot cross eddies within a cascade time. The slow waves are also undamped within a cascade time: although they damp within a waveperiod by Barnes damping, their waveperiod is longer than the cascade time. Consequently, the Kolmogorov density spectrum extends down to the proton gyro scale.

## 1.12 Future Work

In a future paper, we will examine in detail the density spectrum in the solar wind. In another future paper, we will relate the theory of compressible plasma turbulence developed here to observations—primarily those of diffractive scintillation. We will demonstrate that the observed amplitude of small-scale density fluctuations is surprisingly large, especially along certain lines of sight, such as the one toward the Galactic Center. Then we will attempt to determine which astrophysical sources contribute the bulk of the density fluctuations and why they do so.

## Acknowledgments

We thank Jason Maron for analyzing some of his simulations for us, for showing us how to use his numerical code, and for informative discussions. We thank the referee, Ben Chandran, for a very helpful report. Research reported in this chapter was supported by NSF grant 94-14232.

## 1.13 Appendix: Waves in Compressible MHD

In this Appendix we derive the properties of the Alfvén mode, the slow mode, and the entropy mode. The fast mode is not relevant to interstellar scintillation for reasons discussed in the body of the chapter. The Fourier-transformed, linearized equations of ideal MHD, with  $\partial/\partial t \rightarrow -i\omega$  and  $\nabla \rightarrow i\mathbf{k}$ , read

$$\omega n' = (\mathbf{k} \cdot \mathbf{v})n, \quad (\text{mass conservation}) \quad (1.89)$$

$$\omega \mathbf{v} = \mathbf{k} \left[ \bar{c}^2 \frac{n'}{n} + b_z v_A \right] - b v_A k_z, \quad (\text{momentum conservation}) \quad (1.90)$$

$$\omega \mathbf{b} = \hat{z} v_A (\mathbf{k} \cdot \mathbf{v}) - v v_A k_z, \quad (\text{Faraday's law}) \quad (1.91)$$

where  $n$  is number density,  $\rho$  is mass density,  $B$  is the background magnetic field intensity, and  $v_A \equiv B/\sqrt{4\pi\rho}$  is the Alfvén speed. The  $z$ -axis is chosen to lie parallel to the background magnetic field. Some other variables are the perturbed number density,  $n'$ ; the fluid velocity,  $\mathbf{v}$ ; and the perturbed magnetic intensity,  $\mathbf{B}'$ , or in velocity units,  $\mathbf{b} \equiv \mathbf{B}'/\sqrt{4\pi\rho}$ . The sound speed,  $\bar{c}$ , is defined

less conventionally here to be the square root of the ratio of perturbed pressure to perturbed mass density:  $\tilde{c} \equiv (p'/\rho')^{1/2}$ . We can express the equations of motion in terms of  $\mathbf{v}$  as follows:

$$(\omega^2 - k_z^2 v_A^2) \mathbf{v} = [(\mathbf{k} \cdot \mathbf{v})(\tilde{c}^2 + v_A^2) - k_z v_z v_A^2] \mathbf{k} - v_A^2 k_z (\mathbf{k} \cdot \mathbf{v}) \hat{\mathbf{z}} . \quad (1.92)$$

For most of the purposes of this chapter, the energy equation may be left unspecified, and  $\tilde{c}$  may be assumed constant. However, we use the energy equation when we discuss slow mode damping at the cooling scale in §1.5.1. We assume that temperature fluctuations decay in a cooling time,  $t_{\text{cool}}$ ; more precisely,

$$i\omega T s' = \frac{T'}{t_{\text{cool}}} \quad (\text{energy conservation}) , \quad (1.93)$$

where  $s'$  is the perturbed entropy per particle, and  $T$  is the temperature. Combining this equation with the following monatomic ideal gas relations

$$\frac{p'}{p} = \frac{\rho'}{\rho} + \frac{T'}{T} = \frac{2}{3} s' + \frac{5}{3} \frac{\rho'}{\rho} , \quad (1.94)$$

yields

$$\tilde{c}^2 \equiv \frac{p'}{\rho'} = c_T^2 \frac{2 - i5\omega t_{\text{cool}}}{2 - i3\omega t_{\text{cool}}} , \quad (1.95)$$

where  $c_T^2 \equiv p/\rho$  is the square of the isothermal sound speed. When  $\omega t_{\text{cool}} \ll 1$ ,  $\tilde{c}$  is the isothermal sound speed; when  $\omega t_{\text{cool}} \gg 1$ ,  $\tilde{c}$  is the adiabatic sound speed.

### 1.13.1 Alfvén Mode

The Alfvén mode is incompressible;  $\mathbf{k} \cdot \mathbf{v} = 0$ . Thus the term involving the sound speed in the momentum equation vanishes, and the properties of the Alfvén mode are independent of the equation of energy conservation. We obtain the dispersion relation

$$\omega = v_A |k_z| , \quad (1.96)$$

by forming the cross product of equation (1.92) with  $\mathbf{k}$ . The eigenfunction satisfies

$$\mathbf{n}' = \mathbf{k} \cdot \mathbf{v} = \hat{\mathbf{z}} \cdot \mathbf{v} = 0 \quad , \quad \mathbf{b} = -\text{sign}(k_z) \mathbf{v} . \quad (1.97)$$

Note that both  $\mathbf{v}$  and  $\mathbf{b}$  are perpendicular to  $\hat{\mathbf{z}}$ : the Alfvén wave is polarized transverse to the unperturbed magnetic field.

### 1.13.2 Slow Mode

We summarize the properties of the slow mode to lowest order in  $k_z/k \ll 1$ , the limit appropriate to the MHD cascade. To obtain the dispersion relation we assume, subject to verification, that the perturbation in total pressure—i.e., thermal plus magnetic pressure—vanishes to second order in  $k_z/k$ . Note that the perturbation in total pressure is proportional to the terms in square brackets in both equation (1.90) and equation (1.92). From the vanishing of this pressure term in equation (1.92), we then have

$$\mathbf{k} \cdot \mathbf{v} = \frac{v_A^2}{\tilde{c}^2 + v_A^2} \left[ 1 + O\left(\frac{k_z}{k}\right)^2 \right] k_z v_z . \quad (1.98)$$

The z-component of equation (1.92), with  $\mathbf{k} \cdot \mathbf{v}$  given by equation (1.98), then yields the dispersion relation:

$$\omega = \frac{\tilde{c}}{\sqrt{\tilde{c}^2 + v_A^2}} \left[ 1 + O\left(\frac{k_z}{k}\right)^2 \right] v_A |k_z| . \quad (1.99)$$

Next, we solve for the eigenfunction to lowest order in  $k_z/k$ :

$$\frac{n'}{n} \simeq \text{sign}(k_z) \frac{v_A v_z}{\tilde{c} \sqrt{\tilde{c}^2 + v_A^2}} , \quad v_x \simeq -\frac{\tilde{c}^2}{\tilde{c}^2 + v_A^2} \frac{k_z}{k} v_z , \quad v_y = 0 , \quad \mathbf{b} \simeq -\text{sign}(k_z) \frac{\tilde{c} \mathbf{v}}{\sqrt{\tilde{c}^2 + v_A^2}} , \quad (1.100)$$

where the x-axis has been chosen to lie in the plane containing  $\mathbf{k}$  and  $\hat{\mathbf{z}}$ . We now see that our assumption of negligible perturbed pressure is self-consistent to lowest order in  $k_z/k$ . While we have not used the x-component of equation (1.92), both the left-hand side and the right-hand side of this equation are of the same order in  $k_z/k$ .

The vanishing of the slow mode's perturbed pressure may be understood as follows: the period of the slow mode is comparable to the time for a disturbance to cross a parallel wavelength at the slower of  $\tilde{c}$  and  $v_A$ . Total pressure balance is set up within the time that the fast mode—which travels at the faster of  $\tilde{c}$  and  $v_A$ —crosses a wavelength. This may be seen by solving equation (1.92) exactly (treating  $\tilde{c}$  as a constant): the slow mode's perturbed pressure is negligible, and our approximate solution is valid, when  $2(k_z/k)\tilde{c}v_A/(\tilde{c}^2 + v_A^2) \ll 1$ , which implies that  $k_z \times \min\{\tilde{c}, v_A\} \ll k \times \max\{\tilde{c}, v_A\}$ .

Note that both  $\mathbf{v}$  and  $\mathbf{b}$  are nearly parallel to  $\hat{\mathbf{z}}$ : the slow wave polarization is nearly aligned with the unperturbed magnetic field. Moreover, in the limit that  $\tilde{c} \gg v_A$ , the slow mode is nearly incompressible.

### 1.13.3 Entropy Mode

The linearized MHD equations yield four modes; in addition to the Alfvén, slow, and fast modes, there is a lesser known mode: the entropy mode. For adiabatic fluid motions, the energy equation is  $\omega s' = 0$ . The entropy mode has  $\omega = 0$ , and its eigenfunction is given by  $p' = \mathbf{v} = \mathbf{b} = 0$ ,

$$T'/T = -n'/n = 2s'/5.$$

In the following, we calculate the eigenvalue and eigenvector of the entropy mode in the presence of cooling, i.e., when the energy equation is given by equation (1.93). We shall see that the entropy mode decays in a time comparable to  $t_{\text{cool}}$ .

We consider only wavenumbers sufficiently large that the fast mode's crossing time is much faster than the entropy mode's decay time, i.e.,  $k \gg k_{\text{fast}} \equiv [\bar{c}^2 + v_A^2]^{-1/2} t_{\text{cool}}^{-1}$ . Therefore the total pressure perturbation vanishes. Note that  $k > k_{\text{fast}}$  in the vicinity of the cooling scale (eq. [1.39]), where the present calculation is most relevant.

The dispersion relation may be obtained from equation (1.92), after setting the perturbed total pressure—the term in square brackets—to zero. The result is equation (1.99), which has three roots: two counter-propagating slow modes and the entropy mode. To solve for the entropy mode, it is convenient to rewrite equation (1.99) as follows:

$$i\omega t_{\text{cool}} = \frac{4 + 2\beta[1 - (v_A k_z/\omega)^2]}{6 + 5\beta[1 - (v_A k_z/\omega)^2]}, \quad (1.101)$$

where  $\beta \equiv 2c_T^2/v_A^2$ , and where equation (1.95) has been used for  $\bar{c}$ . Presupposing that  $\omega$  is of order  $t_{\text{cool}}^{-1}$ , we see that the right-hand side of this equation has two limiting behaviours, depending on the value of  $k_z$ .

On small scales, where  $\min\{v_A, c_T\} \times t_{\text{cool}} k_z \gg 1$ ,

$$\omega = -i \frac{2}{5} \frac{1}{t_{\text{cool}}}. \quad (1.102)$$

In this limit the slow mode crossing time is faster than cooling, so the thermal pressure perturbation vanishes, as may be seen directly from equation (1.95). Thus, to lowest order in  $(k_z v_A t_{\text{cool}})^{-1}$ , the eigenfunction is the same as for the adiabatic case,  $p' = \mathbf{v} = \mathbf{b} = 0$ ,  $T'/T = -n'/n = 2s'/5$ .

On large scales, where  $k_z v_A t_{\text{cool}} \ll 1$ , equation (1.101) implies that

$$\omega = -i \frac{4 + 2\beta}{6 + 5\beta} \frac{1}{t_{\text{cool}}}, \quad v_A t_{\text{cool}} k_z \ll 1. \quad (1.103)$$

Substituting this into equation (1.95), and using total pressure balance, yields the eigenfunction,  $n'/n = b_z/v_A = -(p'/p)(\beta/2)$ . The remaining non-zero components of the eigenfunction are  $T'/T = -(n'/n)(1 + 2/\beta)$  and  $s' = -(n'/n)(5/2 + 3/\beta)$ .

## Bibliography

- [1] Armstrong, J. W., Rickett, B. J., and Spangler, S. R. 1995, *ApJ*, 443, 209
- [2] Balsara, D. and Pouquet, A. 1999, *Phys. Plasmas*, 6, 89
- [3] Banks, P. M. 1966, *Planet. Space Sci.*, 14, 1105
- [4] Barnes, A. 1966, *Phys. Fluids*, 9, 1483
- [5] Boldyrev, S. and Gwinn, C. 2002, *astro-ph/0204144*
- [6] Braginskii, S. I. 1965, *Rev. Plasma Phys.*, 1, 205
- [7] Cho, J. and Vishniac, E. T. 2000a, *ApJ*, 538, 217
- [8] Cho, J. and Vishniac, E. T. 2000b, *ApJ*, 539, 273
- [9] Cordes, J. M., Weisberg, J. M., and Boriakoff, V. 1985, *ApJ*, 288, 221
- [10] Cordes, J. M., Weisberg, J. M., Frail, D. A., Spangler, S. R., and Ryan, M. 1991, *Nature*, 354, 121
- [11] Goldreich, P. 1998, *AAS*, 192, 4603
- [12] Goldreich, P. and Sridhar, S. 1995, *ApJ*, 438, 763
- [13] Goldreich, P. and Sridhar, S. 1997, *ApJ*, 485, 680
- [14] Higdon, J. C. 1984, *ApJ*, 285, 109
- [15] Higdon, J. C. 1986, *ApJ*, 309, 1342
- [16] Higdon, J. C. and Conley, A. 1998, *AAS*, 192, 4609
- [17] Lambert, H. C. and Rickett, B. J. 2000, *ApJ*, 531, 883
- [18] Maron, J. and Goldreich, P. 2001, *ApJ*, 554, in press
- [19] Mathis, J. S. 1986, *ApJ*, 301, 423
- [20] Miller, W. M. III and Cox, D. P. 1993, *ApJ*, 417, 579
- [21] Monin, A. S. and Yaglom, A. M. 1971, *Statistical Fluid Mechanics* (Cambridge: MIT Press)
- [22] Moran, J. M., Rodriguez, L. R. Green, B., and Backer, D. C. 1990, *ApJ*, 348, 147

- [23] Müller, W. and Biskamp, D. 2000, Phys. Rev. Lett., 84, 475
- [24] Phillips, J. A. and Clegg, A. W. 1992, Nature, 360, 137
- [25] Quataert, E. 1998, ApJ, 500, 978
- [26] Reynolds, R. J. 1991, ApJ, 372, L17
- [27] Rickett, B. J. 1977, ARA&A, 15, 479
- [28] Rickett, B. J. 1990, ARA&A, 28, 561
- [29] Spitzer, L., Jr. 1978, Physical Processes in the Interstellar Medium (New York: John Wiley & Sons)
- [30] Sridhar, S. 1998, talk at conference on *Interstellar Turbulence*, Puebla, Mexico, 1998
- [31] Tennekes, H. and Lumley, J. L. 1972, A First Course in Turbulence (Cambridge: MIT Press)

## Chapter 2 Imbalanced Weak MHD Turbulence

Written with Peter Goldreich; to be submitted to the *Astrophysical Journal*

### ABSTRACT

MHD turbulence consists of waves that propagate along magnetic fieldlines, in both directions. When two oppositely directed waves collide, they distort each other, without changing their respective energies. In weak MHD turbulence, a given wave suffers many collisions before cascading. Imbalance means that more energy is going in one direction than the other. In general, MHD turbulence is imbalanced. A number of complications arise for the imbalanced cascade that are unimportant for the balanced one. We solve weak MHD turbulence that is imbalanced. Of crucial importance is that the energies going in both directions are forced to equalize at the dissipation scale. We call this the pinning of the energy spectra. It affects the entire inertial range. Weak MHD turbulence is particularly interesting because perturbation theory is applicable. Hence it can be described with a simple kinetic equation. Galtier et al. derived this kinetic equation. We present a simpler, more physical derivation, based on the picture of colliding wavepackets. In the process, we explain why Goldreich and Sridhar claimed that perturbation theory is inapplicable, and why this claim is wrong. (Our “weak” is equivalent to Goldreich and Sridhar’s “intermediate.”) We perform numerical simulations of the kinetic equation to verify our claims.

### 2.1 Introduction

MHD turbulence is ubiquitous in astrophysics. For example, it is present in the sun, the solar wind, the interstellar medium, molecular clouds, accretion disks, and galaxy clusters. Theoretical understanding of incompressible MHD turbulence has grown explosively in the last decade. Nonetheless, it remains underdeveloped.

Iroshnikov (1963) and Kraichnan (1965) developed a theory for MHD turbulence. They realized that the magnetic field at the largest lengthscale in a cascade directly affects all of the smaller lengthscales. Small-scale fluctuations can be treated as small-amplitude waves in the presence of a large mean magnetic field. By contrast, the large-scale velocity is unimportant for small-scale dynamics; it can be eliminated by a change of variables, since the equations of MHD are invariant under Galilean transformations.

Despite their realization of the importance of the mean magnetic field, Iroshnikov and Kraichnan assumed that small-scale fluctuations are isotropic. Numerical simulations later showed that this assumption is wrong. Even with isotropic excitation at large scales, fluctuations on smaller scales are elongated along the mean magnetic field (e.g., Montgomery and Turner 1981, Shebalin, Matthaeus,

and Montgomery 1983).

In retrospect, it is not very surprising to find elongated fluctuations. Arbitrary disturbances in incompressible MHD can be decomposed into shear-Alfvén and pseudo-Alfvén waves. Each wave travels either up or down the mean field at the Alfvén speed,  $v_A$ , which is the magnitude of the mean field in velocity units. Consider stirring a magneto-fluid with a spoon that is moving at speed  $v \ll v_A$ , for a time comparable to the spoon’s width divided by  $v$ . (In a turbulent cascade, one would expect  $v \ll v_A$  on small scales, since  $v$  decreases towards small scales, whereas  $v_A$  is unchanged.) Alfvén waves are radiated away from the spoon, parallel to the mean field with speed  $\pm v_A$ . After the disturbance is finished, there are two wavepackets travelling away from each other. Each wavepacket is elongated along the mean field, with parallel-to-transverse aspect ratio  $\sim v_A/v \gg 1$ .

The characteristics of MHD turbulence depend critically on the amount of elongation. When parallel-to-transverse aspect ratios are smaller than  $v_A/v$ , waves collide many times before cascading. Hence the turbulence is weak, and perturbation theory can be used to derive a kinetic equation and a spectrum (Sridhar and Goldreich 1994; see Zakharov, L’vov, and Falkovich 1992 for a general review of weak turbulence). Goldreich and Sridhar (1997) and Ng and Bhattacharjee (1997) deduced the spectrum of the balanced weak cascade from scaling arguments.<sup>1</sup> However, similar scaling arguments are inadequate for the imbalanced cascade (see §2.3.2 of the present chapter). Galtier et al. (2000) derived the kinetic equation for the weak imbalanced cascade. Their balanced spectrum agreed with that of Goldreich and Sridhar (1997) and Ng and Bhattacharjee (1997). They also presented a partial solution for the general imbalanced case. In §2.3.2, we explain why their solution is incomplete; in §2.4 we give the complete solution.

Even if aspect ratios are smaller than  $v_A/v$  on large scales, at a small enough scale they become comparable to  $v_A/v$ . Below this scale perturbation theory breaks down, and weak turbulence becomes strong. Goldreich and Sridhar (1995) worked out the scalings for the balanced strong cascade. They argued that aspect ratios are comparable to  $v_A/v$  at all scales in the strong regime. Strong turbulence is difficult, largely because it is non-perturbative. Although strong and weak turbulence differ in a number of ways, they also share many similarities. One of our main motivations for studying weak turbulence is to gain insight into strong turbulence. In particular, turbulence in the

---

<sup>1</sup>We relegate some of the history to a footnote because it can be confusing. Sridhar and Goldreich (1994) developed the first theory of MHD turbulence that accounted for the anisotropy of fluctuations. They claimed that three-wave processes vanish in weak MHD turbulence, and four-wave processes must be considered (i.e., perturbation theory is trivial to first order, so second order terms are important). As a result, they used four-wave couplings to derive a kinetic equation and a spectrum for weak MHD turbulence. Montgomery and Matthaeus (1995) claimed, and Ng and Bhattacharjee (1996) showed, that Sridhar and Goldreich (1994) are wrong, and three-wave processes do not vanish. Goldreich and Sridhar (1997) explained the contradiction: Sridhar and Goldreich (1994) had unknowingly assumed that the fieldline wander is small; in this case, three-wave couplings are negligible and the kinetic equation based on four-wave couplings is correct. In the more realistic case that fieldlines wander substantially, three-wave processes are important. Goldreich and Sridhar (1997) went on to argue that, in the latter case, perturbation theory is inappropriate, and couplings of all order are of comparable magnitude; so they called this intermediate turbulence. Galtier et al. (2000) argued that perturbation theory is appropriate, even when three-wave processes are important. In the Appendix of the present chapter, we use Goldreich and Sridhar’s picture of wavepackets following wandering fieldlines to clarify the controversy, and to explain why perturbation theory works. Because it does work, we call the cascade weak instead of intermediate.

solar wind is observed to be imbalanced; it cannot be understood without a theory for imbalanced strong MHD turbulence. Yet this theory is unknown. In a future paper, we will work it out by extending the results of the present chapter.

## 2.2 Basic Equations

Ideal incompressible MHD<sup>2</sup> is described by the following equations of motion:

$$\partial_t \mathbf{v} + \mathbf{v} \cdot \nabla \mathbf{v} = -\nabla P + \mathbf{B} \cdot \nabla \mathbf{B} , \quad (2.1)$$

$$\partial_t \mathbf{B} + \mathbf{v} \cdot \nabla \mathbf{B} = \mathbf{B} \cdot \nabla \mathbf{v} , \quad (2.2)$$

$$\nabla \cdot \mathbf{v} = \nabla \cdot \mathbf{B} = 0 . \quad (2.3)$$

The density is set to unity; the fluid velocity is  $\mathbf{v}$ ; the magnetic field in velocity units is  $\mathbf{B} \equiv (\text{magnetic field})/(4\pi)^{1/2}$ ; the total pressure is  $P \equiv p + B^2/2$ , which is the sum of the thermal and magnetic pressures. Viscous and resistive terms are neglected in the above equations; they are important on small scales, and will be included where required.

We decompose the magnetic field into its mean,  $v_A \hat{\mathbf{z}}$ , where  $v_A$  is the Alfvén speed and  $\hat{\mathbf{z}}$  is a unit vector, and into its fluctuating part  $\mathbf{b} \equiv \mathbf{B} - v_A \hat{\mathbf{z}}$ . With this decomposition, the equations of motion may be written in terms of the Elsasser variables,  $\mathbf{w}^\uparrow \equiv \mathbf{v} - \mathbf{b}$  and  $\mathbf{w}^\downarrow \equiv \mathbf{v} + \mathbf{b}$ , as follows:

$$\partial_t \mathbf{w}^\uparrow + v_A \partial_z \mathbf{w}^\uparrow = -\mathbf{w}^\downarrow \cdot \nabla \mathbf{w}^\uparrow - \nabla P , \quad (2.4)$$

$$\partial_t \mathbf{w}^\downarrow - v_A \partial_z \mathbf{w}^\downarrow = -\mathbf{w}^\uparrow \cdot \nabla \mathbf{w}^\downarrow - \nabla P , \quad (2.5)$$

$$\nabla \cdot \mathbf{w}^\uparrow = \nabla \cdot \mathbf{w}^\downarrow = 0 . \quad (2.6)$$

Note that  $P$  is not an independent degree of freedom. Taking the divergence of either equation (2.4) or (2.5) yields

$$P = -\nabla^{-2}(\nabla \mathbf{w}^\uparrow \cdot \nabla \mathbf{w}^\downarrow) , \quad (2.7)$$

where  $\nabla^{-2}$  is the inverse Laplacian. When  $\mathbf{w}^\downarrow = 0$ ,  $\mathbf{w}^\uparrow$  propagates undistorted upwards along the mean magnetic field with speed  $v_A$ . Similarly, when  $\mathbf{w}^\uparrow = 0$ ,  $\mathbf{w}^\downarrow$  propagates downwards at  $v_A$ . Nonlinear interactions occur only between oppositely directed wavepackets. It is these interactions that are responsible for turbulence.

There are three conserved quantities in incompressible MHD. Two of these are immediately apparent from equations (2.4)-(2.6): the energies of the upgoing and of the downgoing waves, i.e.,  $(\mathbf{w}^\uparrow)^2$  and  $(\mathbf{w}^\downarrow)^2$ . (Technically, these are twice the energy per unit mass. We refer to them as

---

<sup>2</sup>In this chapter, we consider only incompressible MHD turbulence; compressibility does not alter the dynamics very much (Lithwick and Goldreich 2001).

simply energies throughout the chapter.) These energies are directly related to the total (kinetic plus magnetic) energy  $\propto (w^\uparrow)^2 + (w^\downarrow)^2$  and to the cross-helicity  $\propto (w^\uparrow)^2 - (w^\downarrow)^2$ . The focus of this chapter is turbulence where the energies in the up and down waves differ, or, equivalently, where the cross-helicity is non-zero. The third conserved quantity is magnetic helicity; however, for reasons explained below, its conservation does not play a role in this chapter.

In MHD turbulence, on lengthscales much smaller than the outer scale, there is effectively a strong mean magnetic field that is due to fluctuations on the largest lengthscales. Gradients transverse to this mean field are much larger than gradients along it (e.g., Shebalin, Matthaeus, and Montgomery 1983, Goldreich and Sridhar 1995, 1997, Ng and Bhattacharjee 1996). This allows the MHD equations to be slightly simplified. The transverse components of equation (2.4), assuming that  $w_z^\downarrow \partial_z \mathbf{w}^\uparrow$  is much smaller than  $\mathbf{w}^\downarrow \cdot \nabla_\perp \mathbf{w}^\uparrow$ , are

$$\partial_t \mathbf{w}_\perp^\uparrow + v_A \partial_z \mathbf{w}_\perp^\uparrow \approx -\mathbf{w}_\perp^\downarrow \cdot \nabla_\perp \mathbf{w}_\perp^\uparrow - \nabla_\perp P, \quad (2.8)$$

where transverse components are denoted with the symbol  $\perp \equiv (x, y)$ . We assume that the parallel component of  $\mathbf{w}^\downarrow$  is either comparable to, or less than, its perpendicular component. We will see below that this is typically the case in the inertial range of a turbulent cascade. From equation (2.7),  $P \approx -\nabla_\perp^{-2}(\nabla_\perp \mathbf{w}^\uparrow : \nabla_\perp \mathbf{w}^\downarrow)$ ; therefore

$$\nabla_\perp \cdot \mathbf{w}_\perp^\uparrow \approx 0. \quad (2.9)$$

Similarly,

$$\partial_t \mathbf{w}_\perp^\downarrow - v_A \partial_z \mathbf{w}_\perp^\downarrow \approx -\mathbf{w}_\perp^\uparrow \cdot \nabla_\perp \mathbf{w}_\perp^\downarrow - \nabla_\perp P, \quad (2.10)$$

$$\nabla_\perp \cdot \mathbf{w}_\perp^\downarrow \approx 0. \quad (2.11)$$

If we change  $\approx$  to  $=$ , equations (2.8)-(2.11) form a closed set. They are called the equations of reduced MHD. They apply also in compressible MHD whenever transverse gradients are larger than parallel ones (e.g., Biskamp 1993). The main goal of this chapter is to solve these equations. Although the complete equations are not much more complicated, it simplifies our discussions to neglect parallel gradients relative to perpendicular ones at the outset. There are two conserved energies in reduced MHD:  $(w_\perp^\uparrow)^2$  and  $(w_\perp^\downarrow)^2$ . The magnetic helicity associated with  $\mathbf{w}_\perp^\uparrow$  and  $\mathbf{w}_\perp^\downarrow$  vanishes, and is therefore unimportant for their evolution.<sup>3</sup>

We also consider the parallel components of equations (2.4) and (2.5). Neglecting parallel gradi-

---

<sup>3</sup>In 3-D MHD, the magnetic helicity is  $\int \mathbf{A} \cdot \mathbf{B} d^3x$ , where  $\mathbf{A}$  is the magnetic potential ( $\nabla \times \mathbf{A} = \mathbf{B}$ ). If the magnetic field is broken up into its mean  $v_A \hat{\mathbf{z}}$ , and into fluctuations  $\mathbf{b}$ , then the only non-vanishing part of the helicity is  $\int \mathbf{a} \cdot \mathbf{b} d^3x$ , where  $\nabla \times \mathbf{a} = \mathbf{b}$ . In reduced MHD,  $\mathbf{b}$  is transverse to  $\hat{\mathbf{z}}$  and  $\mathbf{a}$  is nearly parallel to  $\hat{\mathbf{z}}$ , so the helicity nearly vanishes.

ents relative to transverse ones yields

$$\partial_t w_z^\uparrow + v_A \partial_z w_z^\uparrow \approx -\mathbf{w}_\perp^\downarrow \cdot \nabla_\perp w_z^\uparrow, \quad (2.12)$$

$$\partial_t w_z^\downarrow - v_A \partial_z w_z^\downarrow \approx -\mathbf{w}_\perp^\uparrow \cdot \nabla_\perp w_z^\downarrow. \quad (2.13)$$

Clearly,  $(w_z^\uparrow)^2$  and  $(w_z^\downarrow)^2$  are conserved quantities. The transverse equations describing reduced MHD are unaffected by these parallel equations because the former are independent of  $w_z^\uparrow$  and  $w_z^\downarrow$ . Nonetheless, the parallel equations have observable consequences.

It is conventional to decompose the normal modes of linearized incompressible MHD,  $\mathbf{w}^\uparrow$  and  $\mathbf{w}^\downarrow$ , into shear-Alfvén and pseudo-Alfvén waves. These correspond to the Alfvén and slow waves of compressible MHD. When perpendicular gradients are much larger than parallel ones,  $\mathbf{w}_\perp^\uparrow$  and  $\mathbf{w}_\perp^\downarrow$  are nearly equivalent to shear-Alfvén waves;  $w_z^\uparrow$  and  $w_z^\downarrow$  are nearly equivalent to pseudo-Alfvén waves.

Also observationally relevant is the evolution of a passive scalar  $s$ , which satisfies  $\partial_t s + \mathbf{v} \cdot \nabla s = 0$ . In terms of Elsasser variables, and after neglecting parallel gradients, the passive scalar satisfies

$$\partial_t s \approx -(1/2)(\mathbf{w}_\perp^\uparrow + \mathbf{w}_\perp^\downarrow) \cdot \nabla_\perp s. \quad (2.14)$$

To avoid a proliferation of subscripts, in the remainder of this chapter we drop the  $\perp$  from  $\mathbf{w}_\perp^\uparrow$  and  $\mathbf{w}_\perp^\downarrow$ . To denote the parallel components, we use  $w_z^\uparrow$  and  $w_z^\downarrow$ .

## 2.3 Weak Turbulence: Heuristic Discussion

### 2.3.1 Scaling Relation

MHD turbulence can be understood from the dynamics of  $\mathbf{w}^\uparrow$  and  $\mathbf{w}^\downarrow$  (eqs. [2.8-2.11] for reduced MHD, dropping  $\perp$  subscripts). To linear order,  $\mathbf{w}^\uparrow$  is a wave that propagates up the mean magnetic fieldlines at the Alfvén speed,  $v_A$ ;  $\mathbf{w}^\downarrow$  propagates down at  $v_A$ . Each wave perturbs the mean magnetic fieldlines. Nonlinear terms describe the interaction between oppositely directed waves: each wave nearly follows the fieldlines perturbed by its collision partner.<sup>4</sup>

Consider an upgoing wavepacket that encounters a train of downgoing wavepackets. As the upgoing wave travels up the length of the downgoing train, it is gradually distorted. It tries to follow the perturbed fieldlines in the downgoing train, but these fieldlines wander, i.e., the transverse

<sup>4</sup>The equation for a quantity  $f$  that travels upwards at speed  $v_A$ , while following the magnetic fieldlines of the down-going  $\mathbf{w}^\downarrow$  is  $(\partial_t + v_A \partial_z + \mathbf{w}^\downarrow \cdot \nabla_\perp) f = 0$ . Equation (2.8) for  $\mathbf{w}^\uparrow$  differs from this because of the pressure term, which is required to keep  $\mathbf{w}^\uparrow$  incompressible, while conserving the energy  $(w^\uparrow)^2$ . Thus  $\mathbf{w}^\uparrow$  does not exactly follow the fieldlines of  $\mathbf{w}^\downarrow$ . Nonetheless, we show in the Appendix that this deviation does not greatly affect the behaviour of the turbulence. Dissipation is a second effect that prevents the following of fieldlines. In the present discussion, we consider lengthscales that are sufficiently large that dissipation can be neglected.

separation between any two fieldlines changes. After each downgoing wavepacket, the amount of wander is random; after many wavepackets, the wander tends to increase, as in a random walk. When the up-wave has travelled sufficiently far along the down-waves that the typical amount of wander is comparable to its own transverse size, the up-wave cascades.

To be quantitative, let each downgoing wave in the train have a typical amplitude  $w_\lambda^\downarrow$ , a transverse size  $\lambda$ , and a parallel size  $\Lambda$ , where “transverse” and “parallel” refer to the orientation relative to the mean magnetic field. The most important collisions are between wavepackets of comparable transverse size (see §2.3.4). So let the upgoing wave have transverse size  $\lambda$  as well.

Since each downgoing wavepacket has a typical perturbed magnetic field of magnitude  $\sim w_\lambda^\downarrow$  (neglecting the factor of 1/2), it bends the fieldlines by the angle  $w_\lambda^\downarrow/v_A$ ; the transverse displacement of a fieldline through this wavepacket is  $(w_\lambda^\downarrow/v_A)\Lambda$ ; and the wander of two typical fieldlines through the wavepacket, if they are initially separated by  $\lambda$ , is also  $(w_\lambda^\downarrow/v_A)\Lambda$ .

In weak turbulence, the wander through a single wavepacket is smaller than the wavepacket’s transverse size,

$$\frac{w_\lambda^\downarrow}{v_A}\Lambda \ll \lambda \quad \text{and} \quad \frac{w_\lambda^\uparrow}{v_A}\Lambda \ll \lambda, \quad (2.15)$$

i.e., the parallel-to-transverse aspect ratios are smaller than  $v_A/w_\lambda^\downarrow$  and  $v_A/w_\lambda^\uparrow$ . (When these inequalities are not satisfied, strong turbulence is applicable; see §2.3.4.) An upgoing wavepacket must travel through many downgoing ones before cascading. After  $N$  downgoing wavepackets, fieldlines have wandered a distance  $\sim N^{1/2}(w_\lambda^\downarrow/v_A)\Lambda$ , assuming that wavepackets are statistically independent. The upgoing wavepacket is fully distorted—and hence cascaded—when the fieldlines it is following wander a distance  $\lambda$ , i.e., when  $N \sim (\lambda v_A/\Lambda w_\lambda^\downarrow)^2$ . Since each downgoing wavepacket is crossed in the time  $\Lambda/v_A$ , the cascade time of the upgoing wavepacket is

$$t_{\text{cas}}^\uparrow \sim \left(\frac{\lambda v_A}{\Lambda w_\lambda^\downarrow}\right)^2 \frac{\Lambda}{v_A} \sim \left(\frac{\lambda}{w_\lambda^\downarrow}\right)^2 \frac{v_A}{\Lambda}. \quad (2.16)$$

In this time, the upgoing wavepacket travels a distance  $v_A t_{\text{cas}}^\uparrow$ , which is much larger than  $\Lambda$  (see eq. [2.15]). Consequently, if the upgoing wavepacket also has a parallel size  $\Lambda$ , then as its energy is cascaded to smaller transverse lengthscales, it does not cascade to smaller parallel lengthscales:

$$\Lambda = \text{scale independent} . \quad (2.17)$$

We assume throughout this chapter that the upgoing waves’ parallel lengthscale is the same as that of the downgoing waves,  $\Lambda$ ; the extension to the case when they differ is trivial (as long as the inequalities (2.15) are both satisfied, with the appropriate  $\Lambda$ ’s).

We calculate the steady state energy spectra by using Kolmogorov’s picture of energy flowing from large to small lengthscales. The energy in up-waves flows from lengthscales larger than  $\lambda$  to

those smaller than  $\lambda$  at the rate

$$\epsilon^\uparrow \sim \frac{(w_\lambda^\uparrow)^2}{v_{\text{cas}}^\uparrow} \sim \left[ \frac{w_\lambda^\uparrow w_\lambda^\downarrow}{\lambda} \right]^2 \frac{\Lambda}{v_A}. \quad (2.18)$$

We call this the flux. In steady state, it must be independent of  $\lambda$ , so

$$w_\lambda^\uparrow w_\lambda^\downarrow \propto \lambda. \quad (2.19)$$

### 2.3.2 Insufficiency of Scaling Arguments for the Imbalanced Cascade

When the cascade is balanced, the steady state solution is simple:  $w_\lambda^\uparrow = w_\lambda^\downarrow \propto \lambda^{1/2}$  and  $\epsilon^\uparrow = \epsilon^\downarrow \sim (w_\lambda^\uparrow)^4 \Lambda / \lambda^2 v_A$ , (Goldreich and Sridhar 1997, Ng and Bhattacharjee 1997). When it is imbalanced, a number of complications arise.

By the symmetry between up- and down-going waves, equation (2.18) is also equal to the flux of down-going waves:

$$\epsilon^\downarrow \sim \left[ \frac{w_\lambda^\uparrow w_\lambda^\downarrow}{\lambda} \right]^2 \frac{\Lambda}{v_A}. \quad (2.20)$$

Constancy of  $\epsilon^\downarrow$  is forced by the constancy of  $\epsilon^\uparrow$ , and does not yield new information. One implication is that scaling arguments are insufficient to determine the flux ratio  $\epsilon^\uparrow / \epsilon^\downarrow$ . Physically, any flux ratio should be possible. But without the dimensionless coefficients of equations (2.18) and (2.20),  $\epsilon^\uparrow / \epsilon^\downarrow$  cannot be determined. The coefficients depend on the spectral slope of  $w_\lambda^\uparrow$  (or equivalently of  $w_\lambda^\downarrow \propto \lambda / w_\lambda^\uparrow$ , eq. [2.19]), and cannot be obtained from scaling arguments. Galtier et al. (2000) calculated the coefficients using kinetic equations. (We explain how below.) Therefore these authors were able to relate the flux ratio to the spectral slopes.

However, the arguments presented thus far are still insufficiently constraining. Equations (2.18) and (2.20) constrain only the product  $w_\lambda^\uparrow w_\lambda^\downarrow$ . There are seemingly an infinite number of solutions with given values of  $\epsilon^\uparrow$  and  $\epsilon^\downarrow$ , since  $w_\lambda^\uparrow$  can be multiplied by any constant as long as  $w_\lambda^\downarrow$  is divided by this same constant. Furthermore, we expect on physical grounds that if the values of  $w_\lambda^\uparrow$  and  $w_\lambda^\downarrow$  at a given lengthscale are fixed (instead of the values of  $\epsilon^\uparrow$  and  $\epsilon^\downarrow$ ), the cascade should be completely constrained; however, in this case the constancy of equations (2.18) and (2.20) leaves the spectral slope of  $w_\lambda^\uparrow$  completely undetermined—even given the coefficients derived by Galtier et al. (2000). Do the two spectra cross? Are they cut off by dissipation at the same scale? All of these problems for the imbalanced cascade can be resolved once the dynamics at the dissipation scale is understood.

### 2.3.3 Dynamics at the Dissipation Scale: Pinned Spectra

The main result of the present chapter is that the energies of the up- and down-going waves are forced to equalize—they are “pinned”—at the dissipation scale. This completely constrains the cascade.

It is very surprising that the dynamics at the dissipation scale has such an important influence. In this subsection we explain why pinning occurs. In §2.4, we give the resulting solution of the steady state cascade.

From equation (2.16), the cascade time of the up-going waves is inversely proportional to the energy of the down-going ones:  $t_{\text{cas}}^\uparrow = (\lambda/w_\lambda^\downarrow)^2(v_A/\Lambda)$ , and similarly for the downgoing waves. We consider how the spectra evolve if initially, on lengthscales comparable to the dissipation scale, waves going in one direction are more energetic than the oppositely directed ones. To facilitate the discussion, we refer to Figure 2.2, which presents the results from a numerical simulation that we discuss in detail below. In the middle panels of Figures 2.2a-d, we plot  $e^\uparrow(k) \sim (\lambda w_\lambda^\uparrow)^2$  and  $e^\downarrow(k) \sim (\lambda w_\lambda^\downarrow)^2$  as functions of wavenumber  $k = 1/\lambda$ . Note that  $w_\lambda^\downarrow > w_\lambda^\uparrow$ , so  $t_{\text{cas}}^\downarrow > t_{\text{cas}}^\uparrow$ . We consider a lengthscale-dependent dissipation time,  $t_{\text{diss}}$ , that is the same for both up- and down-going waves.<sup>5</sup> On large lengthscales, the dissipation timescale is much longer than the cascade times. Towards smaller lengthscales,  $t_{\text{diss}}$  decreases faster than both  $t_{\text{cas}}^\uparrow$  and  $t_{\text{cas}}^\downarrow$ . The effects of dissipation are felt on lengthscales where  $t_{\text{diss}}$  is smaller than, or comparable to, either  $t_{\text{cas}}^\uparrow$  or  $t_{\text{cas}}^\downarrow$ . Since  $t_{\text{cas}}^\downarrow > t_{\text{cas}}^\uparrow$  in the vicinity of the dissipation scale, the largest lengthscale at which dissipation effects are felt is where  $t_{\text{cas}}^\downarrow \sim t_{\text{diss}}$ . In Figure 2.2a, this is at  $k \sim 1,000$ . We now let the spectra evolve (Figs. 2.2b-c). Since  $w_\lambda^\downarrow$  feels the dissipative effects at  $k \sim 1,000$ , its spectrum is exponentially cut off at smaller scales. This implies that the cascade time of the up waves,  $t_{\text{cas}}^\uparrow$ , increases exponentially towards smaller scales. As a result, up-wave energy that is being cascaded from large to small scales cannot be cascaded fast enough at  $k \gtrsim 1,000$ . Therefore the up-waves' energy flux is backed up, and the  $w_\lambda^\uparrow$  spectrum rises. Furthermore, as  $w_\lambda^\uparrow$  rises,  $t_{\text{cas}}^\downarrow$  falls, so the cascade time of the down waves on small scales decreases, and the down-wave spectrum falls. The final result is that the two spectra are pinned at the dissipation scale. This pinning occurs very quickly: on the dissipation timescale.

### 2.3.4 Two Peripheral Issues

This subsection may be skipped on a first reading, without affecting our main line of argument.

#### Locality

In §2.3.1, it is assumed that the dominant interaction is between those wavepackets that have comparable transverse lengthscale, i.e., interactions are local in lengthscale. In this section, we justify this assumption.

We focus on the cascading of an upgoing wavepacket by downgoing ones. Let the upgoing wavepacket have transverse size  $\lambda$ , and let the downgoing wavepackets each have transverse size  $l$ , parallel size  $\Lambda$ , and amplitude  $w_l^\downarrow$ . The upgoing wavepacket cascades when the fieldlines it is

<sup>5</sup>For example, in the simulation presented in Figure 2.2,  $t_{\text{diss}} \simeq \lambda^2/\nu$ , where  $\nu$  is both the viscosity and the resistivity.

following wander a distance comparable to its transverse size,  $\lambda$ .

We consider first the case that  $l < \lambda$ . Two fieldlines that are separated by  $\lambda$  at the head of the downgoing wavepackets wander independently of each other. Their transverse separation after  $N$  downgoing wavepackets increases by

$$N^{1/2}(w_l^\dagger/v_A)\Lambda \quad , \quad l < \lambda . \quad (2.21)$$

Conversely, if  $l > \lambda$ , then the magnetic field at two points separated by  $\lambda$  differs by  $\sim w_l^\dagger \lambda/l$ ; consequently, the fieldlines separate by

$$N^{1/2}(w_l^\dagger/v_A)(\lambda/l)\Lambda \quad , \quad l > \lambda , \quad (2.22)$$

as long as this separation is not much larger than a few  $\lambda$ .

For interactions to be local, i.e., for the amount of fieldline wander seen by an up-wave of transverse size  $\lambda$  to be maximized by those down-waves that have  $l \sim \lambda$ , the following two conditions must hold: (i)  $w_l^\dagger$  is an increasing function of  $l$  (eq. [2.21]); and (ii)  $w_l^\dagger/l$  is a decreasing function of  $l$  (eq. [2.22]). So the cascade is local if

$$0 < \frac{d \ln w_\lambda^\dagger}{d \ln \lambda} < 1 . \quad (2.23)$$

The same condition clearly holds for  $w_\lambda^\uparrow$ . In terms of the steady-state scalings,  $w_\lambda^\uparrow \propto \lambda^{(1+\alpha)/2}$  and  $w_\lambda^\dagger \propto \lambda^{(1-\alpha)/2}$ , the condition

$$-1 < \alpha < 1 \quad (2.24)$$

is required for the cascade to be local; otherwise, nonlocal effects are important. Galtier et al. (2000) derived the inequalities in (2.24) from the kinetic equation.

There is a second reason why the condition  $d \ln w_\lambda^\uparrow/d \ln \lambda < 1$  is necessary for our heuristic arguments to be valid. When this condition is violated, the energy in up-waves that have lengthscale  $\lambda$ , i.e.,  $(w_\lambda^\uparrow)^2$ , is smaller than the contribution to the energy at lengthscale  $\lambda$  by upgoing waves with  $l > \lambda$ , i.e.,  $(w_l^\uparrow \lambda/l)^2$ . This is a different kind of non-locality than considered previously: energy cascades directly from large to small lengthscales, skipping over intermediate lengthscales.

### Transition to Strong Turbulence

Weak turbulence is applicable when  $w_\lambda^\dagger \Lambda/v_A \ll \lambda$  and  $w_\lambda^\uparrow \Lambda/v_A \ll \lambda$  (eq. [2.15]). Since  $\lambda$  decreases faster than both  $w_\lambda^\dagger$  and  $w_\lambda^\uparrow$  (eq. [2.23]), even if these inequalities are satisfied at large lengthscales, they are violated at small ones. Thus weak turbulence has a limited inertial range.

Of greater relevance than weak turbulence for describing astrophysical sites such as the solar

wind is strong turbulence, which is applicable when the above inequalities are violated. In this case, the fieldline separation within a single wavepacket is not smaller than the transverse size of the wavepacket. This has two implications. First, equation (2.16) for the cascade time is no longer valid; and second, the parallel size of wavepackets  $\Lambda$  decreases towards smaller scales because the head and tail of a wavepacket are independently cascaded. The balanced strong cascade is worked out by Goldreich and Sridhar (1995); we discuss the imbalanced strong cascade in a future paper. Strong turbulence is more difficult than weak turbulence because perturbation theory is not valid. Nonetheless, a number of the features of weak turbulence that we develop in the present chapter are applicable to strong turbulence. This is our main motivation for studying the weak cascade: to gain insight into the strong cascade.

Since this chapter is concerned with weak turbulence, we choose the dissipation scale to be sufficiently large that the inequalities (2.15) are never violated, and the entire cascade is weak. By choosing a sufficiently small  $\Lambda$ , the lengthscale at which weak turbulence transitions to strong can be made as small as desired.

## 2.4 Steady State Energy Spectra

The steady state energy spectra are simple to calculate given the scaling  $w_\lambda^\uparrow w_\lambda^\downarrow \propto \lambda$  (eq. [2.19]), and the fact that the spectra are pinned at the dissipation scale,  $\lambda_{\text{diss}}$ . We denote the value of  $w_\lambda^\uparrow$  and  $w_\lambda^\downarrow$  at  $\lambda_{\text{diss}}$  by  $w_{\text{diss}}$ . We can then express the energy spectra as follows

$$w_\lambda^\uparrow = w_{\text{diss}} \left( \frac{\lambda}{\lambda_{\text{diss}}} \right)^{(1+\alpha)/2} \quad (2.25)$$

$$w_\lambda^\downarrow = w_{\text{diss}} \left( \frac{\lambda}{\lambda_{\text{diss}}} \right)^{(1-\alpha)/2} . \quad (2.26)$$

These spectra are valid in the inertial range, i.e., on lengthscales larger than the dissipation scale, and smaller than the outer scale, at which the turbulence is stirred. There are three parameters that must be calculated to constrain the spectra:  $w_{\text{diss}}$ ,  $\lambda_{\text{diss}}$ , and  $\alpha$ .

For definiteness, we assume that dissipation is caused by a diffusive process, with a viscous term of the form  $\nu \nabla^2 \mathbf{v}$  in equation (2.1) and a resistive term of the form  $\nu \nabla^2 \mathbf{B}$  in equation (2.2). This implies that the magnetic Prandtl number is equal to one.<sup>6</sup> The dissipative timescale is

$$t_{\text{diss}}(\lambda) \simeq \frac{\lambda^2}{\nu} . \quad (2.27)$$

At the dissipation scale, the cascade time is equal to  $t_{\text{diss}}$ , i.e.,  $t_{\text{cas}}(\lambda_{\text{diss}}) = t_{\text{diss}}(\lambda_{\text{diss}})$ , which implies

---

<sup>6</sup>It is straightforward to consider other forms for the dissipation. We consider hyperviscosity in §2.8.

that

$$\frac{\lambda_{\text{diss}}^2}{\nu} \simeq \left( \frac{\lambda_{\text{diss}}}{w_{\text{diss}}} \right)^2 \frac{v_A}{\Lambda}, \quad (2.28)$$

after using equations (2.16) and (2.27); so

$$w_{\text{diss}} \simeq \left( \frac{\nu v_A}{\Lambda} \right)^{1/2}. \quad (2.29)$$

If the dissipation is caused by a diffusive process, then  $w_{\text{diss}}$  is independent of the energies and the fluxes. This is not true for  $\lambda_{\text{diss}}$  or  $\alpha$ .

To calculate  $\lambda_{\text{diss}}$  and  $\alpha$ , we consider two alternative scenarios: first, the energies at the outer scale are specified, and second the fluxes are specified.

### 2.4.1 Fixed Energy at the Outer Scale

We assume that the energies are specified at the outer scale,  $\lambda_{\text{out}}$ , where  $w_{\lambda}^{\uparrow}$  and  $w_{\lambda}^{\downarrow}$  are denoted by  $w_{\lambda_{\text{out}}}^{\uparrow}$  and  $w_{\lambda_{\text{out}}}^{\downarrow}$ . Since  $w_{\lambda}^{\uparrow} w_{\lambda}^{\downarrow} / \lambda = w_{\text{diss}}^2 / \lambda_{\text{diss}}$ ,

$$\lambda_{\text{diss}} = \frac{\lambda_{\text{out}}}{w_{\lambda_{\text{out}}}^{\uparrow} w_{\lambda_{\text{out}}}^{\downarrow}} \frac{\nu v_A}{\Lambda}, \quad (2.30)$$

after using equation (2.29).

Dividing equation (2.25) by equation (2.26) yields  $w_{\lambda_{\text{out}}}^{\uparrow} / w_{\lambda_{\text{out}}}^{\downarrow} = (\lambda_{\text{out}} / \lambda_{\text{diss}})^{\alpha}$ , so

$$\alpha = \frac{\ln(w_{\lambda_{\text{out}}}^{\uparrow} / w_{\lambda_{\text{out}}}^{\downarrow})}{\ln(\lambda_{\text{out}} / \lambda_{\text{diss}})} = \frac{\ln(w_{\lambda_{\text{out}}}^{\uparrow} / w_{\lambda_{\text{out}}}^{\downarrow})}{\ln(w_{\lambda_{\text{out}}}^{\uparrow} w_{\lambda_{\text{out}}}^{\downarrow} (\Lambda / \nu v_A))}. \quad (2.31)$$

With  $w_{\lambda_{\text{out}}}^{\uparrow} / w_{\lambda_{\text{out}}}^{\downarrow}$  fixed, the cascade is balanced ( $\alpha \rightarrow 0$ ) in the limit that the inertial range is infinitely large ( $\lambda_{\text{out}} / \lambda_{\text{diss}} \rightarrow \infty$ ).

Inserting equations (2.29), (2.30), and (2.31) into the spectrum (eqs. [2.25] and [2.26]) gives the solution to the steady state imbalanced weak cascade, assuming that  $w_{\lambda_{\text{out}}}^{\uparrow}$  and  $w_{\lambda_{\text{out}}}^{\downarrow}$  are specified.

### 2.4.2 Fixed Flux

Heuristic arguments are insufficient for calculating the ratio of the fluxes,  $\epsilon^{\uparrow} / \epsilon^{\downarrow}$  (see §2.3.2). We would like to determine both  $\epsilon^{\uparrow}$  and  $\epsilon^{\downarrow}$  given the spectra of  $w_{\lambda}^{\uparrow}$  and  $w_{\lambda}^{\downarrow}$ . Conversely, we would like to determine the spectra when  $\epsilon^{\uparrow}$  and  $\epsilon^{\downarrow}$  are specified. To accomplish this, the dimensionless coefficients of equations (2.18) and (2.20) are required. For a given power-law solution,  $w_{\lambda}^{\uparrow} \propto \lambda^{(1+\alpha)/2}$  and  $w_{\lambda}^{\downarrow} \propto \lambda^{(1-\alpha)/2}$ , these coefficients depend on  $\alpha$ :

$$\epsilon^{\uparrow} = f(\alpha) \left[ \frac{w_{\lambda}^{\uparrow} w_{\lambda}^{\downarrow}}{\lambda} \right]^2 \frac{\Lambda}{v_A}, \quad (2.32)$$

$$\epsilon^\downarrow = f(-\alpha) \left[ \frac{w_\lambda^\uparrow w_\lambda^\downarrow}{\lambda} \right]^2 \frac{\Lambda}{v_A}, \quad (2.33)$$

where  $f(\alpha)$  is a dimensionless function of  $\alpha$  that must be calculated. By the symmetry between up and down waves,  $\epsilon^\uparrow$  and  $\epsilon^\downarrow$  are both proportional to the same function  $f$ , evaluated at  $\pm\alpha$ . Since heuristic arguments are insufficient to calculate the function  $f$ , it is fortunate that weak turbulence can be analyzed with perturbation theory. We compute  $f$  in the Appendix (eq. [2.85]); Galtier et al. (2000) also computed it.

The ratio of the fluxes is related to  $\alpha$  by

$$\frac{\epsilon^\uparrow}{\epsilon^\downarrow} = \frac{f(\alpha)}{f(-\alpha)}. \quad (2.34)$$

The limit  $|\alpha| \ll 1$  is particularly interesting. For given outer-scale energies, if the inertial range is very large then the steady state cascade is nearly balanced (see the discussion below eq. [2.31]), and  $|\alpha| \ll 1$ . In this limit, we show in the Appendix that  $f(\alpha) \simeq f(0) \cdot (1 + 0.5\alpha)$  (see eq. [2.86]). Thus

$$\frac{\epsilon^\uparrow}{\epsilon^\downarrow} - 1 \simeq \alpha, \quad |\alpha| \ll 1. \quad (2.35)$$

To linear order in  $\alpha$ , the product of the fluxes is independent of  $\alpha$ :

$$\epsilon^\uparrow \epsilon^\downarrow \simeq \left[ \frac{w_\lambda^\uparrow w_\lambda^\downarrow}{\lambda} \right]^4 \left( \frac{\Lambda}{v_A} \right)^2 = \left[ \frac{w_{\text{diss}}^2}{\lambda_{\text{diss}}} \right]^4 \left( \frac{\Lambda}{v_A} \right)^2, \quad |\alpha| \ll 1, \quad (2.36)$$

neglecting the unimportant order-unity multiplicative factor  $[f(0)]^2$ .

In sum, if  $\epsilon^\uparrow$  and  $\epsilon^\downarrow$  are specified, then the spectra of  $w_\lambda^\uparrow$  and  $w_\lambda^\downarrow$  are given by equations (2.25) and (2.26), with  $w_{\text{diss}}$ ,  $\alpha$ , and  $\lambda_{\text{diss}}$  given by equations (2.29), (2.35), and (2.36), in the limit of small  $|\alpha|$ . Note that, to first order in  $\alpha$ , the only relation that depends on the kinetic equation (i.e., on the form of  $f(\alpha)$ ) is equation (2.35).

## 2.5 Kinetic Equations in Weak Turbulence

We show in the Appendix that perturbation theory can be used to describe weak turbulence. As a consequence, the evolution of the energy spectra of the up- and down-waves is described by a closed set of two equations; in other words, the two-point correlation functions evolve independently of all higher-order correlation functions. This is a great simplification.

Evolution equations for the energy spectra—the kinetic equations—were obtained in Galtier et al. (2000, 2001). We present an alternate, more physical, derivation in the Appendix. Such a derivation is useful because it clears up a number of erroneous claims that have been made in the literature—in particular, the claim of Goldreich and Sridhar (1997) that perturbation theory is inapplicable.

In the following, we summarize the result derived in the Appendix. The kinetic equations are given in Fourier-space. We Fourier transform  $\mathbf{w}^\uparrow(x, y, z, t)$  and  $\mathbf{w}^\downarrow(x, y, z, t)$  in  $x$  and  $y$  (but not  $z$ ), and denote the transforms by  $\mathbf{w}_{\mathbf{k}}^\uparrow(z, t)$  and  $\mathbf{w}_{\mathbf{k}}^\downarrow(z, t)$ , where  $\mathbf{k}$  is purely transverse ( $k_z \equiv 0$ ). We define the energy spectra  $e^\uparrow$  and  $e^\downarrow$  such that

$$\langle \mathbf{w}_{\mathbf{k}}^\uparrow(z, t) \cdot \mathbf{w}_{\mathbf{k}'}^\uparrow(z, t) \rangle = e^\uparrow(k, t) \delta(\mathbf{k} + \mathbf{k}') \quad (2.37)$$

$$\langle \mathbf{w}_{\mathbf{k}}^\downarrow(z, t) \cdot \mathbf{w}_{\mathbf{k}'}^\downarrow(z, t) \rangle = e^\downarrow(k, t) \delta(\mathbf{k} + \mathbf{k}') , \quad (2.38)$$

where  $\delta(\mathbf{k})$  is a two-dimensional Dirac delta-function, and angled brackets denote both an ensemble average and an average over  $z$ . (We assume that the turbulence is homogeneous in  $z$ .) Both  $e^\uparrow$  and  $e^\downarrow$  are real. The turbulence is isotropic in the transverse plane, so  $e^\uparrow$  and  $e^\downarrow$  are functions of the magnitude of  $\mathbf{k}$ .

Within an order-unity factor,  $k^2 e^\uparrow \sim (w_\lambda^\uparrow)^2$  when  $\lambda = 1/k$ . Recall from §2.3 that  $w_\lambda^\uparrow$  is the typical value of  $\mathbf{w}^\uparrow$  on lengthscale  $\lambda$ ; more precisely, it can be defined as the square root of the structure function of  $\mathbf{w}^\uparrow$ . Therefore the steady-state scaling  $w_\lambda^\uparrow \propto \lambda^{(1+\alpha)/2}$  (eq. [2.25]) corresponds to  $e^\uparrow \propto k^{-(3+\alpha)}$ ; similarly,  $w_\lambda^\downarrow \propto \lambda^{(1-\alpha)/2}$  corresponds to  $e^\downarrow \propto k^{-(3-\alpha)}$ . In comparing our results with those of Galtier et al. (2000), note that these authors use the one-dimensional spectrum, which they denote  $E^\pm$ , while we use the two-dimensional spectrum. So,  $E^+ \sim k e^\uparrow$  and  $E^- \sim k e^\downarrow$ , within a multiplicative constant.<sup>7</sup>

From equation (2.80) in the Appendix, the kinetic equation for the up-waves is

$$\frac{\partial}{\partial t} \Big|_k e^\uparrow(k, t) = \frac{\Lambda}{v_A} k^2 \int_0^\infty dk_\uparrow k_\uparrow^3 (e^\uparrow(k_\uparrow, t) - e^\uparrow(k, t)) \int_0^{2\pi} d\theta \sin^2 \theta \cos^2 \theta \frac{e^\downarrow(k_\downarrow, t)}{k_\downarrow^2} \quad (2.39)$$

where

$$k_\downarrow \equiv (k^2 + k_\uparrow^2 - 2kk_\uparrow \cos \theta)^{1/2} . \quad (2.40)$$

There must also be a term describing dissipation on small lengthscales. If the dissipation is diffusive and the viscosity ( $\nu$ ) is equal to the resistivity, then  $-\nu k^2 e^\uparrow$  is to be added to the right-hand side of the above equation.

Because of the symmetry between up- and down-waves, the equation for  $e^\downarrow$  is the same as for  $e^\uparrow$ , but with  $e^\uparrow$  and  $e^\downarrow$  everywhere switched. The steady-state relation between the energy and the flux that we use above (eq. [2.32]) is obtained in the Appendix by setting the right-hand side of equation (2.39) zero.

---

<sup>7</sup>The one-dimensional spectrum is defined such that its integral over  $dk$  is proportional to the energy. Similarly, the integral of the two-dimensional spectrum over  $d^2\mathbf{k}$  is proportional to the energy.

## 2.6 Numerical Simulations of Kinetic Equations

In this section we present the results of numerical simulations which verify our previous heuristic discussions: in particular, the pinning of spectra and the scaling of the spectra in steady state.

It is much faster to simulate kinetic equations than the full equations of motion for  $w^\uparrow$  and  $w^\downarrow$ . There are a number of reasons for this. First, the kinetic equations are only one dimensional, since homogeneity has been assumed parallel to the mean magnetic field, and isotropy has been assumed in the plane transverse to the mean magnetic field. Second, and more importantly, the averaged energies  $e^\uparrow$  and  $e^\downarrow$  are much smoother functions of  $k$  than  $w^\uparrow$  and  $w^\downarrow$ . Thus, a logarithmically-spaced grid can be used, which logarithmically reduces the number of variables that need to be evolved. The result is an enormous reduction in computational time. A typical kinetic simulation takes a few hours on a PC to reach steady state. A comparable fully three-dimensional MHD simulation, would require many months, if not years, on the fastest supercomputers.

Galtier et al. (2000) also perform numerical simulations of the kinetic equation. However, their investigation of the imbalanced cascade is very incomplete. In particular, they only plot spectra of the product  $e^\uparrow e^\downarrow$ . They do not discuss the pinning of the spectra at the dissipation scale, which is crucial to the evolution of the cascade.

For our numerical simulations of the kinetic equations (eq. [2.39] and the analogous  $e^\downarrow$  equation), we set  $\Lambda/v_A = 1$ . This corresponds to absorbing  $\Lambda/v_A$  into  $e^\uparrow$  and  $e^\downarrow$ . We evaluate all functions of  $k$  on a fixed, logarithmically-spaced grid with  $k = 2^{i/8}$ ,  $i = 1, \dots, 100$ . At the outer scale,  $k_{\text{out}} = 2^{1/8} = 1.09$  and the maximum  $k$  is  $k_{\text{max}} = 2^{100/8} = 5793$ . The double integral in the kinetic equation is performed by summing the values of the integrand evaluated on the  $k$ -space grid. The factor that depends on  $\theta$  is averaged in the vicinity of each grid point, i.e., at each  $(k_\uparrow, k_\downarrow)$ . Since  $\theta$  is a function of  $k_\uparrow/k$  and  $k_\downarrow/k$ , and since the grid is logarithmic, the averaged angular factor can be precomputed and stored in a two-dimensional matrix, each element of which is the average in the vicinity of  $(k_\uparrow/k, k_\downarrow/k)$ .<sup>8</sup> We integrate in time with second-order Runge-Kutta.

For the discussions of the simulations that follow, recall that the energies of the waves at a given lengthscale  $\lambda = 1/k$  are, within unimportant multiplicative constants,

$$(w_\lambda^\uparrow)^2 \sim k^2 e^\uparrow(k), \quad (w_\lambda^\downarrow)^2 \sim k^2 e^\downarrow(k). \quad (2.41)$$

---

<sup>8</sup>In evaluating the integral near  $k_{\text{out}}$ , it is necessary to use the values of  $e^\uparrow(k_\uparrow)$  and  $e^\downarrow(k_\downarrow)$  for  $k_\uparrow, k_\downarrow < k_{\text{out}}$ . Since these values are off of the grid, some method of extrapolation must be used. In the runs that we present in this chapter, we extrapolate with  $e^\uparrow, e^\downarrow \propto k^{-2}$ . We have also experimented with a flat spectrum for  $k < k_{\text{out}}$ :  $e^\uparrow = e^\uparrow(k_{\text{out}})$ ,  $e^\downarrow = e^\downarrow(k_{\text{out}})$ . While this changes the behaviour near  $k \sim k_{\text{out}}$ —in particular, it leads to a sharp drop in  $e^\uparrow$  and  $e^\downarrow$  between  $k = k_{\text{out}}$  and  $k = 2^{1/8}k_{\text{out}}$  by a factor of around 3—the remainder of the spectrum for  $k > 2^{1/8}k_{\text{out}}$  is nearly unaffected. With the  $k^{-2}$  extrapolation there is also a drop at  $k = k_{\text{out}}$ , as can be seen in the top panel of Figure 2.1d, for example; but this drop is much less drastic than with the flat spectrum extrapolation.

The cascade times of the up- and down-going waves are, respectively,

$$t_{\text{cas}}^{\uparrow}(k) = (k^4 e^{\downarrow}(k))^{-1}, \quad t_{\text{cas}}^{\downarrow}(k) = (k^4 e^{\uparrow}(k))^{-1}, \quad (2.42)$$

(see eq. [2.16]). The dissipation time is

$$t_{\text{diss}}(k) = (\nu k^2)^{-1}, \quad (2.43)$$

(see eq. [2.27]). For the simulations in this section, the viscosity is set to

$$\nu = 3 \cdot 10^{-5}; \quad (2.44)$$

this implies that  $t_{\text{diss}}(k_{\text{max}}) = 0.001$ .

### 2.6.1 Fixed Energy at the Outer Scale

For our first simulation, we fix  $e^{\uparrow}(k_{\text{out}}) = 1$  and  $e^{\downarrow}(k_{\text{out}}) = 0.1$  throughout the simulation. See Figure 2.1. For the initial condition, we use the spectra  $e^{\uparrow} \propto k^{-3}$  and  $e^{\downarrow} \propto k^{-3}$  (Fig. 2.1a). These initial spectra are seemingly valid solutions of the steady-state flux relations (eqs. [2.32] and [2.33]), with  $\alpha = 0$  and  $\epsilon^{\uparrow} = \epsilon^{\downarrow}$ . But the spectra are not pinned. When they are evolved in time, it seen that they become pinned to each other at the dissipation scale. This pinning happens very quickly—at the dissipation timescale (Fig 2.1b). The reason for this pinning was discussed in §2.3.3, and can be traced in Figures 2.1a-c.

The entire  $e^{\downarrow}$  spectrum adjusts to  $e^{\uparrow}$  on the timescale  $t_{\text{cas}}^{\downarrow}(k_{\text{out}}) \sim 1$ . The  $e^{\uparrow}$  spectrum takes longer to adjust, since  $t_{\text{cas}}^{\uparrow}(k_{\text{out}}) \sim 10$ . By  $t = 50$ , steady state is reached (Fig 2.1d). We can compare the behaviour in steady state with our calculations in §2.4. From equation (2.30), the dissipation wavenumber is

$$k_{\text{diss}} = \frac{k_{\text{out}}^3}{\nu} (e^{\uparrow}(k_{\text{out}}) e^{\downarrow}(k_{\text{out}}))^{1/2} \simeq 13,700, \quad (2.45)$$

which is approximately three times larger than the value seen in Figure 2.1d. The reason for this discrepancy can be seen in the bottom panel of this figure: dissipation is important where the cascade times are  $\sim t_{\text{diss}}/3$ , rather than  $\sim t_{\text{diss}}$  as we previously assumed. To account for this difference, we can use an effective viscosity,  $\nu_{\text{eff}} \equiv 3\nu$ , instead of  $\nu$  in our steady state formulae.

Equation (2.31) gives

$$\alpha = \frac{\ln[e^{\uparrow}(k_{\text{out}})/e^{\downarrow}(k_{\text{out}})]}{\ln[k_{\text{out}}^4 e^{\uparrow}(k_{\text{out}}) e^{\downarrow}(k_{\text{out}})/\nu_{\text{eff}}^2]} = 0.14, \quad (2.46)$$

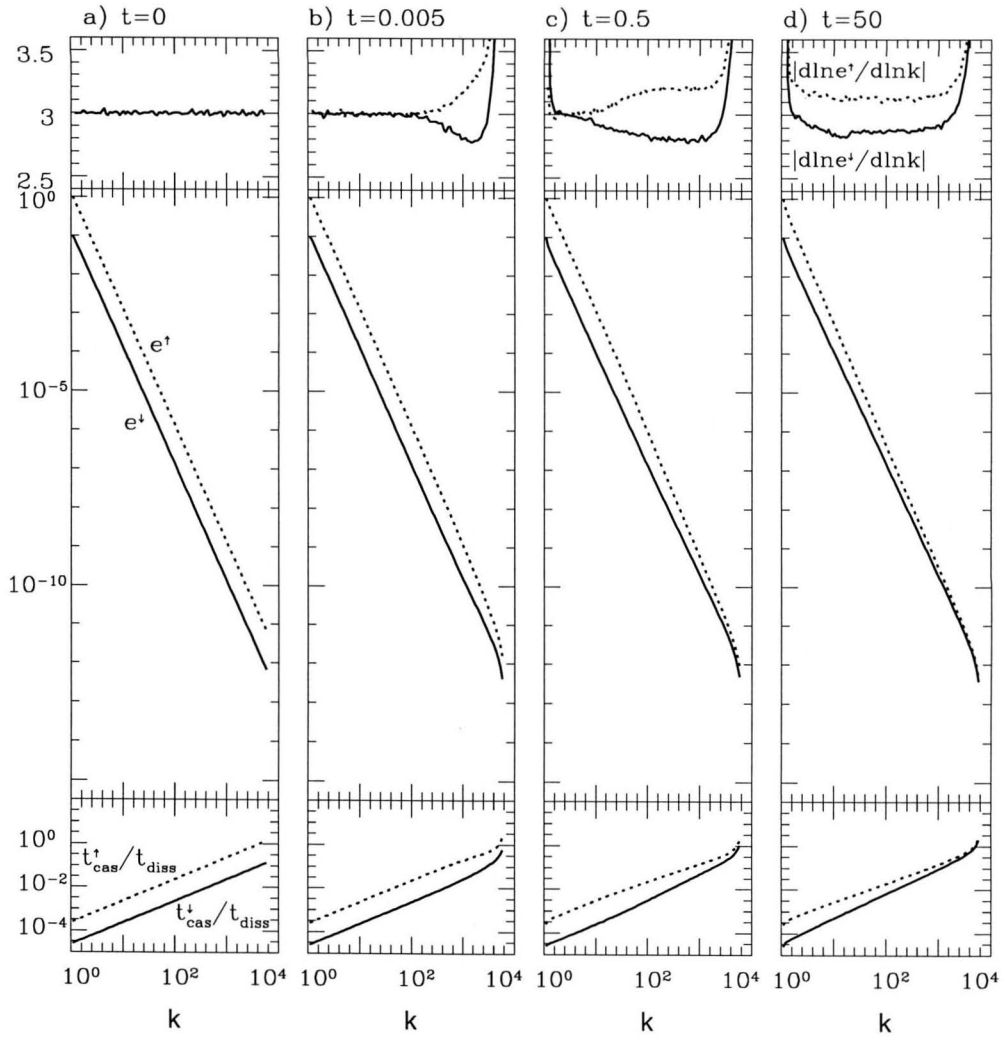


Figure 2.1: Simulation of Kinetic Equations with Fixed Energies at the Outer Scale

so

$$-\frac{d \ln e^\uparrow}{d \ln k} = 3 + \alpha = 3.14 \quad (2.47)$$

$$-\frac{d \ln e^\downarrow}{d \ln k} = 3 - \alpha = 2.86, \quad (2.48)$$

in good agreement with the top panel of Figure 2.1d.

From equation (2.36), the product of the steady state fluxes is approximately

$$\epsilon^\uparrow \epsilon^\downarrow \simeq [k_{\text{out}}^6 e^\uparrow(k_{\text{out}}) e^\downarrow(k_{\text{out}})]^2 = [1.09^6 \cdot 1 \cdot 0.1]^2 = 0.028. \quad (2.49)$$

In the numerical simulation, the values of  $\epsilon^\uparrow$  and  $\epsilon^\downarrow$  in steady state are obtained by outputting the instantaneous decay rates of  $e^\uparrow(k_{\text{out}})$  and  $e^\downarrow(k_{\text{out}})$  when the forcing is turned off. We find that  $(d/dt)e^\uparrow(k_{\text{out}}) = -0.136 = -\epsilon^\uparrow$  and  $(d/dt)e^\downarrow(k_{\text{out}}) = -0.114 = -\epsilon^\downarrow$ , so  $\epsilon^\uparrow \epsilon^\downarrow = 0.016$ , in reasonable agreement with the predicted value.

Recall that heuristic arguments suffice to derive all of the steady-state formulae that we have used thus far in this section, and the kinetic equation is unnecessary. But the kinetic equation is necessary to derive the relative value of the steady state fluxes. From equation (2.35), we should have

$$\epsilon^\uparrow / \epsilon^\downarrow - 1 = \alpha = 0.14, \quad (2.50)$$

if we use the value of  $\alpha$  from equation (2.46). The actual value is  $0.136/0.114 - 1 = 0.19$ , once again in reasonable agreement.

## 2.6.2 Fixed Flux

For our second simulation, we inject energy at a fixed rate at  $k = k_{\text{out}}$ . We use the same injection rate as we found in steady state in the first simulation:

$$\epsilon^\uparrow = 0.136, \quad \epsilon^\downarrow = 0.114. \quad (2.51)$$

Thus  $e^\uparrow(k_{\text{out}})$  and  $e^\downarrow(k_{\text{out}})$  are free to evolve. For our initial condition, we use the spectra obtained in steady state in the first simulation, but multiplied by a constant; specifically,  $e^\uparrow(k) \rightarrow e^\uparrow(k)/10$  and  $e^\downarrow(k) \rightarrow e^\downarrow(k) \cdot 10$  (see Fig. 2.2a). With these fluxes and initial spectra, the flux relations (eqs. [2.32] and [2.33]) are satisfied—since they were satisfied before the multiplication and division by 10. But, once again, this is not a valid steady state solution because the spectra are not pinned at the dissipation scale. When the spectra are evolved in time, the spectra are first pinned (Figs. 2.2a-c). In this simulation, the spectra are initially pinned where  $t_{\text{cas}}^\downarrow \sim t_{\text{diss}}$ , which is at  $k \sim 1,000$ . Therefore the pinning timescale is  $\sim t_{\text{diss}}(k = 1,000) \sim 0.03$ .

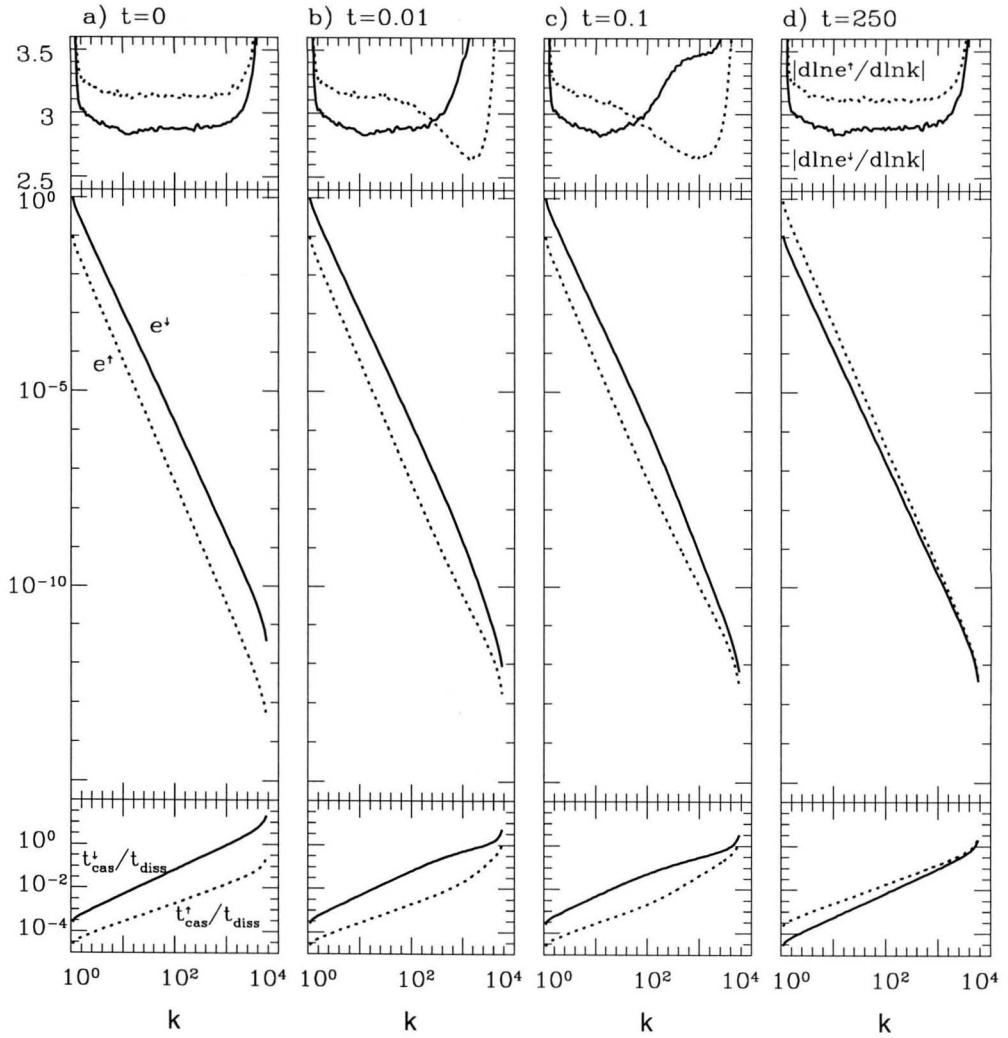


Figure 2.2: Simulation of Kinetic Equations with Fixed Fluxes

As expected, the same steady state is reached as in the first simulation (Fig. 2.2d). In reaching steady state, the two spectra must cross. This happens at  $t \sim 40$ , when both spectra are identical, with slopes equal to  $-3$ , and with outer scale energy equal to  $\sim 0.3$ . The time to reach steady state is considerably longer in the constant flux simulation than in the constant energy one. Steady state is reached at  $t \sim 250$ , as opposed to  $t \sim 50$  in the previous simulation. This may be attributed to the fact that most of the flux that is input at large scales is continuously being lost at small scales. Therefore, the constant flux simulation is less efficient at growing the spectra than is the constant energy spectra.

In sum, these two simulations show that the pinning of the spectra occurs very quickly. In addition, both the evolution of the spectra towards steady state, and the behaviour in steady state, can be understood with simple heuristic arguments. However, there is one exception: the relation between the ratio of the fluxes and the spectral slope,  $\epsilon^\uparrow/\epsilon^\downarrow - 1 \simeq \alpha$ , the coefficient of which (i.e., 1) can only be obtained by considering the steady state kinetic equation.

### 2.6.3 Decaying Turbulence

For our third simulation, we allow the spectra to decay without injecting any energy. The initial condition is the steady state spectra from the previous simulation, see Figure 2.3. At the outer scale, the cascade time of the down-waves is  $\sim 1/e^\downarrow(k_{\text{out}}) \sim 1$ , so  $e^\downarrow(k_{\text{out}})$  decays on this timescale. More precisely, from the values plotted in Figure 2.3,  $e^\downarrow \propto \exp(-0.5t)$  at fixed  $k$ .

The cascade time of the up-waves is much longer. Initially,  $t_{\text{cas}}^\uparrow \sim 10$  at the outer scale; as  $e^\downarrow$  decays,  $t_{\text{cas}}^\uparrow$  increases exponentially. So  $e^\uparrow(k_{\text{out}})$  does not evolve. Nonetheless,  $t_{\text{cas}}^\uparrow$  is smaller at small scales, and there is some evolution of  $e^\uparrow$  at large  $k$ .

The spectra appear to evolve in a self-similar manner, with the spectra remaining pinned at their dissipation scale. The end result is that the energy in the down-waves disappears, while the energy in the up-waves is nearly unchanged. Decaying weak turbulence is unstable: an initial imbalance between up and down waves is magnified exponentially. A similar instability occurs in strong turbulence, as suggested by Dobrowolny et al. (1980) in the context of the solar wind, and as seen in numerical simulations of strong turbulence (Maron and Goldreich 2001, and Cho et al. 2002).

## 2.7 A Model of the Kinetic Equations: Coupled Diffusion Equations

It is instructive to consider a very simple model of the kinetic equations. In this section, we develop a model in the form of two coupled diffusion equations. Investigation of these model equations

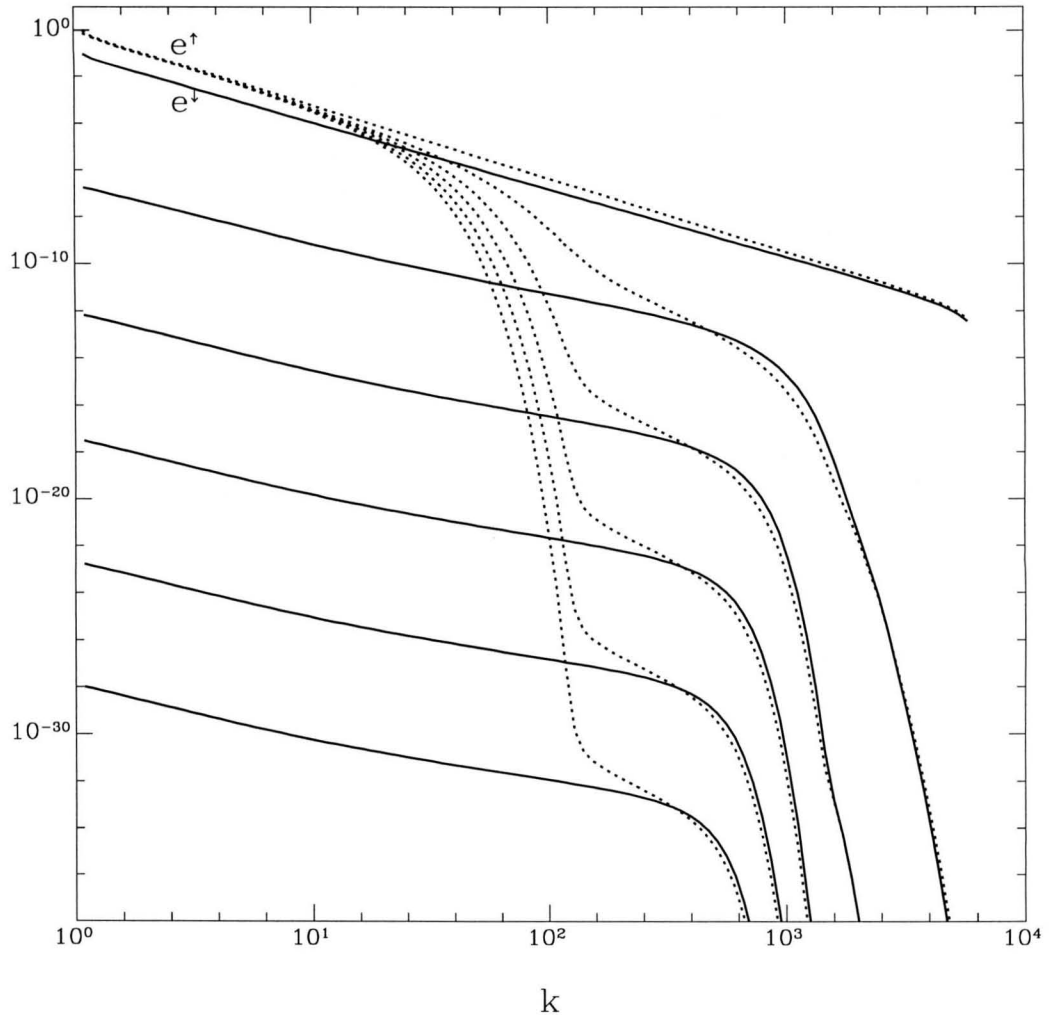


Figure 2.3: Decaying Simulation of Kinetic Equations  
Spectra of  $e^\uparrow$  (dotted lines) and  $e^\downarrow$  (solid lines) at the following times:  $t = 0, 25, 50, 75, 100, 125$  (from top to bottom).

illustrates that the pinning of spectra is quite general; the only requirement is that the cascade time of one type of wave be inversely related to the energy of the other type. A second reason for considering model equations is that they can be simulated much faster and more easily than the kinetic equations. Finally, by contrasting the kinetic equations with the model equations, we can gain insight into the behaviour of the kinetic equations.

### 2.7.1 Derivation of Coupled Diffusion Equations

Our model equation is

$$\frac{\partial}{\partial t} k e^\uparrow = - \frac{\partial}{\partial k} \tilde{\epsilon}^\uparrow, \quad (2.52)$$

where  $\tilde{\epsilon}^\uparrow$  is the flux. Since the energy of the up-waves is proportional to the integral of  $e^\uparrow$  over  $d^2 \mathbf{k}$ ,  $k e^\uparrow$  is proportional to the energy per unit  $k$ . For  $\tilde{\epsilon}^\uparrow$ , we choose a form that depends on the following quantities evaluated at  $k$ :  $e^\downarrow$ ,  $e^\uparrow$ , and  $\partial_k e^\uparrow$ . By contrast, the kinetic equation depends on  $e^\uparrow$  and  $e^\downarrow$  evaluated at a range of wavenumbers, so our model equation is much more local in  $k$  (in fact, it is exactly local). For the cascade time of the energy in the up waves to have the correct form (eq. [2.16]), i.e.,  $t_{\text{cas}}^\uparrow = (\lambda/w_\lambda^\downarrow)^2 (v_A/\Lambda) \sim (k^4 e^\downarrow)^{-1} (v_A/\Lambda)$ , we choose

$$\tilde{\epsilon}^\uparrow = - \frac{\Lambda}{v_A} e^\downarrow k^{6-\beta} \frac{\partial}{\partial k} (k^{\beta+1} e^\uparrow), \quad (2.53)$$

where  $\beta$  is a constant that we specify below. Of course the above relation for the flux gives the correct steady-state scaling:  $e^\uparrow e^\downarrow \propto k^{-6}$ . The evolution equations for  $e^\downarrow$  are the same as for  $e^\uparrow$  (eqs. [2.52] and [2.53]), with  $\uparrow$ 's and  $\downarrow$ 's interchanged.

With  $e^\uparrow \propto k^{-(3+\alpha)}$ ,  $e^\downarrow \propto k^{-(3-\alpha)}$ , we can relate the steady-state fluxes to the energies:

$$\tilde{\epsilon}^\uparrow = \tilde{f}(\alpha) [k^6 e^\uparrow(k) e^\downarrow(k)] \frac{\Lambda}{v_A}, \quad (2.54)$$

$$\tilde{\epsilon}^\downarrow = \tilde{f}(-\alpha) [k^6 e^\uparrow(k) e^\downarrow(k)] \frac{\Lambda}{v_A}, \quad (2.55)$$

where

$$\tilde{f}(\alpha) = 2 + \alpha - \beta. \quad (2.56)$$

These relations are analogous to equations (2.32) and (2.33). To make the analogy closer, we choose  $\beta$  so that  $\tilde{f}$  has the same dependence on  $\alpha$  as does  $f$  in the limit that the cascade is nearly balanced (i.e.,  $|\alpha| \ll 1$ ). Since  $\tilde{\epsilon}^\uparrow/\tilde{\epsilon}^\downarrow = \tilde{f}(\alpha)/\tilde{f}(-\alpha) \simeq 1 + \alpha/(1 - \beta/2)$  in this limit, we see by comparison with equation (2.35) that we should choose  $\beta = 0$ .

Collecting results, our model equations are two coupled diffusion equations:

$$\frac{\partial}{\partial t} e^\uparrow = \frac{\Lambda}{v_A} \frac{1}{k} \frac{\partial}{\partial k} \left( e^\downarrow k^6 \frac{\partial}{\partial k} k e^\uparrow \right) - \nu k^2 e^\uparrow, \quad (2.57)$$

$$\frac{\partial}{\partial t} e^\downarrow = \frac{\Lambda}{v_A} \frac{1}{k} \frac{\partial}{\partial k} \left( e^\uparrow k^6 \frac{\partial}{\partial k} k e^\downarrow \right) - \nu k^2 e^\downarrow, \quad (2.58)$$

after including dissipative terms.

These equations, while much simpler than the kinetic equations, share many of the same features. Since the cascade time of the up-going waves is inversely proportional to the energy of the down-going waves (and vice versa), the argument for the pinning of the spectra in weak turbulence (see §2.3.3) applies here as well. Moreover, in steady state, these diffusion equations suffer from the same degeneracy as does the kinetic equation: the constancy of  $\tilde{\epsilon}^\uparrow$  and  $\tilde{\epsilon}^\downarrow$  is insufficient to determine the scaling of  $e^\uparrow$  or  $e^\downarrow$  separately. This degeneracy is partially broken by the dependence of the fluxes on the slopes (eqs. [2.54] and [2.55]); we have chosen this dependence so that it is the same as for the kinetic equations in the limit that the cascade is nearly balanced ( $|\alpha| \ll 1$ ). In the following section, we present numerical simulations of these equations.

## 2.7.2 Numerical Simulations of Coupled Diffusion Equations

We run two simulations of the coupled diffusion equations. As with the kinetic simulations described in §2.6, the first simulation has fixed energy at the outer scale, and the second simulation has fixed flux. And, as before,  $\Lambda/v_A$  is set to unity, functions of  $k$  are evaluated at  $k = 2^{i/8}$ ,  $i = 1, \dots, 100$ , and the viscosity is  $\nu = 3 \cdot 10^{-5}$ .

### Fixed Energy at the Outer Scale

For our first simulation, we fix  $e^\uparrow(k_{\text{out}}) = 1$  and  $e^\downarrow(k_{\text{out}}) = 0.1$ . The evolution is shown in Figure 2.4. It is very similar to the evolution of the kinetic simulation (Fig. 2.1). As before, the spectra are pinned quickly. And since, by design, the predicted steady state relations for the diffusion equations are the same as those for the kinetic equations (eqs. [2.45]–[2.50]), the steady state behaviour of the two simulations are nearly identical; compare Figures 2.4d and 2.1d. Nonetheless, there are two differences worthy of note. First, the slopes of  $e^\uparrow$  and  $e^\downarrow$  do not have a spike near  $k = k_{\text{out}}$ . The presence of such a spike in the kinetic simulation is due to the extrapolation of the spectra to  $k < k_{\text{out}}$  (see footnote 8). Since the diffusion equations are exactly local in  $k$ , such an extrapolation is unnecessary, and so the behaviour is much smoother near  $k = k_{\text{out}}$ . Second, dissipation is important where the cascade times are  $\sim t_{\text{diss}}/15$  (see bottom panel of Fig. 2.4d), instead of  $\sim t_{\text{diss}}/3$  as for the kinetic simulation. Therefore, we should use an effective viscosity  $\nu_{\text{eff}} = 15\nu$  in the predicted steady state relations. In particular, the prediction for  $\alpha$  (see eq. [2.46]) becomes  $\alpha = 0.17$  with this  $\nu_{\text{eff}}$ .

From the output of the code in steady state, the fluxes are  $\epsilon^\uparrow = 0.308$  and  $\epsilon^\downarrow = 0.260$ . Thus  $\epsilon^\uparrow/\epsilon^\downarrow - 1 = 0.18$ , while the predicted value is  $\alpha$ , i.e., 0.17.

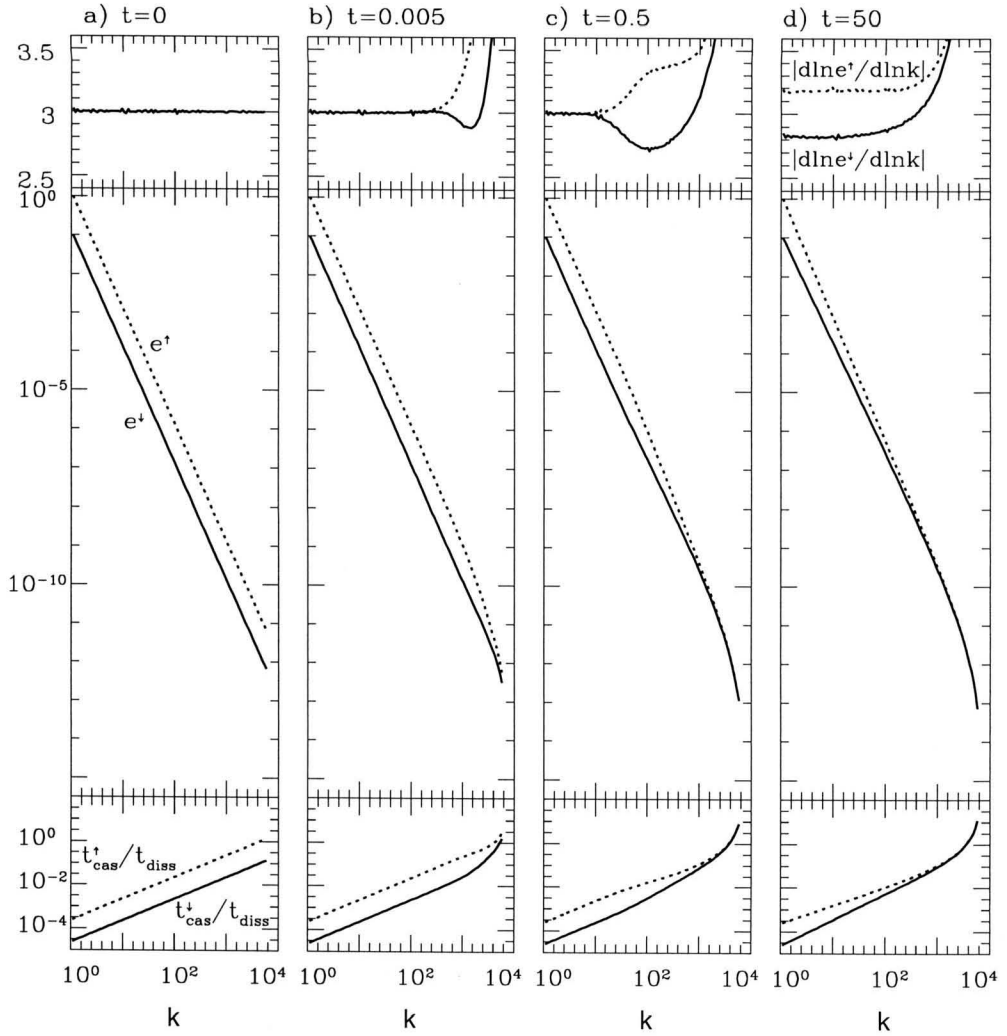


Figure 2.4: Simulation of Diffusion Equations with Fixed Energies at the Outer Scale

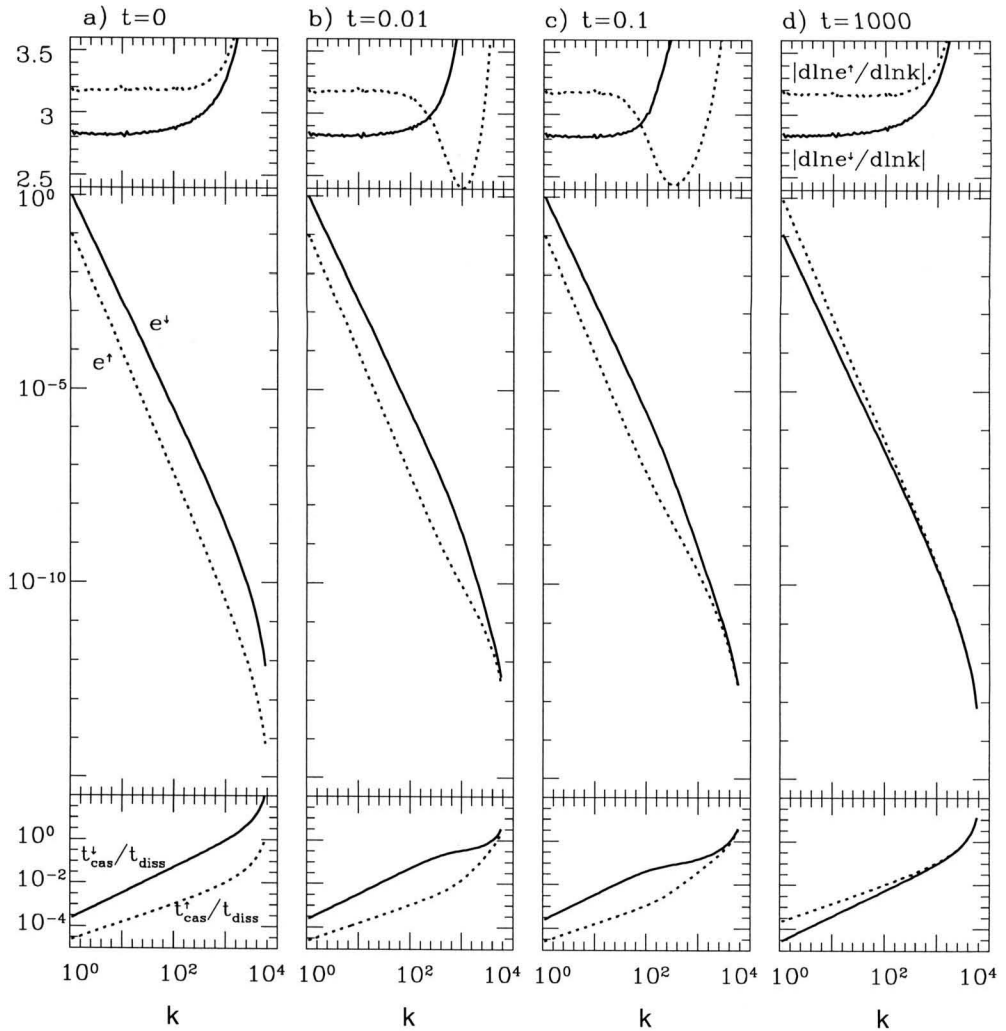


Figure 2.5: Simulation of Diffusion Equations with Fixed Fluxes

### Fixed Flux at the Outer Scale

For the second simulation, we inject energy at  $k = k_{\text{out}}$  at a fixed rate, equal to that found in steady state in the previous simulation; i.e.,  $\epsilon^\dagger = 0.308$  and  $\epsilon^\perp = 0.260$ . For the initial condition, we divide the previously found steady state value of  $e^\dagger$  by 10, and we multiply  $e^\perp$  by 10. The evolution is shown in Figure 2.5. It is very similar to that found in the corresponding kinetic simulation (Figure 2.2).

## 2.8 The Bottleneck Effect

The bottleneck effect appears in numerical simulations of both hydrodynamic and MHD turbulence (e.g., Borue and Orszag 1995, Biskamp 2000). A trick that is commonly used in simulations is that the viscous term is modified from the diffusive value  $\nu k^2 \mathbf{v}$  to  $\nu_n k^n \mathbf{v}$ , where  $n$  is typically 4 or 8, and  $\nu_n$  is the hyperviscosity; the resistivity is modified in a similar manner. This trick makes the dissipation lengthscale slightly smaller. Thus a smaller part of the spectrum is subjected to dissipation, and more of the true undissipated spectrum can be observed for a given dynamic range. Although this trick does work, and the dissipation lengthscale is made smaller, there is a problem: the spectrum on scales slightly larger than the dissipation scales is made flatter. The energy, in effect, is backed up. This is the bottleneck effect. It can be particularly problematic in simulations of strong MHD turbulence, where the energy backup can affect lengthscales considerably larger than the dissipative scales (Biskamp and Müller 2000, Maron and Goldreich 2001, although Cho and Vishniac 2000 show a less extended backup).

This motivates us to investigate the bottleneck effect in weak turbulence. If the bottleneck effect appears, its interpretation will be simpler than in strong turbulence. We perform two simulations of the kinetic equation, one with hyperviscosity of the form  $\nu_4 k^4$ , and the other with  $\nu_8 k^8$ . In each simulation, we fix the energies at the outer scale,  $e^\uparrow(k_{\text{out}}) = 1$ ,  $e^\downarrow(k_{\text{out}}) = 0.1$ , and allow the spectra to reach steady state. The steady state spectra of  $k^6 e^\uparrow e^\downarrow$  are shown in Figure 2.6, offset for clarity. Also shown is the simulation with ordinary viscosity described in §2.6.1. From this figure it is apparent that weak turbulence suffers from the bottleneck effect; the effect becomes larger with increasing hyperviscous exponent.

The bottleneck effect can be understood as follows. Consider an up-wave on a lengthscale slightly larger than dissipative scales. It is cascaded by down-waves that have slightly different lengthscales than its own. Hyperviscosity gives a sharper dissipative cutoff to the down-wave spectrum than ordinary viscosity. Therefore a hyperviscous simulation has fewer down-waves in the vicinity of the dissipation scale, and the cascade time of the up-wave is longer. For the up-wave energy flux to be independent of lengthscale, a longer cascade time implies a larger energy. As a result, the spectrum is flatter on scales slightly larger than dissipative ones. Falkovich (1994) has a similar explanation of the bottleneck effect in hydro turbulence.

## 2.9 Discussion

In this chapter we described imbalanced weak turbulence and solved the steady state cascade. In a future paper, we will extend the result to the strong cascade. One of our ultimate goals is to use the theory of imbalanced strong turbulence to explain turbulence in the solar wind, where imbalance is

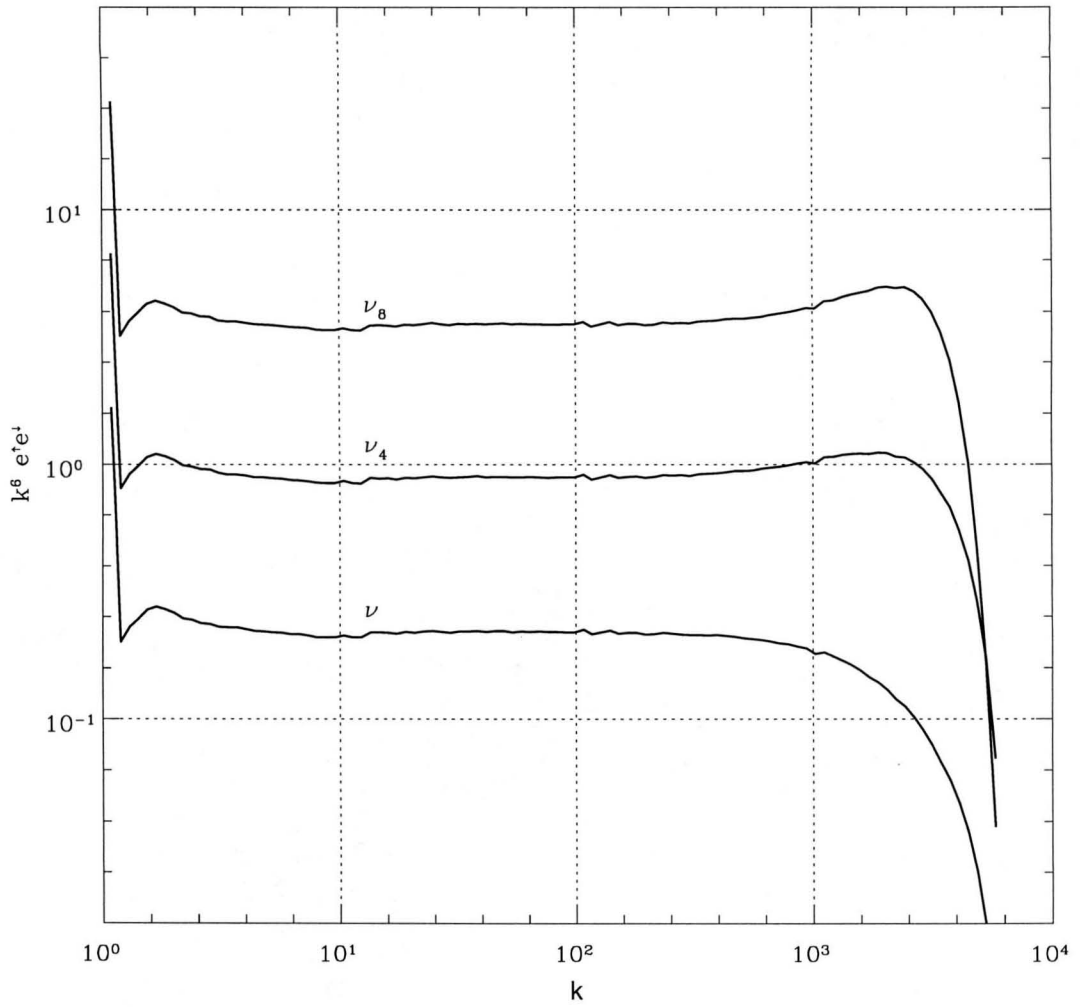


Figure 2.6: The Bottleneck Effect

Three spectra, offset for clarity; the top spectrum has viscous and resistive terms  $\nu_8 k^8$ , the middle has  $\nu_4 k^4$ , and the bottom has  $\nu k^2$ .

observed.

Although strong turbulence is more generally applicable than weak, the latter is a simple and useful model. There are a number of issues in strong turbulence that are not understood. Weak turbulence can be used as the first step in explaining them. For example, in this chapter we found that the bottleneck effect appears in weak turbulence, where its interpretation is straightforward. There are a number of other issues that we intend to investigate in weak turbulence as a prelude to understanding them in strong turbulence; for example, turbulence in the presence of a high magnetic Prandtl number and reconnection.

## 2.10 Appendix: Kinetic Equation in Weak Turbulence

### 2.10.1 Preliminaries

The kinetic equations describing weak turbulence were derived in Galtier et al. (2000) using the theory of weak turbulence. In this appendix, we present a more physical derivation.

We consider the evolution of  $\mathbf{w}^\uparrow$  in a plane that is transverse to  $\hat{\mathbf{z}}$  and moving with velocity  $v_A \hat{\mathbf{z}}$ , i.e., with fixed  $z^\uparrow \equiv z - v_A t$ . (Recall that  $\hat{\mathbf{z}}$  is in the direction of the mean magnetic field.) Changing variables from  $z$  to  $z^\uparrow$  in equation (2.8) gives

$$\left. \frac{\partial}{\partial t} \right|_{x,y,z^\uparrow} \mathbf{w}^\uparrow = -\mathbf{w}^\downarrow \cdot \nabla_\perp \mathbf{w}^\uparrow + \nabla_\perp \nabla_\perp^{-2} (\nabla_\perp \mathbf{w}^\downarrow : \nabla_\perp \mathbf{w}^\uparrow). \quad (2.59)$$

In weak turbulence, the parallel length over which disturbances are correlated,  $\Lambda$ , is small; in particular, in the time that an up-wave crosses a down-going wavepacket,  $\Delta t \sim \Lambda/v_A$ , its distortion is less than unity:  $\Delta w_\lambda^\uparrow / w_\lambda^\uparrow \sim (w_\lambda^\downarrow / v_A) \Lambda / \lambda \ll 1$  (eq. [2.15]).<sup>9</sup> Therefore,  $\mathbf{w}^\uparrow$  undergoes small uncorrelated changes each  $\Delta t \sim \Lambda/v_A$ , and its evolution is analogous to a random walk, with step-size  $\Delta w_\lambda^\uparrow \sim w_\lambda^\uparrow (w_\lambda^\downarrow / v_A) \Lambda / \lambda \ll 1$ .

If, at fixed  $z^\uparrow$ ,  $\mathbf{w}^\downarrow$  is a known function of time, then the evolution equation for  $\mathbf{w}^\uparrow$  is linear in  $\mathbf{w}^\uparrow$ . Nonlinearity arises because  $\mathbf{w}^\uparrow$  modifies  $\mathbf{w}^\downarrow$  (through eq. [2.10]); this modification backreacts on  $\mathbf{w}^\uparrow$  through equation (2.59). Nonetheless, in weak turbulence the backreaction is unimportant for the random walk of  $\mathbf{w}^\uparrow$  at a fixed  $z^\uparrow$ . Every  $\Delta t \sim \Lambda/v_A$ , the backreaction changes  $w_\lambda^\uparrow$  by  $\sim w_\lambda^\uparrow [(w_\lambda^\downarrow / v_A) \Lambda / \lambda] [(w_\lambda^\uparrow / v_A) \Lambda / \lambda]$ , which is smaller than  $\Delta w_\lambda^\uparrow$  by the small factor  $(w_\lambda^\uparrow / v_A) \Lambda / \lambda \ll 1$ . Furthermore, since this backreaction is uncorrelated on timescales larger than  $\Lambda/v_A$ , it only effects a small change in the step-size of the random walk. Therefore, this backreaction can be neglected, and it suffices to consider equation (2.59) as though it were linear in  $\mathbf{w}^\uparrow$ .

Our goal in this appendix is to quantify the random walk; the resulting equation is the kinetic equation. Before doing so, we solve a simpler problem: a one-dimensional linear oscillator, de-

<sup>9</sup>We neglect the factor of 2 associated with the fact that the relative velocity of up and down waves is  $2v_A$ .

scribed by a linear equation with random forcing. The extension to weak turbulence will then be straightforward.

## 2.10.2 A Toy Problem: the Linear Random Oscillator

We consider the evolution of a simple random oscillator  $\psi$ :

$$\frac{d}{dt}\psi(t) = iA(t)\psi(t) , \quad (2.60)$$

where  $\psi$  is a complex scalar and  $A$  is a real random variable; the factor  $i$  ensures that the energy  $|\psi(t)|^2$  is conserved. Our goal is to calculate the evolution of  $\langle\psi(t)\rangle$ , where angled brackets denote an average over an ensemble of  $A$ 's, not over time.<sup>10</sup> We assume that the values of  $A$  at two different times are statistically independent of each other whenever the two times are separated by more than the correlation time,  $\tau_{\text{corr}}$ . (We make this more precise in footnote 11, below.) For simplicity, we take  $A$  to have zero mean ( $\langle A(t) \rangle = 0$ ); the extension to  $A$  with non-zero mean is trivial. Finally, we assume that the statistical properties of  $A$ —such as  $\tau_{\text{corr}}$  and  $A_{\text{rms}} \equiv (\langle A^2 \rangle)^{1/2}$ —vary only on timescales much larger than  $\tau_{\text{corr}}$ . Note that  $\psi$  corresponds to  $w_\lambda^\uparrow$  in equation (2.59);  $A$  corresponds to  $w_\lambda^\downarrow$ , or, more specifically, to  $w_\lambda^\downarrow/\lambda$ ; and  $\tau_{\text{corr}}$  corresponds to  $\Lambda/v_A$ .

There are two limiting regimes for the random oscillator, depending on whether  $A_{\text{rms}}\tau_{\text{corr}}$  is less than or greater than unity. The former case corresponds to weak turbulence, the latter to strong turbulence.

We consider  $A_{\text{rms}}\tau_{\text{corr}} \ll 1$ . The change in  $\psi$  within the time  $\tau_{\text{corr}}$  is of order  $A_{\text{rms}}\tau_{\text{corr}}\psi$ , which is much smaller than  $\psi$ . Since  $A$  is uncorrelated on timescales larger than  $\tau_{\text{corr}}$ ,  $\psi$  undergoes small uncorrelated changes each  $\tau_{\text{corr}}$ , and thus its long-time evolution is a random walk. Intuitively, we expect that the time evolution of the statistical properties of  $\psi$ —in particular,  $\langle\psi\rangle$ —can be represented by a differential equation. Our goal in this section is to derive the differential equation, and to understand the approximations that are made in deriving it.

The solution of equation (2.60) is simply

$$\psi(t) = \psi(0) \cdot \exp(iA^t) , \quad (2.61)$$

where  $A^t \equiv \int_0^t A(t')dt'$ . We expand as follows,

$$\psi(t) = \psi(0) \cdot (1 + iA^t - (AA^t)^t + \dots) , \quad (2.62)$$

where  $(AA^t)^t \equiv \int_0^t A(t') \int_0^{t'} A(t'')dt''dt'$ ; note that  $(1/2)(A^t)^2 = (AA^t)^t$  is an identity for any  $A(t)$ .

<sup>10</sup>For a textbook discussion of the linear random oscillator, see van Kampen (1992). His derivation of the equation governing  $\langle\psi\rangle$  is more rigorous than ours.

Equation (2.62) may be thought of as an expansion in powers of  $A$ ; as we discuss below, the dimensionless expansion parameter is really the ratio of the correlation time to the cascade time.

We evaluate  $\langle\psi(t)\rangle$  as follows. Since  $A(t)$  is unaffected by  $\psi(0)$ ,  $A(t)$  and  $\psi(0)$  must be uncorrelated:

$$\langle\psi(t)\rangle = \langle\psi(0)\rangle \cdot (1 + i \langle A^t \rangle - \langle (AA^t)^t \rangle + \langle \dots \rangle) . \quad (2.63)$$

Since  $\langle A \rangle = 0$ ,  $\langle A^t \rangle = 0$ . Next, we consider  $\langle (AA^t)^t \rangle$ . The values of  $A$  at two different times “statistically overlap” only when the two times are separated by less than the correlation time; i.e.,  $\langle A(t')A(t' + \Delta t) \rangle$  is non-zero only if  $\Delta t < \tau_{\text{corr}}$ . Thus  $\langle AA^t \rangle \simeq A_{\text{rms}}^2 \tau_{\text{corr}}$  when  $t \gtrsim \tau_{\text{corr}}$ , and  $\langle (AA^t)^t \rangle \simeq A_{\text{rms}}^2 \tau_{\text{corr}} t$ .<sup>11</sup>

Therefore

$$\langle\psi(t)\rangle = \langle\psi(0)\rangle (1 - A_{\text{rms}}^2 \tau_{\text{corr}} t) , \quad \tau_{\text{corr}} \lesssim t \lesssim \tau_{\text{corr}} / (A_{\text{rms}} \tau_{\text{corr}})^2 . \quad (2.64)$$

Equivalently,

$$\frac{d}{dt} \langle\psi(t)\rangle = -A_{\text{rms}}^2 \tau_{\text{corr}} \langle\psi(t)\rangle . \quad (2.65)$$

This equation is the main result of this section. Its interpretation is as follows: since  $\psi$  changes by  $\Delta\psi \sim A_{\text{rms}} \tau_{\text{corr}} \psi$  in the time  $\tau_{\text{corr}}$ , then after  $N$  steps, each  $\tau_{\text{corr}}$  long, the change in  $\psi$  is  $\sqrt{N} \Delta\psi$ . Thus for order unity changes in  $\psi$ ,  $(\psi/\Delta\psi)^2$  steps are required. The resulting time is the cascade time:

$$\tau_{\text{cas}} = (\psi/\Delta\psi)^2 \tau_{\text{corr}} \sim 1/(A_{\text{rms}}^2 \tau_{\text{corr}}) , \quad (2.66)$$

as in equation (2.65), and  $\tau_{\text{corr}}/\tau_{\text{cas}} \sim (A_{\text{rms}} \tau_{\text{corr}})^2 \ll 1$ . Although  $\langle\psi(t)\rangle$  decays to zero on the timescale  $\tau_{\text{cas}}$ , the energy  $|\psi|^2$  remains constant; the cascade of  $\langle\psi\rangle$  is analogous to phase mixing.

We may now proceed to derive the kinetic equation in weak turbulence. Before doing so, we consider the linear random oscillator in more detail. If the reader is satisfied with the above derivation of equation (2.65), the following subsection may be skipped.

### The Validity of Perturbation Theory and Goldreich and Sridhar (1997)

Goldreich and Sridhar (1997) incorrectly claim that perturbation theory fails in weak turbulence, i.e., in their intermediate turbulence.<sup>12</sup> We explain their claim and its resolution in the context of the linear random oscillator. In the process, we clarify the validity of the perturbation expansion.

We consider the terms neglected in equation (2.64). For example, the fourth-order term is

<sup>11</sup>For the expression  $\langle (AA^t)^t \rangle \simeq A_{\text{rms}}^2 \tau_{\text{corr}} t$  to be approximately valid, we see how fast  $A$  must decorrelate:  $\langle A(t')A(t' + \Delta t) \rangle$  must go to zero faster than  $1/\Delta t$  for large  $\Delta t > \tau_{\text{corr}}$ ; otherwise,  $\langle (AA^t)^t \rangle$  rises faster than the first power of  $t$ , and our derivation is invalid. In addition, any order unity constant that multiplies the right-hand side of this equation can be absorbed into the definition of  $\tau_{\text{corr}}$ , so in the following we set  $\simeq$  to  $=$ .

<sup>12</sup>A note on terminology: the turbulence that we and that Galtier et al. (2000) call weak, Goldreich and Sridhar (1997) call intermediate. They call it intermediate precisely because of their claim that perturbation theory is invalid.

$\langle \psi^{(4)} \rangle / \langle \psi(0) \rangle = \langle \{A[A(AA^t)^t]^t\}^t \rangle$ . In this quadruple time integral,  $A$  is evaluated at four different times. Whenever two of these times are separated by less than  $\tau_{\text{corr}}$ , the values of  $A$  at these two times “statistically overlap,” and hence can give a non-zero contribution to the total integral. When two of the times are separated by less than  $\tau_{\text{corr}}$ , and the other two times are also separated by less than  $\tau_{\text{corr}}$ , but the first two times are separated from the second two times by more than  $\tau_{\text{corr}}$ , then this gives a contribution of  $\langle \psi^{(4)} \rangle / \langle \psi(0) \rangle \sim (A_{\text{rms}}^2 \tau_{\text{corr}} t)^2 = (t/\tau_{\text{cas}})^2$ .

Since  $\langle \psi^{(2)} \rangle / \langle \psi(0) \rangle = -A_{\text{rms}}^2 \tau_{\text{corr}} t = -t/\tau_{\text{cas}}$ , the contribution of the fourth-order term is as large as the second-order term after the time  $t = \tau_{\text{cas}}$ . Similarly, if we consider the contribution to  $\langle \psi^{(2n)} \rangle / \langle \psi(0) \rangle$  from correlating pairs of  $A$ , the result is  $\sim (t/\tau_{\text{cas}})^n$ ; so all terms are of comparable value when  $t = \tau_{\text{cas}}$ , and it seems that the lowest order term is inadequate. This, in effect, is the claim that Goldreich and Sridhar (1997) make in the context of weak turbulence.

It is incorrect; although equation (2.64) for  $\langle \psi(t) \rangle$  is only valid for  $t \ll \tau_{\text{cas}}$ , equation (2.65) for  $(d/dt) \langle \psi(t) \rangle$  is approximately valid for all times, with corrections of order powers of  $\tau_{\text{corr}}/\tau_{\text{cas}} \ll 1$ . Since  $\psi(t)$  undergoes small uncorrelated changes every timestep of length  $\tau_{\text{corr}}$ , we expect on physical grounds that the evolution of its statistical properties should be governed by a differential equation that is invariant under time translations.<sup>13</sup> Equation (2.65) is the only such equation whose small-time behaviour is given by equation (2.64). Its right-hand side may be interpreted as the lowest term in a perturbative expansion in  $\tau_{\text{corr}}/\tau_{\text{cas}}$ . All of the contributions to  $\langle \psi(t) \rangle$  that are of order  $(t/\tau_{\text{cas}})^n$  must be derivable from equation (2.65). For example, if  $A_{\text{rms}}^2 \tau_{\text{corr}} \equiv 1/\tau_{\text{cas}}$  is constant, then equation (2.65) has the solution  $\langle \psi(t) \rangle / \langle \psi(0) \rangle = \exp(-t/\tau_{\text{cas}}) = 1 - t/\tau_{\text{cas}} + (1/2)(t/\tau_{\text{cas}})^2 + \dots$ . Terms of order  $(t/\tau_{\text{cas}})^n$  in  $\langle \psi \rangle$  are generated from the lowest order term.

We can solve the one-dimensional oscillator exactly when  $A(t)$  is Gaussian, and thereby illustrate the validity of equation (2.65). If  $A(t)$  is a zero-mean Gaussian random variable, then so is  $A^t$ , and  $\langle \exp(iA^t) \rangle = \exp(-\langle (A^t)^2 \rangle / 2)$ .<sup>14</sup> It follows from equation (2.61) that

$$\langle \psi(t) \rangle = \langle \psi(0) \rangle \cdot \exp(-\langle (AA^t)^t \rangle). \quad (2.67)$$

Equivalently,

$$\frac{d}{dt} \langle \psi \rangle = -\langle AA^t \rangle \langle \psi \rangle, \quad (2.68)$$

which agrees with equation (2.65) when  $\langle AA^t \rangle = A_{\text{rms}}^2 \tau_{\text{corr}}$ .

Although we are mainly concerned with the limit  $A_{\text{rms}} \tau_{\text{corr}} \ll 1$ , we conclude this subsection by briefly discussing the opposite limit,  $A_{\text{rms}} \tau_{\text{corr}} \gg 1$ , which is particularly interesting because it corresponds to strong turbulence. Perturbation theory is inapplicable because  $\psi$  does not undergo small uncorrelated changes every  $\tau_{\text{corr}}$ . Rather, its cascade time is  $\sim 1/A_{\text{rms}}$ , which is much shorter

<sup>13</sup>It should be invariant on the timescale  $\tau_{\text{corr}}$ ;  $A_{\text{rms}}$  and  $\tau_{\text{corr}}$  are effectively constants on this timescale.

<sup>14</sup>Proof: a zero-mean Gaussian  $x$  has probability distribution  $P(x) = (2\pi x_{\text{rms}}^2)^{-1/2} \exp(-x^2/2x_{\text{rms}}^2)$ ; so  $\langle \exp(ix) \rangle = \int_{-\infty}^{\infty} P(x) \exp(ix) dx = \exp(-x_{\text{rms}}^2/2)$ .

than the correlation time of  $A$ . Therefore  $A$  is nearly constant in the time that  $\langle \psi \rangle$  cascades. The inapplicability of perturbation theory makes strong turbulence difficult, if not impossible, to solve. Nonetheless, we can solve the one-dimensional oscillator in the strong limit. Equations (2.67) and (2.68) are still valid, but  $\langle AA^t \rangle \sim A_{\text{rms}}^2 t$ , so  $\langle \psi \rangle \propto \exp(-A_{\text{rms}}^2 t^2)$ , and equation (2.68) is not invariant under time translations.

### 2.10.3 Derivation of Kinetic Equation

We take the Fourier transform of equation (2.59) by transforming in  $x$  and  $y$  (but not  $z$ ). We denote the Fourier transform of  $w^\uparrow$  by  $w_{\mathbf{k}}^\uparrow$ :

$$w_{\mathbf{k}}^\uparrow \equiv \int d^2 x_\perp w^\uparrow \exp(-i\mathbf{k} \cdot \mathbf{x}_\perp), \quad (2.69)$$

where  $\mathbf{k}$  is purely transverse ( $k_z \equiv 0$ ); similarly,  $w_{\mathbf{k}}^\downarrow$  is the Fourier transform of  $w^\downarrow$ .

Since  $w_{\mathbf{k}}^\uparrow$  is perpendicular to both  $\mathbf{k}$  and  $\hat{z}$ , it only represents a single degree of freedom. Hence it is convenient to use a scalar potential  $\psi_{\mathbf{k}}^\uparrow$ , defined by  $w_{\mathbf{k}}^\uparrow = i(\hat{\mathbf{k}} \times \hat{z})\psi_{\mathbf{k}}^\uparrow$ , with  $\hat{\mathbf{k}} \equiv \mathbf{k}/k$ . Similarly,  $w_{\mathbf{k}}^\downarrow = i(\hat{\mathbf{k}} \times \hat{z})\psi_{\mathbf{k}}^\downarrow$ . The Fourier transform of equation (2.59) is then

$$\frac{\partial}{\partial t} \Big|_{\mathbf{k}, z^\uparrow} \psi_{\mathbf{k}}^\uparrow(t) = \int d^2 \mathbf{p} A_{\mathbf{k}, \mathbf{p}}(t) \psi_{\mathbf{p}}^\uparrow(t), \quad (2.70)$$

where

$$A_{\mathbf{k}, \mathbf{p}}(t) \equiv a_{\mathbf{k}, \mathbf{p}} \psi_{\mathbf{k}-\mathbf{p}}^\downarrow(t) \equiv \frac{1}{(2\pi)^2} \hat{z} \cdot (\mathbf{k} \times \mathbf{p}) \hat{\mathbf{k}} \cdot \hat{\mathbf{p}} \frac{\psi_{\mathbf{k}-\mathbf{p}}^\downarrow(t)}{|\mathbf{k}-\mathbf{p}|}. \quad (2.71)$$

We suppress the functional dependences of  $\psi^\uparrow$  and  $\psi^\downarrow$  on  $z^\uparrow$  because this equation is evaluated at fixed  $z^\uparrow$ ; in the following, we replace the partial time derivative by a total derivative, with the understanding that  $z^\uparrow$  is fixed.<sup>15</sup>

We use angled brackets to denote an ensemble average, in a plane with fixed  $z^\uparrow$ . We define the spectral energy densities  $e^\uparrow$  and  $e^\downarrow$  as follows

$$\langle w_{\mathbf{k}}^\uparrow(t) \cdot w_{\mathbf{k}'}^\uparrow(t) \rangle = \langle \psi_{\mathbf{k}}^\uparrow(t) \psi_{\mathbf{k}'}^\uparrow(t) \rangle = e^\uparrow(\mathbf{k}, t) \delta(\mathbf{k} + \mathbf{k}') \quad (2.72)$$

$$\langle w_{\mathbf{k}}^\downarrow(t) \cdot w_{\mathbf{k}'}^\downarrow(t) \rangle = \langle \psi_{\mathbf{k}}^\downarrow(t) \psi_{\mathbf{k}'}^\downarrow(t) \rangle = e^\downarrow(\mathbf{k}, t) \delta(\mathbf{k} + \mathbf{k}'), \quad (2.73)$$

where  $\delta(\mathbf{k})$  is a two-dimensional Dirac delta-function that is required by homogeneity (i.e., by the assumption that  $\langle w^\uparrow(\mathbf{x}_\perp) \cdot w^\uparrow(\mathbf{x}_\perp + \Delta \mathbf{x}_\perp) \rangle$  is independent of  $\mathbf{x}_\perp$ ); note that  $e^\uparrow$  and  $e^\downarrow$  are real.

<sup>15</sup>Since  $w^\uparrow$  is real,  $w_{\mathbf{k}}^\uparrow = (w_{-\mathbf{k}}^\uparrow)^*$ , where  $*$  denotes the complex conjugate, and so  $\psi_{\mathbf{k}}^\uparrow = (\psi_{-\mathbf{k}}^\uparrow)^*$ ; similarly,  $\psi_{\mathbf{k}}^\downarrow = (\psi_{-\mathbf{k}}^\downarrow)^*$ . Note that  $A_{\mathbf{k}, \mathbf{p}} = A_{-\mathbf{k}, -\mathbf{p}}^*$  and  $a_{\mathbf{k}, \mathbf{p}} = a_{-\mathbf{k}, -\mathbf{p}}^*$ , as required by the reality of  $w^\uparrow$ . The differential energy in up-waves within the  $k$ -space area  $d^2 \mathbf{k}$  is proportional to  $d^2 \mathbf{k} |w_{\mathbf{k}}^\uparrow|^2 = d^2 \mathbf{k} |\psi_{\mathbf{k}}^\uparrow|^2$ . So  $A_{\mathbf{k}, \mathbf{p}} = -A_{\mathbf{p}, \mathbf{k}}^*$  and  $a_{\mathbf{k}, \mathbf{p}} = -a_{\mathbf{p}, \mathbf{k}}^*$ , as required by the conservation of up-wave energy.

From §2.10.1,  $\psi^\dagger$  (and hence  $A_{\mathbf{k},\mathbf{p}}$ ) can be viewed as evolving independently of  $\psi^\dagger$ , since the backreaction is negligible at fixed  $z^\dagger$ . Therefore, equation (2.70) is similar to the simple random oscillator (eq. [2.60]), with  $A_{\mathbf{k},\mathbf{p}}$  a random function that has correlation time  $\Lambda/v_A$ . We solve it in the same manner, using perturbation theory. Since  $\langle \psi_{\mathbf{k}}^\dagger \rangle = 0$ , we derive the evolution equation for the bilinear quantity  $\langle \psi_{\mathbf{k}}^\dagger \psi_{\mathbf{k}'}^\dagger \rangle$ ; from equation (2.70),

$$\frac{d}{dt}[\psi_{\mathbf{k}}^\dagger \psi_{\mathbf{k}'}^\dagger] = \int d^2\mathbf{p} A_{\mathbf{k},\mathbf{p}}[\psi_{\mathbf{k}}^\dagger, \psi_{\mathbf{p}}^\dagger] + (\mathbf{k} \leftrightarrow \mathbf{k}'), \quad (2.74)$$

where  $(\mathbf{k} \leftrightarrow \mathbf{k}')$  represents a second term that is the same as the first, but with  $\mathbf{k}$  and  $\mathbf{k}'$  interchanged. We expand in  $A_{\mathbf{k},\mathbf{p}}$ ; to zeroth order,

$$[\psi_{\mathbf{k}}^\dagger \psi_{\mathbf{k}'}^\dagger]^{(0)} = \text{constant}. \quad (2.75)$$

To first order,

$$[\psi_{\mathbf{k}}^\dagger \psi_{\mathbf{k}'}^\dagger]^{(1)} = \int d^2\mathbf{p} A_{\mathbf{k},\mathbf{p}}^t [\psi_{\mathbf{k}}^\dagger, \psi_{\mathbf{p}}^\dagger]^{(0)} + (\mathbf{k} \leftrightarrow \mathbf{k}'), \quad (2.76)$$

where  $A_{\mathbf{k},\mathbf{p}}^t \equiv \int_0^t A_{\mathbf{k},\mathbf{p}}(t') dt'$ . To second order,

$$[\psi_{\mathbf{k}}^\dagger \psi_{\mathbf{k}'}^\dagger]^{(2)} = \int d^2\mathbf{p} d^2\mathbf{q} \left\{ (A_{\mathbf{k},\mathbf{p}} A_{\mathbf{p},\mathbf{q}}^t)^t [\psi_{\mathbf{k}}^\dagger, \psi_{\mathbf{q}}^\dagger]^{(0)} + (A_{\mathbf{k},\mathbf{p}} A_{\mathbf{k}',\mathbf{q}}^t)^t [\psi_{\mathbf{p}}^\dagger, \psi_{\mathbf{q}}^\dagger]^{(0)} \right\} + (\mathbf{k} \leftrightarrow \mathbf{k}'). \quad (2.77)$$

The sum of these last three equations is directly analogous to equation (2.62) for the simple oscillator. Using the same reasoning here as we did for the oscillator in deriving equation (2.65), we take the time derivative of the expected value of equation (2.77); we get, after setting  $\langle A A^t \rangle = (\Lambda/v_A) \langle A A \rangle$  (with the appropriate subscripts on  $A$ ), and after using equation (2.72) and integrating out the delta functions on the right-hand side:

$$\delta(\mathbf{k} + \mathbf{k}') \frac{d}{dt} e^\dagger(\mathbf{k}, t) = \frac{\Lambda}{v_A} \int d^2\mathbf{p} \left\{ \langle A_{\mathbf{k},\mathbf{p}} A_{\mathbf{p},-\mathbf{k}'} \rangle e^\dagger(\mathbf{k}', t) + \langle A_{\mathbf{k},\mathbf{p}} A_{\mathbf{k}',-\mathbf{p}} \rangle e^\dagger(\mathbf{p}, t) \right\} + (\mathbf{k} \leftrightarrow \mathbf{k}'). \quad (2.78)$$

We use equations (2.71) and (2.73) and  $e^\dagger(\mathbf{k}, t) = e^\dagger(-\mathbf{k}, t)$  to re-express this as

$$\frac{d}{dt} e^\dagger(\mathbf{k}, t) = 2 \frac{\Lambda}{v_A} \int d^2\mathbf{p} (e^\dagger(\mathbf{p}, t) - e^\dagger(\mathbf{k}, t)) |a_{\mathbf{k},\mathbf{p}}|^2 e^\dagger(\mathbf{k} - \mathbf{p}, t). \quad (2.79)$$

Since each upgoing plane with fixed  $z^\dagger$  interacts with many statistically independent downgoing waves before cascading, it is reasonable to assume isotropy in planes transverse to  $\hat{\mathbf{z}}$ ; after inserting equation (2.71) for  $a_{\mathbf{k},\mathbf{p}}$  and changing variables,

$$\frac{d}{dt} e^\dagger(\mathbf{k}, t) = \frac{\Lambda}{v_A} k^2 \int_0^\infty dk_\uparrow k_\uparrow^3 (e^\dagger(k_\uparrow, t) - e^\dagger(k, t)) \int_0^{2\pi} d\theta \sin^2 \theta \cos^2 \theta \frac{e^\dagger(k_\downarrow, t)}{k_\downarrow^2}, \quad (2.80)$$

where

$$k_{\downarrow} \equiv (k^2 + k_{\uparrow}^2 - 2kk_{\uparrow} \cos \theta)^{1/2} . \quad (2.81)$$

We have redefined  $\Lambda$  to absorb the factor of  $\pi$ , i.e.,  $\Lambda/\pi \rightarrow \Lambda$ . Thus far, we have only considered a single plane with fixed  $z^{\uparrow}$ . If we assume that the turbulence is homogeneous in  $z$ , the  $z$ -average of the above equation is trivial. Similarly, we re-interpret angular brackets to denote  $z$ -averages in addition to an ensemble average.

### 2.10.4 Steady State Fluxes

In steady state, we set the right-hand side of equation (2.80) to zero. We try power law solutions,  $e^{\uparrow}(k) \propto k^{-(3+\alpha_{\uparrow})}$ ,  $e^{\downarrow}(k) \propto k^{-(3+\alpha_{\downarrow})}$ , in which case the right-hand becomes

$$\left[ e^{\uparrow}(k_0) e^{\downarrow}(k_0) k_0^{6+\alpha_{\uparrow}+\alpha_{\downarrow}} \frac{\Lambda}{v_A} \right] k^2 \int_0^k dk_{\uparrow} k_{\uparrow}^3 \left( k_{\uparrow}^{-(3+\alpha_{\uparrow})} - k^{-(3+\alpha_{\uparrow})} \right) \left( 1 - (k_{\uparrow}/k)^{\alpha_{\uparrow}+\alpha_{\downarrow}} \right) \cdot \int_0^{2\pi} d\theta \sin^2 \theta \cos^2 \theta \left( k^2 + k_{\uparrow}^2 - 2kk_{\uparrow} \cos \theta \right)^{-(5+\alpha_{\downarrow})/2} . \quad (2.82)$$

Note that the square-bracketed term is independent of  $k_0$ . The above expression follows after breaking the  $k_{\uparrow}$  integral into two pieces: one from 0 to  $k$ , and the second from  $k$  to  $\infty$ . Then, the change of variables  $k_{\uparrow} \rightarrow k^2/k_{\uparrow}$  is made in the second piece (a Zakharov transformation), so that its limits are now from 0 to  $k$ . Finally, this second piece is combined with the first.

In steady state, equation (2.82) must vanish, so

$$\alpha_{\downarrow} = -\alpha_{\uparrow} . \quad (2.83)$$

Since  $w_{\lambda}^{\uparrow} \sim (k^2 e^{\uparrow})^{1/2} \propto k^{-(1+\alpha_{\uparrow})/2}$ , and similarly for  $w_{\lambda}^{\downarrow}$ , equation (2.83) is equivalent to  $w_{\lambda}^{\uparrow} w_{\lambda}^{\downarrow} \propto \lambda$  (eq. [2.19]). The vanishing of  $\partial_t e^{\downarrow}$  in steady state yields the same relation as equation (2.83), and so does not give new information.

The flux associated with  $e^{\uparrow}$  is given by integrating the right-hand side of equation (2.80) over  $d^2 \mathbf{k}$  from 0 up to any particular  $k$ . The steady state flux is thus given by integrating equation (2.82), with  $\alpha_{\downarrow} = -\alpha_{\uparrow}$ . The result of the flux integration is

$$\epsilon^{\uparrow} = f(\alpha_{\uparrow}) \left[ e^{\uparrow}(k_0) e^{\downarrow}(k_0) k_0^6 \frac{\Lambda}{v_A} \right] , \quad (2.84)$$

where  $f(\alpha_{\uparrow})$  is a dimensionless function of  $\alpha_{\uparrow}$ :

$$f(\alpha_{\uparrow}) = 2\pi \int_0^1 dx x^3 \ln x (x^{-(3+\alpha_{\uparrow})} - 1) \int_0^{2\pi} d\theta \sin^2 \theta \cos^2 \theta (1 + x^2 - 2x \cos \theta)^{-(5-\alpha_{\uparrow})/2} , \quad (2.85)$$

A technical note: although equation (2.82) vanishes in steady state, its integral over  $d^2 \mathbf{k}$  gives a

factor of  $\alpha_{\uparrow} + \alpha_{\downarrow}$  in the denominator, which also vanishes in steady state. This 0/0 ambiguity can be resolved by considering the limit as  $\alpha_{\uparrow} + \alpha_{\downarrow} \rightarrow 0$  (L'Hôpital's rule).

Equation (2.84) and the corresponding equation for  $\epsilon^{\downarrow}$ , are equivalent to those used in the heuristic discussion (eqs. [2.32] and [2.33]).

Galtier et al. (2000) plot the function  $f(\alpha)$  after numerically integrating the steady-state flux integral.<sup>16</sup> They show that  $-1 < \alpha < 1$ , that the steeper spectrum always carries more flux (i.e.,  $f(\alpha)/f(-\alpha)$  is a monotonically increasing function of  $\alpha$ ), and that in the limit that  $\alpha \rightarrow 1$ ,  $\epsilon^{\uparrow}/\epsilon^{\downarrow} \rightarrow \infty$ . (Clearly, this also implies that in the limit  $\alpha \rightarrow -1$ ,  $\epsilon^{\uparrow}/\epsilon^{\downarrow} \rightarrow 0$ .) In §2.3.4, we explain the physical reason why  $-1 < \alpha < 1$ . When this condition is violated, the cascade becomes nonlocal. Galtier et al. (2000) find infinite fluxes when these inequalities are saturated because they consider an infinitely extended spectrum, which leads to unphysical results when the cascade is nonlocal.

As discussed in §2.4.2, in steady state we are primarily concerned with the case that the up- and down-going fluxes are comparable, so  $|\alpha| \ll 1$ . In this limit, we linearize  $f$  about  $\alpha = 0$ , yielding approximately

$$f(\alpha) \simeq f(0) \cdot (1 + 0.5\alpha) \quad , \quad |\alpha| \ll 1 \quad , \quad (2.86)$$

This result is used in §2.4.2 to calculate the energy spectra given the fluxes  $\epsilon^{\uparrow}$  and  $\epsilon^{\downarrow}$ .

---

<sup>16</sup>More precisely, their figure 2 is proportional to  $[f(\alpha)f(-\alpha)]^{-1/4}$ , and their figure 3 shows  $f(\alpha)/f(-\alpha)$ .

## Bibliography

- [1] Biskamp, D. 1995, *Nonlinear Magnetohydrodynamics* (Cambridge: Cambridge University Press)
- [2] Biskamp, D. 2000, *Magnetic Reconnection in Plasmas* (Cambridge: Cambridge University Press)
- [3] Biskamp, D. and Müller, W.-C. 2000, *Phys. Plasmas*, 7, 4889
- [4] Borue, V. and Orszag, S.A. 1995, *Europhys. Lett.*, 29(9), 687
- [5] Cho, J., Lazarian, A., and Vishniac, E. 2002, *ApJ*, 564, 291
- [6] Cho, J. and Vishniac, E. T. 2000, *ApJ*, 539, 273
- [7] Dobrowolny, M., Mangeney, A., and Veltri, P. 1980, *Phys. Rev. Lett.*, 45, 144
- [8] Falkovich, G. 1986, *Phys. Fluids*, 29, 701
- [9] Galtier, S., Nazarenko, S. V., Newell, A. C., and Pouquet, A. 2000, *J. Plasma Phys.*, 63, 447
- [10] Galtier, S., Nazarenko, S. V., Newell, A. C., and Pouquet, A. 2002, *ApJ*, 564, L49
- [11] Goldreich, P. and Sridhar, S. 1995, *ApJ*, 438, 763
- [12] Goldreich, P. and Sridhar, S. 1997, *ApJ*, 485, 680
- [13] Iroshnikov, P. 1963, *Soviet Astron.*, 7, 566
- [14] Kraichnan, R. 1965, *Phys. Fluids*, 8, 1385
- [15] Lithwick, Y. and Goldreich, P. 2001, *ApJ*, 562, 279
- [16] Maron, J. and Goldreich, P. 2001, *ApJ*, 554, 1175
- [17] Montgomery, D. and Matthaeus, W.H. 1995, *ApJ*, 447, 706
- [18] Montgomery, D. and Turner, L. 1981, *Phys. Fluids*, 24, 825
- [19] Ng, C.S. and Bhattacharjee, A. 1996, *ApJ*, 465, 845
- [20] Ng, C.S. and Bhattacharjee, A. 1997, *Phys. Plasmas*, 4, 605
- [21] Shebalin, J.V., Matthaeus, W.H., and Montgomery, D. 1983, *J. Plasma Phys.*, 29, 525
- [22] Sridhar, S. and Goldreich, P. 1994, *ApJ*, 432, 612

- [23] van Kampen, N.G. 1992, Stochastic Processes in Physics and Chemistry, Chapter XVI (Amsterdam: Elsevier Science Publishers)
- [24] Zakharov, V.E., L'vov, V.S., and Falkovich, G. 1992, Kolmogorov Spectra of Turbulence I (Berlin: Springer)